Development of microwave synthetic routes to silica and gadolinium oxide nanoparticles for potential bio-imaging applications

Charles Weir

Supervisor: Dr Serena Corr

A thesis submitted to the University of Kent for the degree of Master by Research in Chemistry

Declaration

No part of this thesis has been submitted in support of an application for any other degree or qualification of the University of Kent at Canterbury or any other university.

28th July 2015

Abstract

The main aim of this research was to develop microwave synthetic pathways to monodisperse silica nanoparticles, which have potential uses in bio-imaging. Functionalisation of these nanoparticles was also attempted, using the fluorescent dye, Rhodamine B. Microwave synthesis was also investigated as a route to metal oxide nanoparticles, specifically gadolinium oxide and doped-gadolinium oxide nanoparticles, which find uses as magnetic resonance contrast agents.

A novel method to produce silica nanoparticles using a one-pot microwave synthesis has been developed. It has been demonstrated that small monodisperse silica nanoparticles can be prepared at temperatures as low as 50°C for a reaction time of as little as 30 minutes. This has been achieved using a combination of the traditional Stöber process and the use of microwave irradiation, with tertraethoxyorthosilicate as a precursor, in ethanol, water and ammonium hydroxide. A systematic study has been carried out, varying the reaction times and temperatures to identify the optimum synthetic conditions. The temperatures used were 50, 75, 85 and 100°C and the reaction times used were 0.5, 1, 2 and 5 h. To analyse particle size (Z-average) and polydispersity, dynamic light scattering (DLS) were employed. Scanning electron microscopy was also used to image the nanoparticles. It was found that typically smaller particles, with an average size of 65 nm or lower, displayed high monodispersity, compared to larger particles.

Fluorescent doping of silica nanoparticles was also demonstrated using the dye Rhodamine B. These particles were larger in size compared to the pure silica nanoparticles analogues, but remained highly fluorescent, even two months after synthesis.

Gadolinium oxide and europium-doped gadolinium oxide nanoparticles were also prepared using a combination of microwave irradiation and polyol synthesis. Both sets of particles displayed fluorescent properties, which could make them useful in future bioimaging applications.

Acknowledgements

I would firstly like to thank my supervisor Dr Serena Corr for her continued support throughout my Masters project. She has been behind me every step of the way supporting my decisions and offering guidance whenever asked. Without her continued encouragement, none of this would have been possible.

I would also like to thank my colleagues for their academic and personal support during my time as a postgraduate student at the University of Kent. They kept me in high spirits and were always there to bounce ideas off of. This includes, Kate Belsey, Charlie Holland, Arron Kliene, Gemma Osborne, Connor Bruton, Adrien Amigues and Darren Wells. They helped me through data when it was just not making sense and made every day a joy.

A special thanks goes to Marc Williams and Steve Hall as fellow members of Dr Corr's research group. Together they made each day enjoyable, whether this was through laughter or just talking through particularly repetitive data analysis. They provided assistance in my analytical processes and nothing was ever too much trouble.

A large thank you to Jon James for unrestricted access to glassware and machinery, as well as his constant good humour.

My appreciations also goes to The School of Physical Sciences as well as the Head of School for allowing me to conduct my research. Thank you to the Functional Materials Group for their support as well as a place to discuss all ideas, listening with continued interest.

A final thank you to my friends and family for their continued support through my entire academic life. They have always believed in my ability and their faith never waivered, even through the sleepless nights of worrying over small data differences or the continued typing and proof reading without prior chemistry experience.

Table of Contents

Abbreviations

SiO_2 – Silica nanoparticles

RhB-SiO_2 – Rhodamine B doped silica nanoparticles

Gd_2O_3 – Gadolinium oxide nanoparticles

Eu:Gd_2O_3 – Europium doped gadolinium oxide nanoparticles

TEOS – Tetraethethyl orthosilicate

EtOH – Ethanol

FITC – Fluorescein Isothiocyanate

APTES – (3-Aminopropyl)triethoxysilane

DLS – Dynamic Light Scattering

FTIR – Fourier Transform Infra-Red Spectroscopy

SEM – Scanning Electron Microscopy

TEM – Transmission Electron Microscopy

PdI – Polydispersity Index

Z-ave – Z-average (average particle size intensity

1. Introduction

1.1 General introduction

Nanoparticles attract considerable interest in a wide range of fields, such as cosmetics,

[1] textiles,[2] biomedical imaging,[3]and electronics in the form of flat panel displays.[4] There is a variety of nanoparticles that can be used in these fields, such as quantum dots and metal oxides.[5] This is due to their small size, which may bestow new properties which are not observed in the bulk form. To this end, choice of synthetic approach is essential to determining nanoscale size and unlocking these size-dependent properties. Nanoparticles may be prepared using a range of techniques, including co-precipitation, solvothermal methods, microemulsions, sol-gel methods and microwave synthesis.[6] Currently, there is great interest in developing new routes to these types of important materials which allow for the preparation of nanoparticles of uniform size. Through the control of particle size it is possible to affect the chemical and electronic properties of the particles.[7] Preparing uniform particles of a determined size may be very useful, since it would then be possible to see how effective a particular size is in any given application. When compared to their bulk counterparts, nanoparticles have a greater surface area. Additional functionality can be introduced to these particles by attaching functional materials to the surface. Traditional synthetic approaches and functionalisation strategies will be discussed in greater detail later.

1.2 Synthesis and Properties of Silica Nanoparticles

Silica nanoparticles are of particular interest due to their biocompatibility[8], low toxicity[9] and the possibility of functionalisation since a large number of functional groups may be conjugated to the silica particle surface. These properties make silica nanoparticles ideal for medical use and as hosts of biological molecules. Further functionalisation may include the incorporation of hydrophilic capping ligands or coatings.[10] Silica nanoparticles possess surface hydroxyl groups, which can be employed for further chemical modification. These surface groups render silica nanoparticles hydrophilic, which can be very useful when they are being used in a biological host.

The low toxicity of silica nanoparticles is extremely beneficial when considering their potential medical applications, since for use within a biological system this is a necessary trait.[11] Low toxicity prevents any serious damage when coming into contact with host organelles. In the case of silica nanoparticles, large concentrations of particles can be

removed by macrophages preventing any large build up, which will be discussed in greater detail further on.[42]

When considering nanoparticles for biomedical applications, the particle size is of great concern. Therefore, preparing silica nanoparticles for such uses, the synthetic route employed is vital in determining the final particle size. Different synthetic conditions can lead to particles of varying size and shape. Many efforts have been made to prepare monodisperse silica nanoparticles and a number of techniques have been employed.[6] Silica nanoparticle size can be affected by the concentration of each starting component, which includes tetraethyl orthosilicate (TEOS), ethanol, water and an acid or a base which acts as a catalyst, represented by Figure 1.1. When synthesising silica nanoparticles, ammonia is commonly used as a base while an acid is often employed for the preparation of a sol-gel.[48] A schematic for a typical synthesis is shown in Figure 1.1.

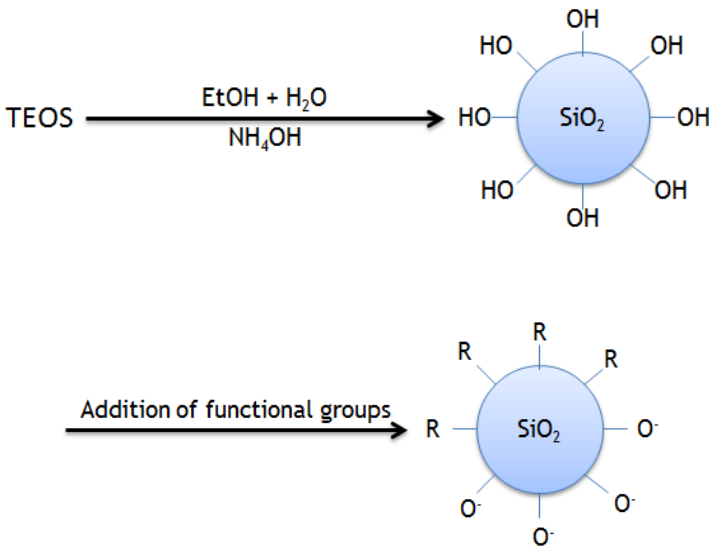

Figure 1.1 Schematic representation of the preparation of silica nanoparticles by the base-catalysed condensation of tetraethyl orthosilicate (TEOS). Additional functionality may be introduced (labelled 'R' groups here) through surface modification. These reactions may be performed in a one-pot reaction.[39]

The relative amounts of ammonia and water, for example, can have a great influence on the final particle size and morphology. The ammonia acts as a base, catalysing the condensation of TEOS. The concentration of water and ammonia are shown to affect the

nucleation rate of silica nanoparticles. As the concentration of both increases, the nucleation rate of the silica nanoparticles also increases. For water to affect this increase in nucleation rate, it requires a change in concentration from 1.1 M to 4.4 M, with ammonia having a concentration of 0.01 M. However, with water remaining at the lower concentration, nucleation rate can still increase as the concentration of ammonia increases.[12]

The size of silica nanoparticles may be tuned (anywhere between 5 nm and 1 μm) depending on the synthetic route employed and through the careful variation of experimental parameters.[13,14] The seminal paper in this field, by Werner Stöber and coworkers, provides a great insight into the synthesis of silica nanoparticles.[13] Through the hydrolysis of alkyl silicates and condensation of silicic acid in alcoholic solutions, silica particles of a uniform size were obtained. Using ammonium hydroxide for base-catalysed condensation, TEOS was reacted in an alcoholic solution. Here, ammonium hydroxide behaves as a catalyst and can have a great influence on the final particle morphology. The presence of ammonium hydroxide causes the formation of silica spheres.[13]

Without this catalyst there would be no spheres, only flakes. The choice of alcohol is an important consideration. It has been shown that the greater the molecular mass of the alcohol employed, the larger the resulting particle size. For example, the use of methanol results in a faster reaction rate with small particle sizes as low as 100 nm, whereas butanol was slower with larger particles formed up to 2 μm. The polydispersity of the samples was more prevalent with the higher alcohols. The formation of particles is noted by a colour change in the reaction vessel from colourless to a cloudy white, indicative of the presence of a precipitate. This is the nucleation phase where seed particles are formed. After particle formation, a growth stage follows after which the final particle size may be measured using electron microscopy. These processes (nucleation, seed formation and growth) may be represented by a LaMer diagram, shown in Figure 1.2.

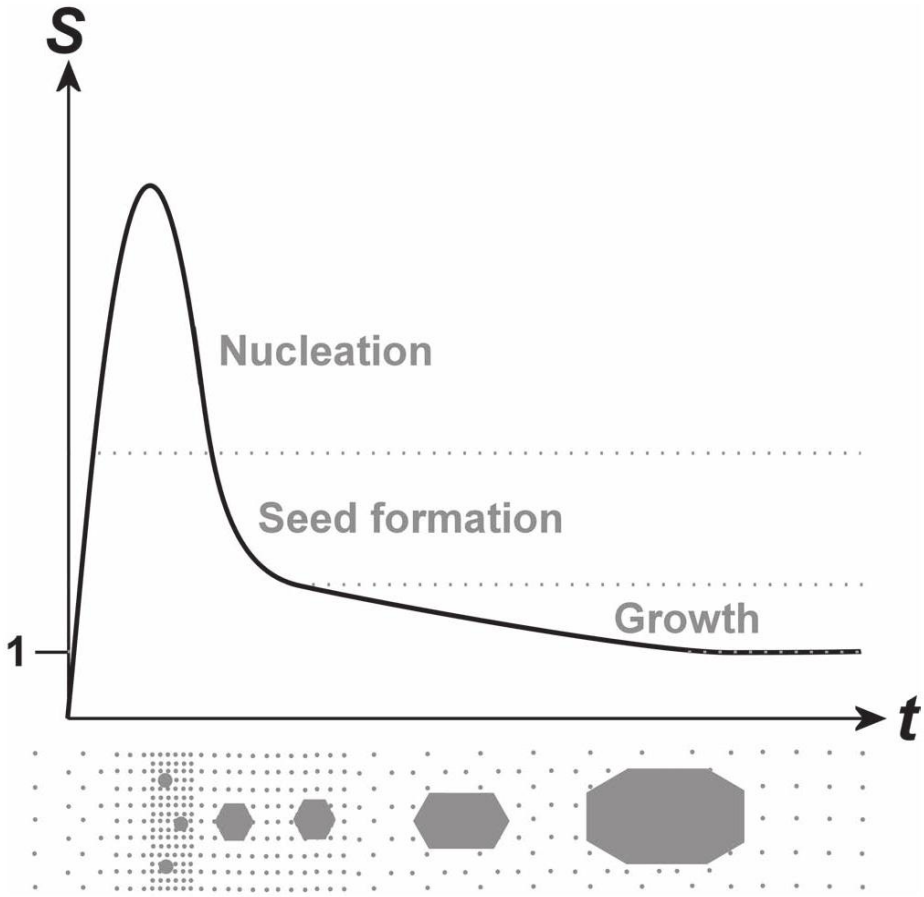

Figure 1.2 LaMer diagram depicting the stages of particle formation, including nucleation, seed formation and growth over time. Supersaturation of particles S, measured against time t.[15]

The condensation times in the above reactions can range from less than one minute (for a size of less than 0.2 μm) up to 24 hours (for a size around 2 μm). This condensation rate depends strongly on the water content. A greater volume of water causes a slower condensation rate. Altering the concentration of ammonia solution also affects particle size, with higher concentrations yielding larger particles. However, issues remain with particle size reproducibility and in maintaining monodisperse nanoparticles. A major advantage of producing monodisperse particulate suspensions is that they allow for an easier identification of the physical and chemical properties of these systems.

The LaMer diagram in Figure 1.2 shows the stages of nucleation, seed formation and growth by nanoparticles. The length of time spent in each of these regimes can influence particle size. The nucleation rate is related to supersaturation, as this determines the amount of activation energy required for nucleation to begin. Once a certain threshold is reached,

nucleation ends and then there is a rapid growth into seed particles. Seed mediated growth is used in a lot of spherical particle synthesis.[13] These seeds are the most important stage for shape control. Once shape is set at this stage, growth occurs, where final particles have an identical shape to that of the seed particles.

In a recent report, Davies *et al.* have demonstrated the use of statistical analysis to systematically investigate how reaction conditions can be varied to tailor the resulting nanoparticle size.[14] This approach, called a 2^2 factorial design, is very efficient as it allows for the direct comparison of how variations in reaction parameters affect the outcome, together with an analysis of the interactions of these parameters. Solutions of varying constituent concentrations were heated and agitated, resulting in a colloidal suspension of SiO_2 nanoparticles. Reaction times were also varied. Agitation was achieved *via* three methods: (i) magnetic stirring, (ii) ultrasonic bath (5 – 60 Hz) and (iii) ultrasonic tip (20 kHz). It was shown that the ratio of water to ethanol was pivotal in determining particle size. For example, with a 1:2 ratio (ethanol:water), the average particle size reached 262 nm. The particle sizes were confirmed using photon correlation spectroscopy (PCS). However when the ratio is inverted and volumes halved, the average size is 140 nm. Particle sizes were also confirmed using electron microscopy. The optimum conditions for the smallest particle sizes were identified as 70 mmol TEOS, 3 mmol ammonia, 0.4 mol ethanol and 0.2 mol water. This produced particles with an average size of 5 nm ±1 nm.[14] As well as having a very low standard deviation and very small particle size, the polydispersity of the sample was found to be low when using PCS. This is an indication of the monodispersity of the sample. The results identified in this publication are dependent on the agitation methods highlighted above. These authors also attempted the same synthesis with a conventional microwave, but abandoned this technique due to difficulties in reproducibility and control.

Another method of synthesis reported is the semi-batch process conducted by Park *et al.*[16] The average size of the particles prepared in the optimised procedure was 13.7 nm. The semi-batch process feeds a solution of TEOS and ethanol, using a controlled flow rate micro feed pump, into a secondary solution of ethanol, ammonia and water. The second solution is in a reactor suspended in a water bath. This procedure can provide nanoparticles of a wide range of sizes (from 10 nm up to 350 nm) compared to some other methods. However, the standard deviation values can be inconsistent.

The sequential synthesis used by Rao *et al*. achieved particle sizes as low as 20 nm.[17] This procedure involves agitating the alcohol through sonication for up to 10 minutes before adding the next component. This continued until all components were in solution. Although the particle size is not as low as other methods, uniformity was better, shown through a low standard deviation (less than 3 nm). By using sonication, it is more probable that the solutions will react fully. Sonication uses ultrasound to agitate the mixture. Sound waves are generated using a sonicating water bath and will pass through the solutions suspended in it. Sonication ensures the constant interaction between the components in solution.

Gao *et al*. have reported the synthesis of silica nanoparticles from oil shale ash (OSA), which contains a large quantity of SiO_2.[18] The OSA is heated to just below melting point and then stirred with a sulfuric acid solution, then heated once more. This mixture was filtered and washed with distilled water to remove all of the acid. A sodium silicate solution was produced by mixing more OSA with a sodium hydroxide solution, causing the silica to dissolve. A silica gel was formed on addition of PEG and a sulphuric acid solution. After aging this mixture and heating to 550ºC for 2 hours to remove any surfactant, silica nanoparticles were obtained. This method was very time consuming and involved a large number of processes. The particles obtained were quite polydisperse and large aggregates are formed.[18]

Bagwe *et al.* have recently reported a microemulsion synthesis which leads to the formation of monodisperse silica particles with a high degree of control over the particle size.[19] This procedure involves mixing surfactant, co-surfactant and organic solvent with an aqueous solution of dye, water and ammonia. This process yields nanoparticles of 14 nm, 29 nm and 130 nm.[19]

The particle sizes obtained are dependent on the structure of the microemulsion droplets, the temperature the reaction is performed and the organic solvent employed. In a microemulsion, water droplets are dispersed in a constant environment of oil. These droplets of water are nanosized liquid bodies, which function as nanoreactors for nanoparticle synthesis. The generation of these nanoreactors means that the synthesis does not require extreme pressure or temperature to drive the reaction. The size and shape of the nanoparticles can be controlled by changing the parameters of the microemulsion. Identifying which parameters influence size allows for more control over the final size.[19] The dye used in this synthesis was Tris(2,2'-bipyridyl)dichlororuthenium(II) (Ru(bpy)). This dye demonstrated a

red-shift when an anionic surfactant was used or if the concentration of ammonium hydroxide was increased. It was also found that the co-surfactant had no effect on the fluorescent emission properties of the dye molecules. However, the make-up of the microemulsion systems did have an effect on the maximum fluorescence intensity. When the mixture was dioctyl sulfosuccinate, heptane and water the fluorescence intensity was 2.7×10^6, but when the mixture was polyoxyethylene nonyl phenol ether, cyclohexane and water, the intensity was 1.7×10^6.

Another common route to nanoparticles is the coprecipitation method. Coprecipitation is a synthetic method which uses aqueous silica salt solutions. Bases are then added to this while at room temperature and under an inert gas environment (e.g. nitrogen). The resulting particle size and shape depend on the salt used, the temperature of the reaction, the pH and the ionic strength of the solution. This is easily reproduced once the above factors have been set. Unfortunately, size tuning is more difficult with this process and typically polydisperse particles are produced.[20]

Silica nanoparticles are prepared commercially through acidification of aqueous solutions of sodium silicate, which is made from sand.[21] When this process is performed at high temperatures, silicic acid is formed in supersaturated solutions. These acidic solutions are thermodynamically unstable when in pure water. This instability is due to condensation polymerisation through hydrolysis, which causes the production of small nuclei. The nuclei will continue to grow until they become stable in suspension. Due to the nature of the precursor being natural, there is a certain amount of aluminium contaminant contained within the structures. In order to remove the particles from suspension, the solution is placed into an evaporator. The current applications of aqueous silica nanoparticles are in the manufacture of electrical and thermal insulators, thin film and electronic substrates, and humidity sensors.[21]

Another method of silica nanoparticle synthesis reported by Li *et al*. describes porous hollow silica nanoparticles.[22] The main advantage of these particles is that they could be used as carriers, e.g. for drug delivery. This not only aids in prevention of drug loss but is also useful as a host to carry its load across a barrier which is usually inaccessible. This method requires the use of a calcium carbonate template which the silica surrounds, shown in Figure 1.3. Once fully formed, the template is washed away leaving porous hollow silica nanoparticles. However, the procedure required to hold the drug requires an addition high pressure step. In order to ensure the drug is held by the nanoparticles, a high pressure, of 30

MPa for 24 hours, is required. Though this procedure effectively contains the drug within the nanoparticle core, it is not viable in a standard lab due to the excessive pressures necessary.[22]

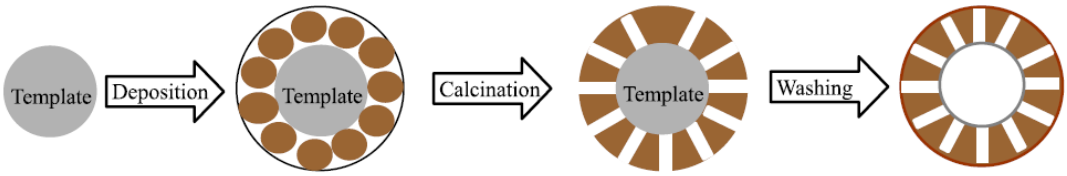

Figure 1.3 Graphical representation of the process of forming $CaCO_3$ nanoparticle templates, followed by preparing silica nanoparticles around this to create a porous structure. After removal of the template by washing, hollow porous silica nanoparticles remain.[22]

One synthesis method attracting increasing interest is microwave-assisted route. Typically microwave techniques are used in organic synthesis, but its use in the preparation of inorganic nanoparticles is growing. This is an inexpensive, quick and versatile technique.[23] These are proven by the power and time control, low complexity of the system and low loss of heat during synthesis. The microwave can also be programmed to maintain a set temperature and pressure for a set time. Microwave irradiation provides uniform heating by two mechanisms: dipolar polarisation due to contributions of the solvent and ionic conduction through contributions of the ions in the sample.[26] This uniformity of heating speeds up the rate of the reaction. The molecules rotate through the application of microwave irradiation and the dipole moment becomes disorientated. On returning to its original orientation, heat is generated from molecular friction. The amount of heat generated depends on the frequency at which microwave radiation is applied combined with the dipole nature.[24]

Choice of solvent is therefore important, as a solvent which absorbs microwave irradiation will allow for uniform heating. One example of a family of solvents which behave in this manner is ionic liquids which, with their low vapour pressures, couple to microwaves efficiently.[25] The ability of the solvent to absorb microwave irradiation (ε') as well as the ability to turn that absorbed radiation into heat (ε'') is given by the loss tangent (tan δ) value:

$$tan\delta = \varepsilon''/\varepsilon'$$

This calculates the ratio between the dielectric constant (ε') and the loss factor (ε''). Using the above equation it is possible to determine good candidate solvents for microwave synthesis. It is found that ethanol and ethylene glycol have high loss tangents of 0.941 and

1.350 respectively, compared to that of acetone which has a very low loss tangent of 0.054.[24,26] This shows that for use in a microwave reaction where the solvent couples strongly to the microwave irradiation, ethylene glycol is better than ethanol, which in turn is better than acetone.

Microwave-assisted synthesis has been employed by Bilecka *et al.* to reduce reaction times and produce highly pure, crystalline ZnO nanoparticles through efficient and controlled heating.[27] Niederberger and co-workers have established the success of benzyl alcohol as a solvent when synthesising crystalline metal oxide nanoparticles, such as ZnO and Fe_3O_4, in a matter of minutes.[28] The metal oxides were prepared using metal alkoxides, acetates and acetylacetonates heated to 60 °C so that they would dissolve in the benzyl alcohol. Homogenous nucleation was then achieved through rapid heating in a microwave synthesiser to 200 °C. Crystal growth occurs at this temperature and can be tailored using further heating. It is also possible to alter the particle size if different precursors are used, which was shown for the case of Fe_3O_4 nanoparticles. The sizes found were 11 nm from $Fe(acac)_2$, 7 nm with $Fe(ac)_2$ and 5 nm from $Fe(acac)_3$. It was also possible to identify the varying reaction pathways to ZnO nanoparticle formation through microwave synthesis and autoclave synthesis. The initial difference between the techniques is reaction times: the use of microwaves reduces reaction times to a few minutes compared to the autoclave which requires several hours. It was found that both methodologies use ester elimination from the formation of benzyl acetate. The benzyl acetate could be seen to form through a highly polar transition state caused by the nonthermal microwave effect. This could be the reason for the accelerated microwave synthesis compared to the slower solvothermal autoclave preparation.[28]

Reports of microwave preparations of silica nanoparticles are limited. However, microwave-assisted synthesis has been used by Lovegood *et al.* to synthesise silica nanoparticles.[29] These particles were synthesised by irradiating solutions, formed using the Stöber method identified above, at 2.45 GHz. The resultant nanoparticles ranged from 30 nm to more than 250 nm in diameter. The growth of these nanoparticles was seen to be quick, accurate and precise. The solution of tetramethyl orthosilicate (TMOS) and hydrochloric acid was diluted with acetone in volumetric ratios. The solutions were heated to 125 °C by setting the microwave power to 300 W, which was then reduced to around 65 W after reaching this desired temperature. It was found that the resultant SiO_2 particles had a transparent nature

which means that characterisation techniques such as UV-vis and photoluminescence is limiting. Therefore techniques such as Dynamic Light Scattering are more effective at quickly and easily measuring the average particle size. The precision of the microwave-assisted synthesis is shown through repeated growth of silica nanoparticles at specific diameters. The five syntheses of smaller particles had an average size of 57 ± 4 nm and the six syntheses of larger particles had an average size of 212 ± 15 nm. The syntheses showed that irradiating the solutions at 125 °C for longer and increasing the concentration of TMOS resulted in larger average particle sizes. The solutions were only heated for minutes which greatly increased the ability for a large number of repeated syntheses. The ability to maintain accuracy through specifying heating times, at specific power levels and pressure limits allowed for excellent reproducibility.

1.3 Modified Silica Nanoparticles

As mentioned previously, post-synthetic functionalisation can bestow multifunctionality on the silica nanoparticles. Coatings or capping agents may allow for passage through cell walls and the generation of a drug-delivery shuttle. For example, TEOS can be used to produce silica coatings of a controlled thickness on the surface of metal oxide nanoparticles and 3-aminopropyltriethoxysilane (APTES) can be used to introduce amine functionality to a particle surface.[30] As Chekina *et al.* have previously shown, a possible coating is fluorescein isothiocyanate (FITC), which has an emission intensity displaying pH dependence. The FITC was made as a solution in acetone and water, which was then added to silica-hematite nanoparticles modified with amine groups from an earlier reaction with APTES. The reaction ran for 12 h at 23 °C in the dark. Once amine groups are present from the addition of APTES to the surface, it is possible for FITC to then form an amine bond. FITC displays greater fluorescence in a pH range between 5 and 8. The advantage of this range is that fluorescent magnetic nanoparticles can act as pH sensing probes for imaging. The bloodstream has a pH of 7.4, with inflamed tissue being slightly acidic at a pH of 6.5 and some endosomes measuring a pH of 5. The above range encompasses all of these and so nanoparticles can be monitored throughout the body.

Two possible methods to prepare dye functionalised silica nanoparticles are to include a dye when preparing the particles, or to graft the dye onto the pre-formed nanoparticle surface.[31] When preparing these nanocomposites, the problem of self-quenching and photobleaching of dyes must be considered, which will be explored later. Van Blaaderen *et*

al. have employed the Stöber method to prepare silica nanoparticles, which were then functionalised with an FITC dye molecule *via* conjugation to 3-aminopropyl trimethoxysilane (APTES) shown in Figure 1.4.[32] Addition of dye molecules has to be accurately calculated, since with a high concentration of dye molecules, π-π stacking can exist between neighbouring molecules and self-quenching can then occur, leading to a decrease in fluorescence intensity.

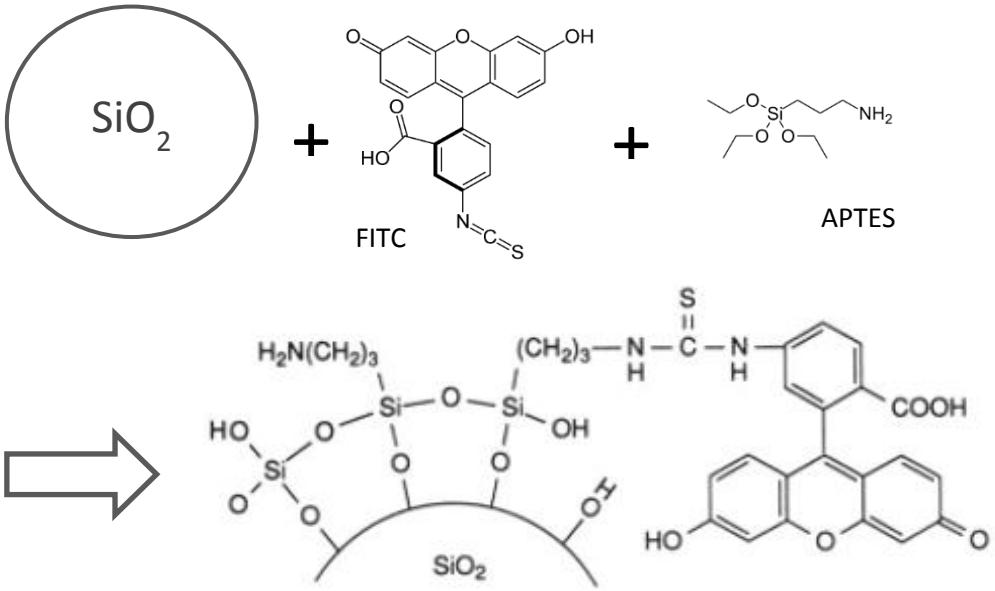

Figure 1.4 A schematic representing the addition of FITC and APTES to the surface of silica nanoparticles. Firstly the APTES binds to the FITC through the formation of amide bonds. The APTES is held to the silica nanoparticle surface through strong Si-O-Si bonds.[32]

Drug moieties may also be conjugated to the surface of silica nanoparticles. In some cases, drug molecules may have adverse effects on healthy cells. An advantage of silica nanoparticles is that they can reduce the toxicity of molecules attached to their surface. This is demonstrated in a study by Botella *et al*. who have attached the drug camptothecin to silica nanoparticles.[33] Camptothecin (CPT) can cause highly adverse reactions such as myelosuppression and hemorrhagic cystitis. Though it is used in the treatment of cancerous cells, its associated cytotoxicity can cause a lot of harm to healthy cells too. It was demonstrated here that CPT conjugates to the silica particles in high quantities, due to the large nanoparticle surface area. This allows for the administration of smaller doses. A resultant effect of this bonding is an excellent stability in biological fluids and the prevention of an untimely release. CPT is not covalently bonded directly to the silica nanoparticles, but

rather through ester bonds to trihydroxysilylpropyl carboxylate (THSC) groups, which are attached to the silica nanoparticle surface.

Surfactants may be employed on the surface of silica nanoparticles to enhance their uptake into cells. For example, the use of phospholipids is beneficial when considering drugs which are often found to be hydrophobic in nature. Phospholipids are present in the structure of every cell. Therefore, using them to coat drug loaded silica nanoparticles could be effective at facilitating transfer across cell membranes. The attachment of targeting ligands to phospholipids is done through conjugation between carboxylic groups and primary amines. For example, folic acid has been conjugated to silica nanoparticles in this manner, allowing for stealth movement from the reticuloendothelial system and increased circulation time.[34] Surface charge can be just as important in functionalisation and stability in a colloidal suspension. This stability can be indicated by a highly negative or highly positive zeta potential.

Once the nanoparticles have been synthesised, it is necessary to remove them from suspension for further characterisation using a variety of analytical techniques. The morphology of the silica spheres is of importance and so the most effective method for achieving a highly spherical nature is required. As noted earlier a large surface area is necessary to enable multifunctionality through surface modifications. This large surface area is best achieved by a spherical shape. Cho *et al.* highlight the ratio of the surface area between particles sized 50 nm, 100 nm and 200 nm. The particles at 50 nm and 100 nm have a surface area four times and two times larger (respectively) than that held by the 200 nm particles.[54] Procedures for particle retrieval reported by Rahman *et al*. involve oven drying or alcohol dehydration.[35] The oven drying technique can result in an alteration to the morphology and a slightly increased average size of 7.1 nm compared to alcohol dehydration where the particle size is 6.7 nm and the morphology remains intact. It was also reported that alcohol dehydration does not cause particle aggregation, compared to oven drying.[35]

1.4 Biomedical Applications of Silica Nanoparticles

Due to their small size, ease of chemical modification and biocompatibility, silica nanoparticles can be used in several biomedical applications, with one example being bio-imaging.[7] The low toxicity and high degree of compatibility means these particles can pass through the body without detection and removal by the immune system, making this an ideal mediator for drug delivery or cellular interactions.[36] Surface modifications, discussed below,

may also be employed to avoid removal by biological agents. There is also the advantage of the silica being biocompatible, allowing any tethered dye molecules to remain in the body without being attacked.[36]

By taking advantage of the surface chemistry of these particles, several entities may be combined to form a nanocomposite which displays multifunctionality.[38] The combination of several properties in one composite gives the benefits of all properties in one entity. While these multimodal materials can be effective for biomedical use, there can be some difficulties encountered in their preparation. For example, in the combination of magnetic nanoparticles with fluorescent entities, quenching may occur.[37] Here, the use of a silica shell can be instrumental in providing a spacer between the magnetic core and the fluorescent dye to prevent quenching. These important composites are very useful since they can be used to track cells and with a combination of magnetic resonance (MR) and fluorescence imaging they can image and then treat those cells.[37]

Multifunctionality can be achieved through a number of different ways, depending on the desired outcome. Using target specific moieties attached to the surface of the nanoparticles, it is possible to not just target cells but then use the optical properties of fluorescent dyes for confocal imaging and the magnetic properties for MR imaging.[38] The use of silica enables incorporation of dyes easily as it is optically transparent.[37] When introducing functional groups to the surface of silica nanoparticles, Achatz *et al.* have reported a one-pot synthesis where a reduction in agglomeration has been noted.[39] This is in comparison to a previous report from Mader *et al*., where dispersions of nanoparticles in toluene are heated with reagents under reflux conditions for 24 h.[40] It is found that this method generates small nanoparticles with an average size of between 30 to 40 nm. Although small particle size is achieved, these authors note a high degree of agglomeration. Comparatively, the one-pot synthesis resulted in particles of an average size of 25 nm and demonstrated very little clustering.

Due to silica's hydrophilic nature it may be difficult to pass through cell membranes, because of the nature of the cellular bilipid layer. Non-polar, or lipophilic, molecules are easily able to pass through membranes through diffusion.[41] However, using these kinds of molecules to ensure this transfer is achieved can affect the efficacy of a drug being transported. For example, the drug retention time may be hindered. To increase retention time, it is possible to attach polyethylene glycol (PEG) to the surface of the nanoparticles.

This PEGylation step forms a covalent bond between the PEG molecule and a therapeutic drug, resulting in a masking effect, preventing renal clearance. This 'Trojan horse'-type strategy is shown in Figure 1.5.

Without this masking procedure, the nanoparticles will be absorbed by macrophages in the body and removed. The increased retention times afforded by this procedure have been demonstrated by Torchilin and coworkers.[42] It is found that longer PEG blocks result in longer retention and circulation times. This in turn has a lower uptake by the reticuloendothelial system. Longer retention times are also reported by Yamamoto *et al*. who have used a PEG shell to surround drug moieties.[43] This shell then makes it possible to prevent capture and uptake by the reticuloendothelial systems that transport foreign bodies to the liver, spleen and kidneys for excretion. Yokoyama *et al*. have shown that the addition of PEG maintains water solubility.[44] They have also evidenced that covalently bonded PEG can be used to make fluorescent particles more stable. This stability is demonstrated by comparison of Adriamycin and PEG-poly(aspartic acid). When both are kept in the dark, it is seen that the absorbance remains higher for longer.

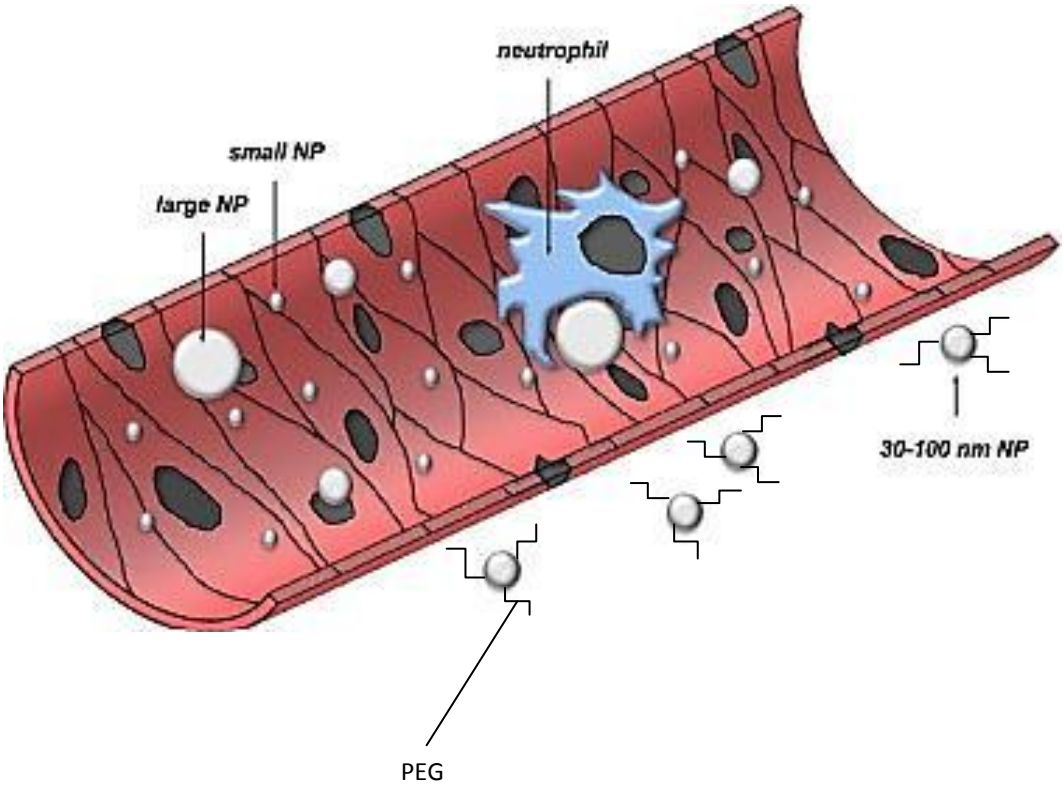

Figure 1.5 Typical representation of the inside of a blood vessel. Smaller nanoparticles of 30-100 nm may avoid clearance, due to size or through masking by PEG, while larger particles are cleared more efficiently by the reticuloendothelial system (highlighted in blue).[41]

The choice of dye for preparing these kinds of nanocomposites is important, since some dyes may be destroyed by continuous light exposure in a process known as photobleaching. Commonly used fluorescent probes, such as fluorescein isothiocyanate (FITC), may be severely photobleached on exposure to UV light. Since dyes being employed as probes may require exposure to continuous light excitation, photobleaching gives cause for concern for real-time viewing. Dyes such as tris(bipyridine)ruthenium (II) chloride (Ru(bpy)) and Rhodamine B are less prone to bleaching and are commonly employed to allow for good imaging.[45] It has been found that by incorporating these dyes into nanoparticles, this photobleaching effect may be overcome.

Sharma *et al*. have found that while organic dyes can succumb to photobleaching quickly, the encapsulation of this dye within silica nanoparticles can improve its photostability.[46] This stability is improved both *in vivo* and *in vitro*. This method of dye-doping means oxygen cannot easily access the organic dye. This reduction in oxygen interaction reduces photodegradation of the dye molecules. It is also possible for surface modifications to still be

made, such as enhanced hydrophilic character and cell uptake through the addition of biomolecules such as proteins.

The synthetic method employed can also play a major role in stability. Using reverse microemulsion techniques to synthesise fluorescent silica nanoparticles can sometimes result in difficulties when incorporating non-polar molecules, such as drugs or organic dyes, into a silica matrix. Often, leaching and reduction in brightness may be observed. This is due to a lack of any covalent bonding between the particles and the dye molecules.[47] To prevent or at least reduce the leakage mentioned above, the reverse-micelle microemulsion process can allow for strong electrostatic attractions between silica nanoparticles and the polar organic dyes.[47] This attraction is found when using a polar dye. The relationship between the negatively charged silica nanoparticles and positively charged dye allows for strong intermolecular attractions. Figure 1.6 demonstrates how the fluorescent silica nanoparticles prepared using this method have been used to image leukaemia cells in a rat. The image shows how effective these nanoparticles can be when antibodies such as Immunoglobulin E are attached to the surface to provide targeted bioimaging.[49]

Ow *et al.* have reported that by incorporating dye molecules of tetramethylrhodamine isothiocynate (TRITC) into silica, photostability is increased and the dye molecules are protected from photobleaching.[48] The organic dye is firstly conjugated to the silica precursor which is then condensed. This action causes dye rich cores to form. Then silica monomers, prepared using the sol-gel method, were added to cause a dense silica encapsulation around the core. The surrounding silica moieties shield the TRITC dyed core from interacting with the environment and therefore this increases photostability. This would in turn extend the fluorescent lifetime of the dye. This method is described as heterogeneous nucleation. If the TRITC were added externally as a free dye, it was found to have a brightness of 0.08 kHz/particle, however when encapsulated in the silica core the brightness was at around 1.2 kHz/particle.

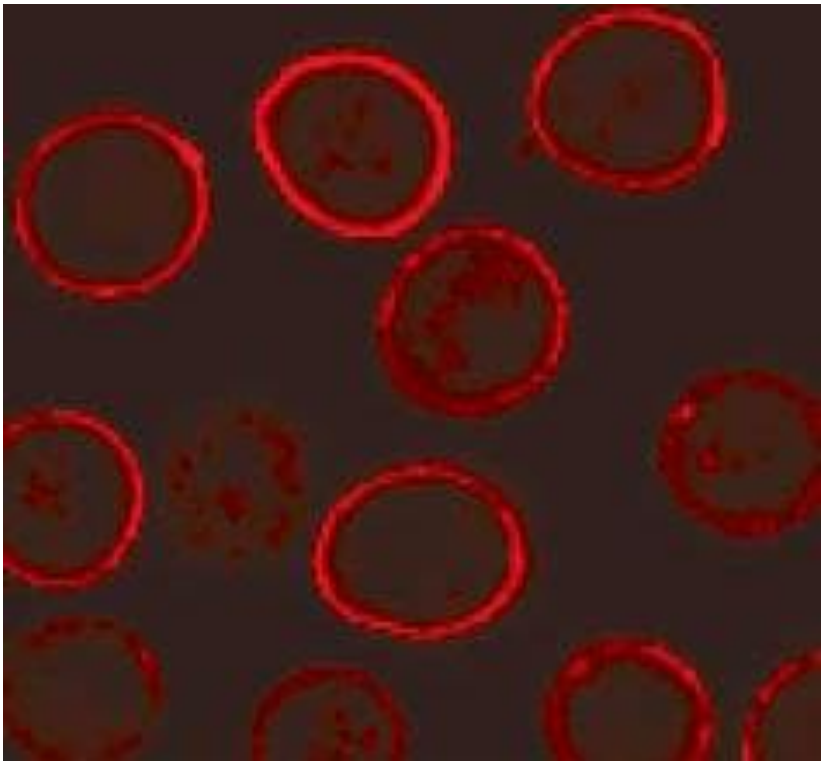

Figure 1.6 Confocal image of fluorescent core–shell silica nanoparticles (red) non-covalently bonded to an Immunoglobulin E antibody. This antibody is then explicitly attached to the FceR1 cell surface receptor of rat basophilic leukaemia cells. The interaction between the antibodies and receptors allows for bioimaging of the leukaemia cells.[49]

The multifunctionality of fluorescent-silica nanoparticles can be advanced by using peptides, proteins and enzymes encapsulated in the nanoparticles, which can be used to identify target cells and for example administer an attached drug. By taking advantage of the fluorescent properties, it could also be possible to follow the progress of that cell using confocal imaging. Concerns when preparing polymer based nanocomposites of this form include the possible degradation or denaturation of biological molecules, which hinders the therapeutic efficacy of the proteins. Evidence of this has been observed by Panyam *et al.* where tetanus toxoid (a vaccine for tetanus) activity was reduced by 30 %.[50] This reduction in activity is from the 100 % activity before introduction into the nanocomposite system. This reduction in activity is possibly caused by protein degradation. If the proteins in the vaccine are exposed to organic solvents, this would cause denaturation. However, the preparation of nanoparticles requires solvents to be present. Due to the denaturising effect of these solvents thorough washing would be necessary to prevent any contact between the proteins and

solvent. Degradation of the proteins can also occur if the environment is too acidic, which can be prevented through the use of a buffering base.

In some cases, there is little change in enzyme activity when they are covalently bound to silica nanoparticles. Shang *et al.* have found a 10 % change in RNase A enzyme activity from being free to being attached to the surface of the silica nanoparticles.[51] Stability of the surface modified silica particles is dependent upon the interactions between negative charges on the nanoparticles surface and the positive charge on the enzymes. These interactions rely on the surface area of the contact points between the enzymes and the silica. Therefore larger surface areas strengthen this interaction, as will a higher surface potential.[51]

Although silica nanoparticles are well tolerated biologically, larger sized particles may cause problems. Particles larger than 5 μm in size can block blood vessels. However, if the particles are too small, they could accumulate together and block blood flow possibly causing stroke or embolism.[41] Silica particulates on the micron scale have been associated with a number of diseases, such as rheumatoid arthritis, renal disease and lupus.[52,53]

Larger fluorescent silica nanoparticles (on the order of 100 nm to 200 nm) have been found to cause some minor inflammation when collected in the liver.[54] However, this damage does not appear to be long term and can be eased after 12 to 24 hours. Nanoparticles of 50 nm also show some inflammatory response, but this was not as significant as the case of the larger particles. Particles of 50 nm were excreted faster than those of 100 nm and 200 nm, and after one week, all particles had been removed. This retention time can be an important consideration, depending on how long these particles are required to deliver any attached molecules.

For targeted nanoparticles delivery, size also plays an important role. Peptides and antibodies can be used as biological markers in active targeting. They need to be attached to the surface of the nanoparticles to do this.[55] However, a combination of active and passive targeting can result in a very effective nanoparticle delivery system. Active targeting is when the surface of the nanoparticles is functionalised through the use of a natural ligand linked to a biological moiety. Passive targeting is when physiological parameters will act as a filtration system and this becomes important when particles are too large to enter specific sites. Due to the tailoring of therapies to specific diseases, the delivery of pharmaceutical agents to specific cells is more advantageous than blanket delivery. These agents can be transported to the

specific sites necessary without compromising their integrity. The nanoparticles would be able to protect the drug molecules, preventing degradation or loss *via* efflux. With particle sizes of between 30 nm and 100 nm required for local injections, it is possible for these nanoparticles to avoid reticuloendothelial clearance. Size is again an important concern when using these particles for tumour cell targeting. If the particles are too large, then only certain cells will take them up. For example, passive targeting is employed when targeting phagocytic antigen presenting cells. By using 5 μm particles, smaller cells will not be able to take up these particles and so they will have an effect on those cells specifically.

After cell entry and subsequent load delivery, it may take some time to clear the nanoparticles from the system and they will eventually be collected in the kidneys or taken up by macrophages to the liver and spleen, and then removed from the body. Both before and after delivery, the nanoparticles can be trapped by macrophages. However, being trapped by macrophages can depend on the size of the nanoparticles. It was found that the larger the particles were, in this case 200 nm, the more quickly they can be taken up. The silica nanoparticles may then be transported to the spleen and liver where they can remain for up to 4 weeks before being excreted. This is shown in Figure 1.7, where the nanoparticles are stained red.

Excretion via the kidneys can be much faster, as it was noted that there was no presence detected after 1 week. A major concern is that while in the liver and spleen, these nanoparticles could aggregate and block essential pathways. However, remaining in the liver and spleen prevents them from building up in blood vessels.[54] As Figure 1.7 shows, there is a larger build-up of silica 200 nm nanoparticles than the smaller 50 nm particles. There is also an appreciable population of macrophage cells (shown in green) present around the larger particles. These macrophages were stained using rat anti-mouse F4/80 antibody and the silica nanoparticles were prepared with rhodamine isothiocyanate. This difference could be caused by macrophages not being able to pick up the smaller nanoparticles. This prevents aggregation of smaller particles in the spleen, but also means that the nanoparticles have avoided absorption. Conversely, the larger particles do not avoid the macrophages so easily and are more readily transported to the spleen.

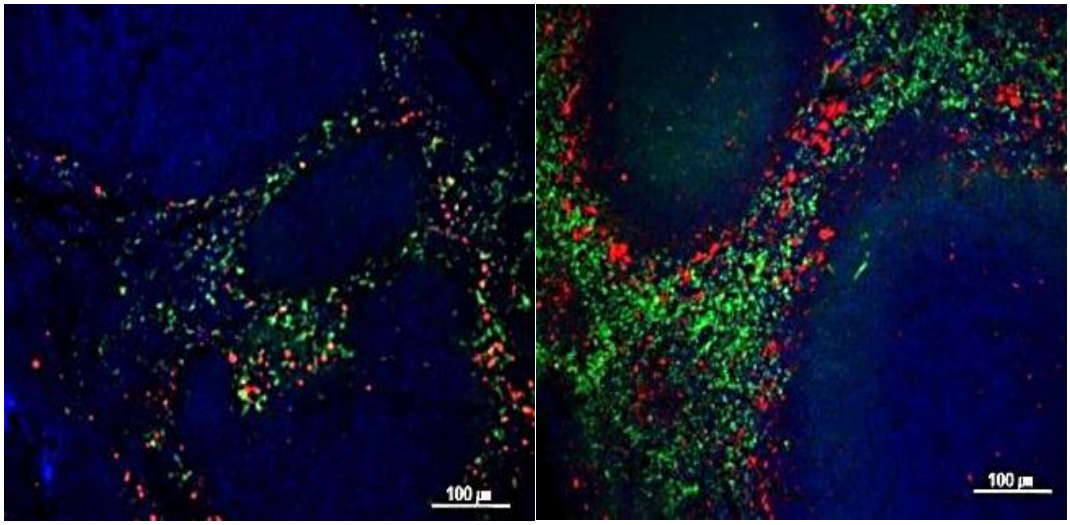

Figure 1.7 Immunohistochemical staining of silica nanoparticles and macrophages in the spleen, 12 hours after injection. Nanoparticle sizes of 50 nm (left) and 200 nm (right) show that size causes a difference in the amount of silica nanoparticles (red) and macrophages (green) that have built-up.[54]

1.5 Synthesis, Properties and Applications of Gadolinium Oxide Nanoparticles

In addition to silica nanoparticles, the current work addresses the preparation of metal oxide nanoparticles using similar synthetic approaches (in this case, microwave synthesis). In particular, gadolinium oxide nanoparticles, Gd_2O_3, are extremely useful for magnetic resonance imaging (MRI), owing to their magnetic properties.[56] This is due to the highly paramagnetic nature of the gadolinium ions. Gd(III) has seven unpaired electrons and a long electronic relaxation time, an important consideration for contrast agent behaviour. Since gadolinium metal is highly toxic *in vivo*, it has traditionally been employed in chelated form. However, for good contrast large concentrations (greater than one gram) are required, which limits imaging quality as there will be accumulation in high quantities.[56] Recently, a polyol synthesis of Gd_2O_3 nanoparticles has been developed, which have shown good potential as contrast agents.[57] Polyol synthesis can be used to prepare a number of metallic powders through reduction of the inorganic compounds.[58] High boiling point alcohols are employed, which is necessary here due to the high temperature at which seed gadolinium oxide nanoparticles grow. The alcohol acts as a stabiliser, limiting particle growth, and also helping to reduce agglomeration.[59] Once formed, the nanoparticles are colloidally stable suspensions in diethylene glycol (DEG). The DEG will not conjugate to the nanoparticles, allowing it to be removed easily through centrifugation and ethanol washings. Another advantage of this method is that the suspension is colloidally stable for weeks after

synthesis.[60] The polyol synthesis above involves treating a mixture of gadolinium(III) chloride hexahydrate and sodium hydroxide in DEG at temperatures of 140 °C and 180 °C.[57] By performing the reaction at ramped temperatures (an initial heating at 140 °C for 1 hour, followed by heating at 180 °C for 4 hours), the nucleation and growth mechanisms may be controlled. The very small size of the nanoparticles obtained (3.1 ± 0.9 nm) is beneficial, as they have the ability to pass through cell walls. However, particles of this small size may be filtered into small capillaries, away from the targeted areas. As well as this, they would go undetected by macrophages. While this is a desirable property, there is the possibility that these particles may not be removed from the body and could build up in large quantities. Therefore, surface modifications can be employed to ensure that the particles are of an optimum size: not too big to be removed from the body and not too small to build up in the body. In this case, the authors employed the silane (3-mercaptopropyl)trimethoxysilane (MPTS) in order to attach PEG, which enhances the stability and biocompatibility.

Other reports of the use of polyol synthesis for metal oxide nanoparticles, include yttrium, zinc and manganese.[59] In this procedure, metal precursors are dissolved in DEG with a predetermined amount of water before heat treatment. Again, the heating regime is two-fold. Here, DEG acts as a chelating ligand limiting the particle growth. The secondary effect is found to be the prevention of clustering of nanoparticles. Size can be tailored through temperature and time of the reaction, as well as the concentration of components. This method resulted in metal oxide nanoparticles being formed with a range of 30 to 200 nm in size.

Gadolinium oxide has further potential applications if it were to be doped with fluorescent lanthanide materials. This fluorescent nature makes lanthanide materials very useful for applications such as biolabelling. F-block, or lanthanide, ions can emit in the visible region, displaying sharp emission spectra which, combined with long lifetimes and reduced photobleaching, make their compounds extremely beneficial for use in bioimaging. Excitation occurs when light is absorbed through a coordinating crystal and electrons are promoted from the ground to the excited state. In the +3 oxidation state, lanthanide ions adopt on an electron configuration of [Xe]$4f^n$ and this shell is filled through the series of lanthanides. However the shielding of this shell is not perfect and so the electrons in this shell will be drawn to the closed shell configuration of the xenon ($5s^2 5p^6$). This effect is the lanthanide contraction.[61] An electrostatic interaction is then formed between the 4f electrons

and the external environment. This electrostatic interaction means that Stark splitting of the 4f level is small. Stark splitting refers to the splitting of the spectral lines. This results in sharp narrow bands representing 4f(III) ions in emission spectra which are weakly dependent on environment, shown in Figure 1.8.

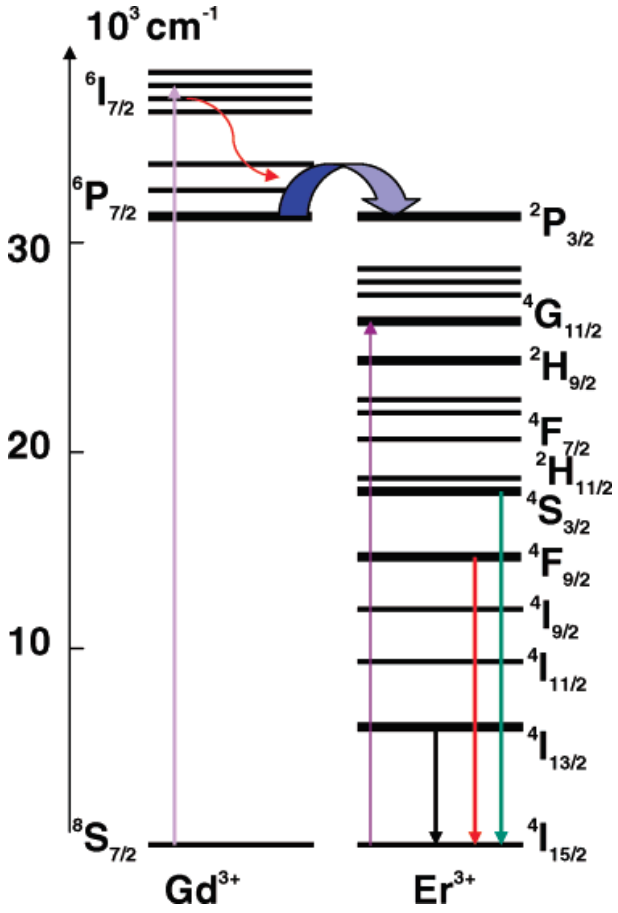

Figure 1.8 Schematic of energy levels in Er^{3+} and Gd^{3+} ions in cubic Gd_2O_3 nanocrystals[62]

The emission wavelength of lanthanide oxide nanoparticles is not related to the particle size. The Bohr radius is very small, therefore nanoparticle size is not relevant for the fluorescent properties exhibited from these elements. However it is possible that on incorporation of other rare-earth ions into these nanoparticles, their fluorescence and lifetime characteristics may be altered. This could be down to any imperfections in the host particles, as well as particle surface effects. Currently lanthanide oxides are used as commercial phosphors. Their use in biolabelling would be effective as they will have better

photostability, when compared to lanthanide doped polystyrene nanoparticles which are used commercially.[63]

1.6 Aims and objectives

The main aim of this research is to develop new microwave routes to nanoparticle synthesis. First, silica nanoparticles will be prepared using a modified Stöber approach in combination with microwave irradiation. Since reaction conditions such as time and temperature have previously been shown to be of immense importance in controlling final particle size, these will be systematically varied. The growth stages of nanoparticle preparation will be monitored using dynamic light scattering tools in order to check when this stage has gone to completion. Particle precipitations will also be performed in an effort to collect particles of a uniform size. Particle size will also be monitored using electron microscopy, in an attempt to find the optimal conditions for (i) small nanoparticles and/or (ii) monodisperse nanoparticles.

Upon examination of these results, the conditions for best particle preparation will be identified and employed to prepare a bimodal nanocomposite, incorporating a fluorescent dye, in this case, Rhodamine B, during synthesis. Another consideration would be to look at the effect of nanoparticle size on the fluorescence, which is affected by the Bohr radius, which is the approximate radius of the exciton which is set up between an electron and a positive hole in a semi-conducting material.

In an attempt to provide a quicker, more energy efficient route to gadolinium oxide nanoparticles, similar microwave approaches will be tested. It is envisaged that the delivery of microwave energy to the solution will provide uniform heating throughout the sample, which should ensure a monodisperse particle size.

The major objective of this work is to show that microwave synthesis is a fast, effective and straightforward method for the preparation of monodisperse populations of nanoparticles with a desired size. Particles prepared in this work could find future applications in both confocal and MR imaging.

2. Experimental

2.1 Theory and Instrumentation

2.1.1 Microwave synthesis

Microwave synthesis, equipment shown in Figure 2.1, uses microwave radiation to heat uniformly, by taking advantage of the molecule dipole moment. The radiation gives rotational energy to all the particles. The electric field generated by the microwave is what causes the flipping of the dipole moments. The dipole is forced to rotate against its original orientation, and as the frequency of radiation changes it will rotate back and forth between these positions. This flipping causes the molecules to rub against each other creating friction and this generates heat. The amount of heat generated then depends on the frequency at which microwave radiation is applied combined with the dipole nature.[64] As mentioned previously (Chapter 1), solvents may be characterised by their loss tangent values. These values can affect how strongly they couple to microwaves. Some common solvents are shown in Table 2.1, with their corresponding tan δ values.

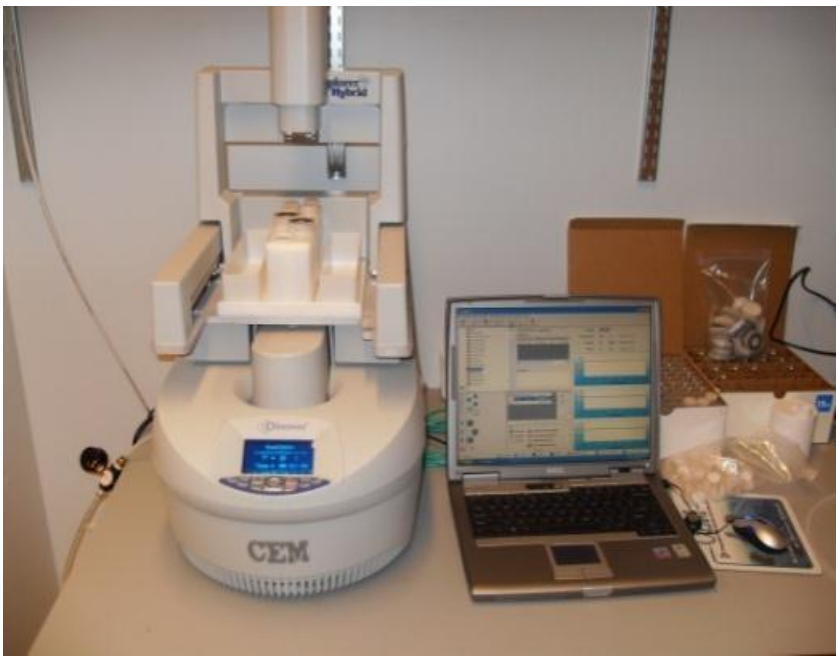

Figure 2.1 Microwave synthesiser used for the preparation of silica nanoparticles

Table 2.1 Common solvents and their loss tangent values. Higher tan δ values mean the solvent will couple more strongly to microwaves.[65]

Solvent	***Tan δ***	***Solvent***	***Tan δ***
Ethylene Glycol	1.350	*DMF*	0.161
Ethanol	0.941	*1,2-dichloroethane*	0.127
Water	0.123	*Acetonitrile*	0.062
Methanol	0.659	*Toluene*	0.040
2-propanol	0.799	*Hexane*	0.020
formic acid	0.722	*Tetrahydrofuran*	0.047
1,2-dichlorobenzene	0.280	*Acetic acid*	0.174
Acetone	0.054	*Dichloromethane*	0.042

In order to calculate the values for the above table it is necessary to first know the ability of the solvent to absorb microwave irradiation (ε') and also the ability to convert the radiation that has been absorbed into heat (ε''). Using both of these factors it is then possible to calculate the loss tangent (tan δ) values, where

$$tan\ \delta = \varepsilon''/\varepsilon'$$

As seen from Table 1, the tan δ values can vary greatly and therefore choice of solvent is important for microwave synthesis, depending on whether the solvent is being used to help increase the rate of heating or to act as a heat sink. Some of the most effective solvents for quicker heating are polar solvents such as ethylene glycol (tan δ 1.350), ethanol (tan δ 0.941) and 2-propanol (tan δ 0.799). Correspondingly, non-polar (or only slightly polar) solvents such as hexane, toluene and dichloromethane have low tan δ values. The kinetics of microwave heating is such that the mechanism is controlled by a fast phase boundary which causes increasing rates of nucleation. The reaction kinetics are evidenced through the use of electron microscopy which shows small, spherical crystals. Microwaves can have shorter reaction times through uniform heating. This heating enhances diffusion rates. All these together can permit the formation of kinetic solid state products over more thermodynamically stable products.[66] The time, pressure and temperature are

programmable so that exact specifications can be maintained throughout. This is all performed in a closed system, with an air venting system which can be used to steadily cool the sample.

2.1.2 Dynamic Light Scattering

Dynamic Light Scattering (DLS) is a non-invasive technique that allows for easily repeatable analyses. DLS measures Brownian motion; this is then related to the particle sizes. Brownian motion is the movement of particles due to random collisions with surrounding molecules. Small particles move quickly and larger particles move more slowly. This relationship between particle size and speed within solution is defined by the Stokes-Einstein equation[67]:

$$D = \frac{RT}{N_A} \frac{1}{6\pi\eta r}$$

As the particles move, the waves will fluctuate causing intensity to do the same. This fluctuation is then used to calculate particle sizes.[68] The Stokes-Einstein equation calculates the diffusion coefficient (D) of a particle undergoing Brownian motion (RT) in a fluid of viscosity (η) and the spherical particle radius (r) in accordance with Avagadro's constant (N_A).

In a DLS experiment, the particles are illuminated with a laser and the intensity fluctuations in the scattered light are analysed. As the laser strikes the particles, light will be scattered in all directions. These scatterings will cause propagated waves that are detected and then shown as an average intensity.[69] DLS can therefore be used to determine the size distribution of small particles in suspension. There is a number of size average values of all the particles that can be mapped, such as the Z-average, intensity, volume and number, shown in Figure 2.2. The Z-average gives a mean particle size by fitting a single exponential to the correlation function obtained during the scattering experiment.[70]

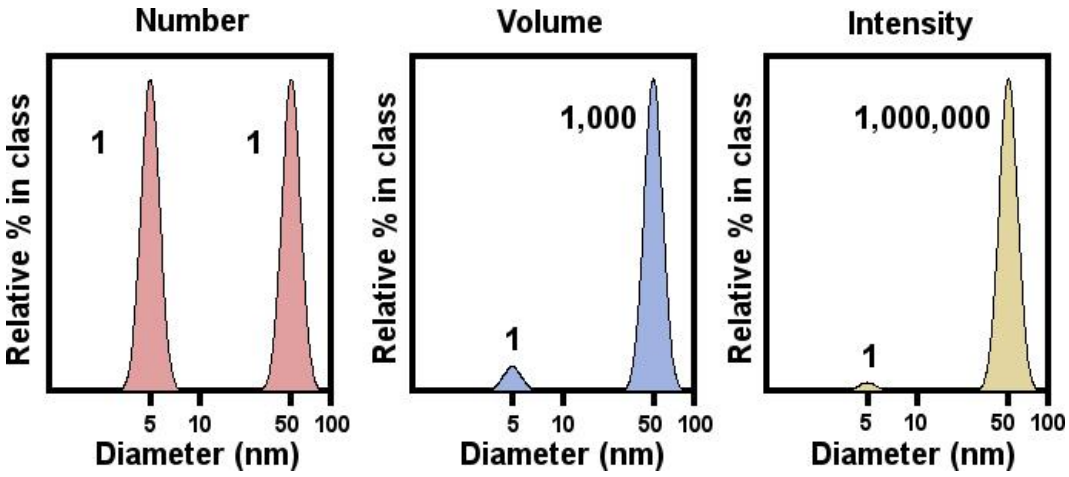

Figure 2.2 Number, volume and intensity distributions of a bimodal mixture of nanoparticles (5 nm and 50 nm) present in equal numbers.[71]

The polydispersity index, or PdI, is an estimation of the width of the distribution and give information on the uniformity of the particles. This is especially useful when monodispersive particles are required. A laser passes into the sample and is deflected when it strikes a particle.[72] This is then detected uncovering a range of values between 0 and 1. Samples which have a value close to 0, are said to be monodisperse. Conversely samples with values closer to 1 are polydisperse. The PdI value is not to be confused with the standard deviation; standard deviation is how much an entire sample differs from the average. This can take into account a few particles being largely different and then having a very large standard deviation, while PdI measures uniformity with arbitrary units, identifying how similar all the particles are and would not show such a large change for only a few particles as intensity is also a factor when it is calculated.[73]

2.1.3 Fourier Transform Infrared Spectroscopy

Infra-red radiation is electromagnetic radiation which has frequencies and energies lower than those of visible light. Infrared radiation is passed though the sample being tested. The molecules absorb the radiation as it strikes them, at discrete frequencies, which correspond to changes in rotational and vibrational energies of the bonds within these molecules. Some of the radiation passes through, known as transmission, and the resultant spectra show the absorption and transmission of the sample. This allows for information on the surface of the nanoparticles to be obtained, allowing for identification of characteristic absorption frequencies.

Identification of the functional groups is possible when comparing with spectra of known compounds.[74] FTIR can also be used to determine quality and consistency of a sample. The time taken for this characterisation varies, depending on the range of frequencies being examined and the number of scans being performed on the sample in a single run. The overall speed of the analysis is quite fast due to the ability for all frequencies to be looked at simultaneously. The sample is placed onto the diamond anvil and then the sample run takes place. This is advantageous as the sample is recoverable. Due to the speed, sensitivity setting and simple sample preparation, this technique is extremely accurate and reproducible. The FTIR instrument used for characterisation was the Shimadzu IR Affinity-1.

2.1.4 Scanning Electron microscopy

Scanning electron microscopy may be used to image a sample by using a high energy beam of electrons. These electrons interact with the atoms in the sample, providing information on the sample morphology, topology and composition. A scanning electron microscope (SEM), shown in Figure 2.3, incorporates the use of an electron optical column, a vacuum system, electronics, and software. Compared to a TEM, the column is much shorter as there are less lenses required. An SEM only needs a lens above the specimen which focuses the electrons to the surface of the specimen. In an SEM, electrons are accelerated and so carry large amounts of kinetic energy, which come into contact with the sample and are then dissipated as a variety of signals. The signals produced include secondary electrons and backscattered electrons (when electrons are reflected off the sample) which are the signals used to create SEM images. Some electrons may also be absorbed by the specimen.[75] The SEM focuses the electron beam into a fine point which is then scanned in a rectangular pattern for imaging as a grid of pixels on a monitor. The SEM is capable of measurements as low as 50 nm and the accelerating voltages are in a range from 50 to 30,000 volts. In order to obtain high quality images the samples are loaded onto discs which are then coated with 10 nm of gold. This does mean that the sample is not recoverable or reusable for other techniques. However after this gold film encapsulates the sample it can be viewed through the SEM as many times as necessary. The SEM requires minimal sample preparation and all calibration is done automatically. The acquisition of images of a sample can take just a few minutes.

The SEM used in this work was a Hitachi S3400-N. In the case of much smaller nanoparticles, transmission electron microscopy (TEM), shown in Figure 2.3, can provide information on the primary particle size, shape and, in some cases, composition.[76] Electron density variations in the objective lens are inverse or negative images of what is seen in a TEM image. The incident beam is fixed allowing the projection of the image onto a viewing screen in the microscope column.[77]

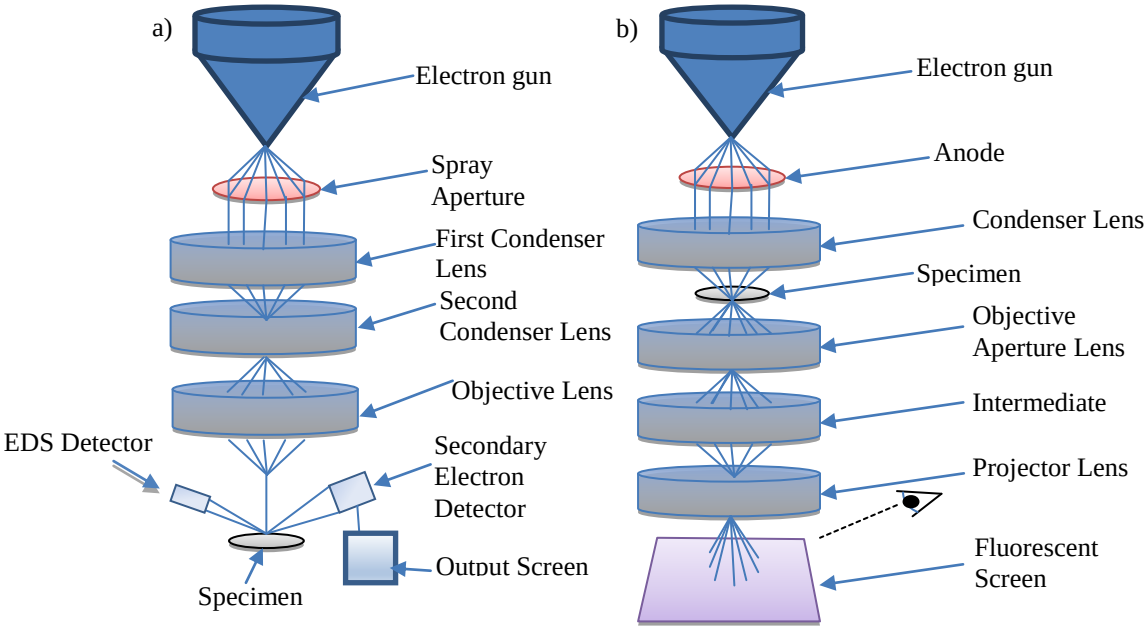

Figure 2.3 Schematic diagram of a) Scanning Electron Microscope and b) Transmission Electron Microscope, identifying the path the electrons take from the gun, through a) a spray aperture, condenser lenses, objective lens and onto the specimen causing electrons to be scattered and detected, which is then shown on an output screen and b) anode, condenser lens, passing through the sample, until it is projected onto a fluorescent screen where it is viewed.[77]

2.1.5 Fluorescence Spectroscopy

Fluorescence spectroscopy is a method of measuring the fluorescence of a sample. Fluorescence occurs when molecules absorb energy and are excited from their ground state to higher vibrational levels. After this occurs, the bond order decreases, the atoms relax and then emit a photon and return to the ground state.[76] The emission spectra produced from a fluorescence spectrometer is a plot of emission against wavelength of the exciting light. A fluorescence spectrometer,

shown in Figure 2.4, is capable of exciting molecules at desired wavelengths depending on the molecules known light excitation wavelength. If the wavelength is not known then analysis can be performed over a wider range, but this will take a considerable amount of time.

Depending on what range of light is being looked into, whether it is UV or UV-vis, then specific lamps are utilised. A mercury lamp will effectively identify UV light in low pressure gas, and UV-vis light in medium and high pressure. Mercury lamps can be limiting due to their outputs relating to specific excitation wavelengths. Alternatively, a tungsten-halogen lamp will provide a continuous excitation across a broader range of wavelengths.

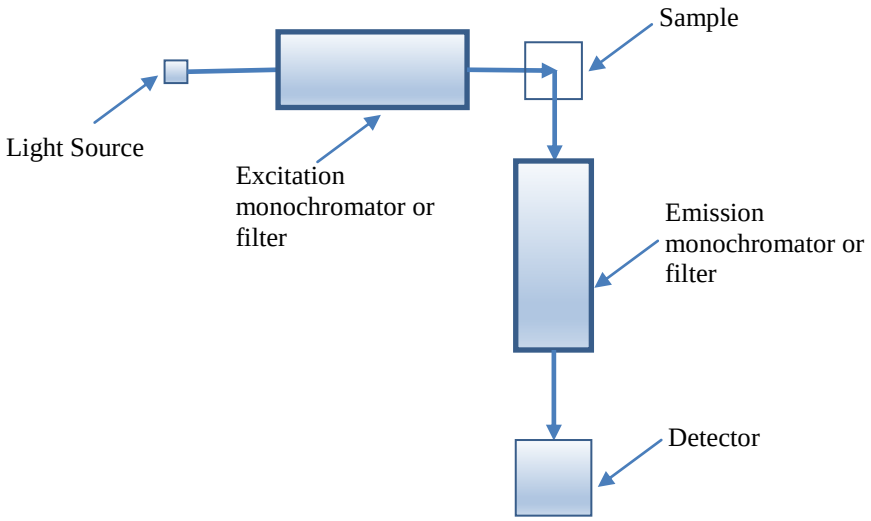

Figure 2.4 Schematic diagram of a Fluorescence spectrometer, identifying the path the light travels from a source, through a monochromator and to the sample.[78] The sample is excited and then releases energy as it returns to its ground state in the form fluorescence, which passes through the emission monochromator and then to the detector which translates this into a visible spectra.

2.2 Synthesis and Characterisation

2.2.1 Silica nanoparticles

Ethanol (9.22 ml; 0.200 mol), water (1.80 ml; 0.100 mol) and TEOS (tetraethyl orthosilicate) (7.29 ml; 35.0 mmol) were pipetted into a 35 ml glass microwave vessel under nitrogen gas. Ammonium hydroxide (0.0550 ml; 1.60 mmol) was added, along with a magnetic flea, before the reaction vessel was placed into the

microwave synthesiser. The desired temperature and time were set, with constant stirring throughout experiments. The microwave synthesiser used in this project is a CEM Discover SP Microwave Synthesiser. Experimental details are given in Table 2.2.

Table 2.2 Experimental conditions for the preparation of silica nanoparticles at varying temperatures (50 °C, 75 °C, 85 °C and 100 °C) and reaction times (0.5 h, 1 h, 2 h and 5 h)

Sample	Temp (°C)	Time (hours)
NP1	50	0.5
NP2	50	1.0
NP3	50	2.0
NP4	50	5.0

Sample	Temp (°C)	Time (hours)
NP5	75	0.5
NP6	75	1.0
NP7	75	2.0
NP8	75	5.0

Sample	Temp (°C)	Time (hours)
NP9	85	0.5
NP10	85	1.0
NP11	85	2.0
NP12	85	5.0

Sample	Temp (°C)	Time (hours)
NP13	100	0.5
NP14	100	1.0
NP15	100	2.0
NP16	100	5.0

Once the reactions had run to completion, the solution turned from colourless to a cloudy white suspension. The suspensions were kept in the dark and DLS analyses were performed each week to check the resulting particle size and monodispersity. To perform the analysis 1 ml of the suspension and 1 ml of acetone was placed into a cuvette which was then placed in the DLS at 25 °C and standard pressure for 2 minutes to establish an equilibrium then run 3 times at high resolution.

For each reaction performed above an identical reaction was also carried out. Immediately after the microwave reaction the particles were isolated from the

reaction mixture. This recovery was performed by transferring the samples from the microwave vessels to sample tubes. These tubes were then placed in a centrifuge and run for 15 minutes at 3000 rpm. These samples were then drained and washed 3 times using 15 ml of acetone, repeating the above centrifuge process. After the final spin the samples were then dried in an oven at around 40 °C at standard pressure, ready for further characterisation.

Silica nanoparticles were prepared using a microwave synthesiser, as shown in Figure 2.1. The starting components were ethanol, water, tetraethyl orthosilicate (TEOS) as a precursor and ammonium hydroxide as a base. The mixture was constantly stirred throughout the reactions. Reactions were carried out at different temperatures (50 °C, 75 °C, 85 °C and 100 °C). For each temperature, several reactions were also carried out to increase the time systematically: 0.5 hours, 1 hour, 2 hours and 5hours. The resulting white solution was decanted into sample tubes for further workup and analysis. These suspensions were monitored using DLS each week to check for continued particle growth. Each reaction was repeated in order to collect a set of nanoparticles precipitated immediately after microwave irradiation. The second approach halted the ageing process and enabled closer analysis through SEM imaging at 10,000 volts. This also allowed for FTIR analysis to be performed on the dried particles to confirm that silica nanoparticles had been formed. The FTIR was set to run for 32 scans between the wavelength of 1000 cm^{-1} and 2000 cm^{-1}.

In order to monitor the growth of silica particles over time, the mean size (Z-average) and polydispersity index were recorded initially and at subsequent weekly intervals using dynamic light scattering (DLS). The DLS instrument used in these experiments is a Zetasizer Nano ZS. The characteristics that can be measured are particle size, zeta potential and molecular weight. This analytical instrument provides a level of sensitivity between 0.6 nm and 6 µm. There is also an available temperature function, which means that any heat sensitive samples can be analysed, within the range of 2 °C to 90 °C. These measurements were performed in order to establish if reactions have gone to completion and determine the extent of particle aggregation over time. DLS is highly sensitive to nanoparticle aggregation, which will manifest itself in a larger Z-average due to clustering of the particles and, if several cluster sizes exist, an increase in polydispersity.

2.2.2 Rhodamine B-doped silica nanoparticles

Using the same procedure as above, Rhodamine B doped silica nanoparticles were prepared. Firstly A solution of Rhodamine B (0.00210 g; 0.00600 mmoles) in ethanol (100 ml) was prepared. 200 μl of this solution was pipetted into a reaction vessel containing ethanol (9.22 ml; 0.200 mol), water (1.80 ml; 0.100 mol) and TEOS (tetraethyl orthosilicate) (7.29 ml; 35.0 mmol) under nitrogen gas. The solution was a translucent pink colour. Ammonium hydroxide (0.0550 ml; 1.60 mmol) was added, along with a magnetic flea, before the reaction vessel was placed into the microwave synthesiser. The reaction temperature and time were set to 50 °C and 0.5 h. Upon completion, a cloudy pale pink colloidal suspension formed. The particles were recovered through the use of a centrifuge. This centrifuge ran for 15 minutes at 3000 rpm. The samples were then washed using acetone and then dried in an oven at around 40 °C at standard pressure. The precipitate formed was a pale pink powder and when subjected to UV light, fluoresced bright pink.

2.2.3 Gadolinium oxide nanoparticles

$GdCl_3.6H_2O$ (0.740 g; 0.200 mol) and NaOH (0.080 g; 0.200 mol) were added to a glass microwave vessel in a glove box. Water (0.36 ml) and diethylene glycol (10 ml) were added. This cylinder was then placed in a microwave synthesiser along with a magnetic flea. The microwave was set for a two stage run. This began by initially heating at 140 °C for 30 minutes, with medium stirring. The second stage then ramped up to 180 °C and remained at this temperature for 3 hours, under continued medium stirring. The resultant precipitate was a white powder. The gadolinium oxide nanoparticles were only precipitated out on the addition of acetone. Without this they remained suspended. The sample was then centrifuged for 15 minutes at 3000 rpm. The powder dropped to the bottom of the tube and the solution was decanted away. This solution then had more acetone added to it and centrifuged to make sure that no further gadolinium nanoparticles remained. Once this was confirmed the white samples were washed using acetone 3 more times and centrifuged as before between each washing. The particles were then kept covered in an oven to dry at around 40 °C at standard pressure. This resultant dried powder was subjected to fluorescence spectroscopy and the sample was excited at 250, 271.65, 274.36 and 277.32 nm.

2.2.4 Europium-doped gadolinium oxide nanoparticle preparation

$GdCl_3.6H_2O$ (0.740 g; 0.200 mol) and NaOH (0.080 g; 0.200 mol) were added to a glass microwave vessel in a glove box. Water (0.36 ml) and diethylene glycol (10 ml) were added. Then the addition of $EuCl_3.6H_2O$ (0.0150 g; 4.00 mmol) was made immediately after diethylene glycol. This cylinder was then placed in a microwave synthesiser along with a magnetic flea. The microwave was set for a two stage run. This began by initially heating at 140 °C for 30 minutes, with medium stirring. The second stage then ramped up to 180 °C and remaining at this level for 3 hours, continuing medium stirring. The precipitate that formed was also a white powder. However under UV light the powder fluoresced blue. The Eu doped gadolinium oxide nanoparticles were again precipitated out using acetone. The sample was then centrifuged for 15 minutes at 3000 rpm as before. The white suspension dropped to the bottom of the tube and the remaining solution was decanted away. This solution then had more acetone added to it and centrifuged to make sure that no further europium doped gadolinium nanoparticles remained. Once this was confirmed the white samples were washed using acetone 3 more times and centrifuged as before between each washing. The particles were then kept in the dark, in an oven to dry at around 40 °C at standard pressure. This resultant dried powder was then analysed using fluorescence spectroscopy, which was excited between 250, 271.65, 274.36 and 277.32 nm.

3. Silica and Rhodium B-doped nanoparticles

3.1 General introduction

The major aim of this work is to prepare monodisperse nanoparticles using novel and environmentally benign routes. To achieve this, microwave synthetic routes have been employed. This synthesis is also aimed to be cleaner, quicker and a more efficient route to silica nanoparticles compared to some more traditional routes. By varying the reaction temperature and time, it should be possible to identify the conditions for optimum results, be that small particle size or monodispersity. The success of this work will be measured through comparison with other techniques and results. In order to monitor the desired outcome, some of the samples have been analysed weekly to observe particle growth over time. Other samples have been precipitated immediately after synthesis to analyse particles not subject to a further growth phase. Analyses of all silica nanoparticles suspensions were performed on a dynamic light scattering (DLS) system. These measurements provide information regarding the hydrodynamic radius, which is measured in term of the cumulative mean, or Z-average, and the polydispersity index (PdI) of the nanoparticles. The Z-average is the intensity mean, calculated from signal intensity. It is important to remember that the Z-average can be misinterpreted if the particle size dispersity is large, i.e. polydisperse. For this reason, the polydispersity index must be considered in conjunction with the Z-average.

The preparation of all silica nanoparticle samples involved mixing the starting constituents, then heating using microwave irradiation. For one set of samples, aging over several weeks was allowed to occur to monitor particle growth, if any, over time. In order to probe the particles prepared immediately after microwave treatment, a second set of experiments were performed using the same conditions where precipitation of the particles occurred without the additional several weeks aging step. In this case, the particles were centrifuged and dropped out of suspension. Several washing steps were performed to remove any unwanted compounds, such as ammonium hydroxide. This type of post synthesis preparation was necessary for purifying the products before further characterisation using DLS and SEM. For DLS, the precipitated particles were re-suspended in water while for electron microscopy, dried sample was deposited on a carbon disc attached to an alumina stub for further analysis. For use in biological imaging, a hydrodynamic radius of close to

100 nm has been identified as most desirable.[79] A high polydispersity index is indicative of a large variation in the particle size. For an indication of high homogeneity, a PdI of < 0.3 is desirable.[80]

3.2 Results for the Preparation of Silica Nanoparticles

3.2.1 Preparation at 50 °C.

Table 3.1 summarises the DLS results obtained for experiments performed at 50 °C for 0.5 h, 1 h, 2 h and 5 h. Measurements were recorded immediately after synthesis and then monitored on a weekly basis to check for further particle growth over time. By monitoring these samples at regular intervals it is possible to gain an overview of how the particles behaved as they aged. This would show whether the particles grew and the rate at which they did so. It would also be possible to see if the particles agglomerate as time went on, or if they maintained a monodispersive state. Each measurement is repeated three times and the results in Table 3.1 are the averages of these repeat measurements.

Immediately after synthesis, the Z-average is 115 nm for the 0.5 h reaction. A significant increase in mean size to 163.6 nm is observed for the 1 h reaction. Upon increasing the reaction times to 2 h and 5 h, decreases in Z-average to 68.5 nm and 108 nm respectively, are noted. However, these smaller average sizes also display the largest polydispersity values, indicating that particle monodispersity is sacrificed for smaller particle size and that several particle size populations exist. The greater amount of reaction time reduces the supersaturation of particles as nucleation and seed formation has more time to complete reducing agglomeration.[81] Further detailed examination of these results is presented below.

Table 3.1: DLS results obtained for silica nanoparticle growth at 50 °C, recorded over eight weeks. These Figures are taken from averaging the multiple runs performed by the analysis program, and typically show an increase in the mean size (Z-average, nm) for the particles with time and a maximum standard deviation of 2.916 nm and a maximum of 0.036 for PdI measurements.

Sample	**Time**	**Initial**		**Week 1**		**Week 2**		**Week 3**		**Final week**	
	(h)	**Z-ave**	**PdI**	**Z-ave**	**PdI**	**Z-ave**	**PdI**	**Z-ave**	**PdI**	**Z-ave**	**PdI**
(a)	**0.5**	115.0	0.105	127.8	0.178	139.7	0.162	143.2	0.168	166.0	0.170
Standard Deviation		1.054	0.012	2.108	0.014	0.289	0.009	1.044	0.017	0.513	0.0125
(b)	**1**	163.6	0.166	191.5	0.197	188.2	0.192	181.6	0.196	215.5	0.179
Standard Deviation		0.819	0.014	1.375	0.018	0.814	0.005	2.916	0.009	0.265	0.013
(c)	**2**	68.5	0.210	84.5	0.323	113.1	0.271	91.4	0.320	99.9	0.311
Standard Deviation		0.730	0.007	0.835	0.036	0.781	0.011	0.157	0.004	0.907	0.002
(d)	**5**	108.0	0.260	113.5	0.270	113.1	0.270	112.7	0.280	125.2	0.300
Standard Deviation		0.351	0.008	0.808	0.017	0.781	0.011	0.3786	0.007	0.850	0.010

For the reaction carried out at 50 °C for 0.5 h, Figure 3.1 shows the steady growth in mean particle size and polydispersity with the standard deviation for both not rising above 2.108 nm and 0.017 respectively over a 7 week period, together with a plot of the Z-average intensities for the initial (week 0) and final readings (Week 8) for this sample.

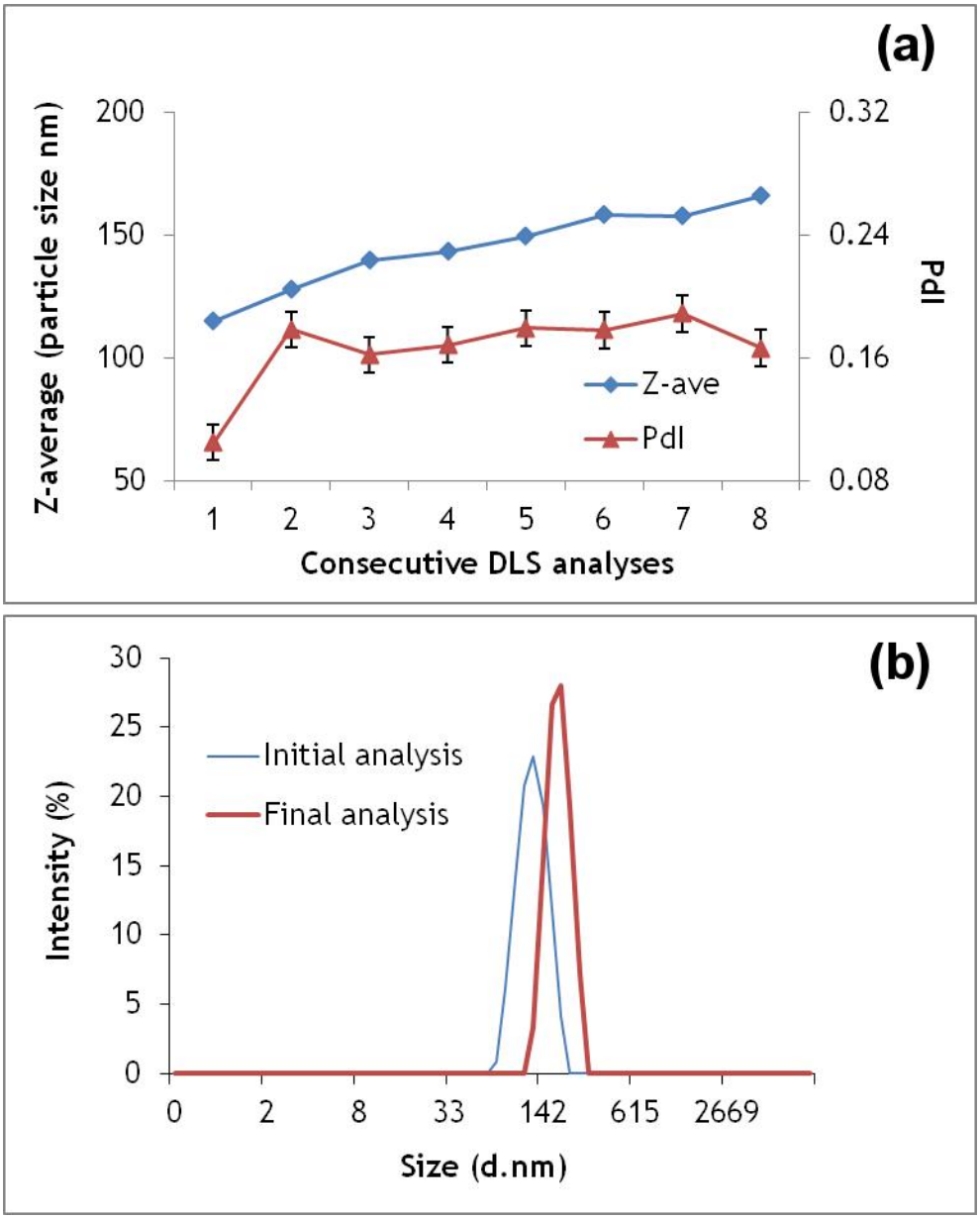

Figure 3.1 (a) Plot of Z-average (blue) and PdI (red) over eight analyses and (b) Z-average plots for silica nanoparticles prepared at 50 °C for 0.5 h, obtained from DLS measurements taken immediately (blue) and after seven weeks (red). Error bars are also included.

Figure 3.1(a) shows that for the reaction carried out at 50 °C for 0.5 h, the Z-average increases at a steady rate. This observed increase is most likely due to the agglomeration of the silica nanoparticles over time. Since the reaction was allowed to proceed for only 30 minutes, it is highly likely that there is some unreacted TEOS still present in the reaction vessel after removal from the microwave reactor. This unreacted TEOS may hydrolyse over time to cause the intergrowth of the nanoparticle assemblies. The polydispersity index of this sample initially increases but then appears to flatten out over time, indicating that while the particle clusters may be increasing in size, over time they become more monodisperse. Spectra for other reaction times are shown in the Appendix.

Figure 3.2 shows a comparison of the first and last analysis of each batch of silica nanoparticles for 1 h, 2 h and 5 h reactions. Studies of the DLS intensity plots for silica nanoparticles prepared at 50 °C for increasing reaction times reveal that, on average, the Z-average decreases as the reaction time increases. However, this is at the expense of the monodispersity of the samples. The PdIs of these samples increase as the reaction time increases which is also noted in the plots in Figure 3.2 where several peaks begin to appear. Intensity plots in DLS are heavily biased by the presence of larger particles, so it is vital to consider the polydispersity indices in conjunction with Z-average measurements. In the case of a 1 h reaction, DLS results indicate a monomodal size distribution with a single peak observed in the intensity plots for the initial and final data collections. An increased PdI value of 0.166 (compared to 0.105 for the 0.5 h reaction) is noted initially and this increases to 0.179 in the final week. Upon increasing the reaction time to 2 h, a smaller particle size is noted (68.5 nm). While small particle size is an aim of this research, careful examination of the intensity plot reveals two peaks, indicating a bimodal population distribution. This is confirmed by the large PdI value (0.210). While the final result shows a disappearance of one of these peaks, the increase in PdI to 0.311 indicates the polydispersity in this sample persists. Increasing reaction times to 5 h also increases the particle polydispersity, with evidence for bimodal particle distributions in the initial and final weeks seen in the appearance of two peaks in the intensity plots. The high PdIs of these samples (0.260 initial, 0.300 final) confirms the lack of monodispersity.

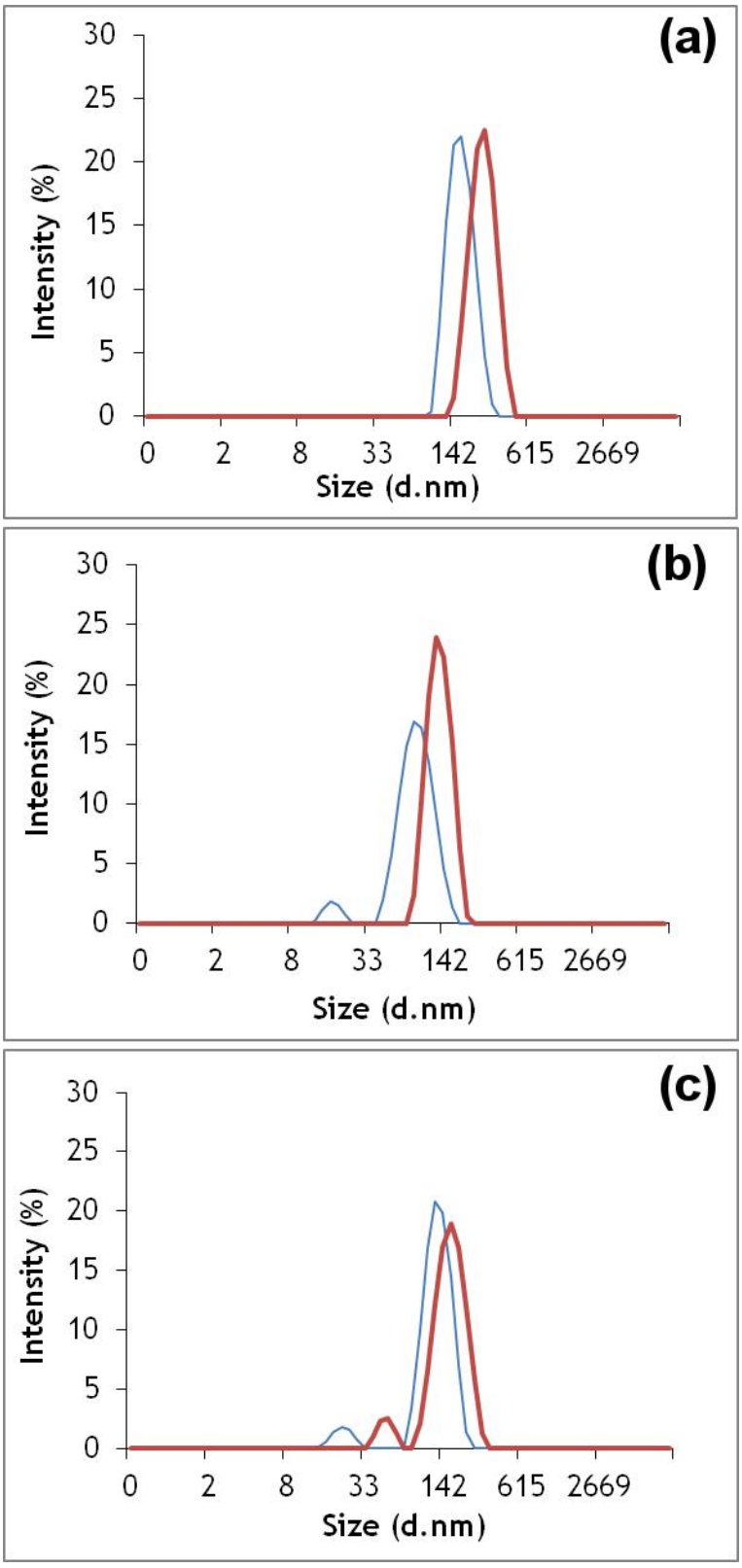

Figure 3.2 DLS intensity plots for silica nanoparticle aqueous dispersions prepared at 50 °C for (a) 1 h, (b) 2 h and (c) 5 h. The multimodal nature of particles prepared at longer reaction times is confirmed by the appearance of several peaks. Blue line is initial analysis and red line is final analysis after 8 weeks.

It is clear from these results that with increasing reaction time comes increasing polydispersity. The best results obtained at 50 °C are the 0.5 h reactions. Leaving this reaction to proceed for several weeks leads to an increase in particle size and polydispersity. In order to combat this, these particles were precipitated immediately after synthesis and studied using DLS and SEM. Particles were also precipitated out for the 1 h, 2 h and 5 h reactions immediately after synthesis for comparison. Figure 3.3 shows IR spectra collected for these dried nanoparticle samples. An absorption peak at 1375 cm^{-1} is observed in all cases. This is due to the presence of Si-O-Si bonds. For samples prepared at higher temperature regimes (75 °C, 85 °C and 100 °C), similar IR spectra were recorded and these are included in the appendices.

Figure 3.3 IR spectra of dried silica nanoparticles prepared at 50 °C for 0.5 h (red), 1 h (purple), 2 h (blue) and 5 h (green).

SEM images collected for the 0.5 h reaction show clearly defined, spherical particles (Figure 3.4(a)). These particles also appear to be the most monodisperse of all samples prepared at 50 °C. For example, Figure 3.4(b) shows for particles prepared at 1 h there are very small particles and larger particles in the range of 0.5 μm and 1 μm present. Similar observations are noted for samples prepared at 2 h (Figure 3.4(c)) and 5 h (Figure 3.4(d)), where smaller particles are observed alongside much larger, micron-sized particles.

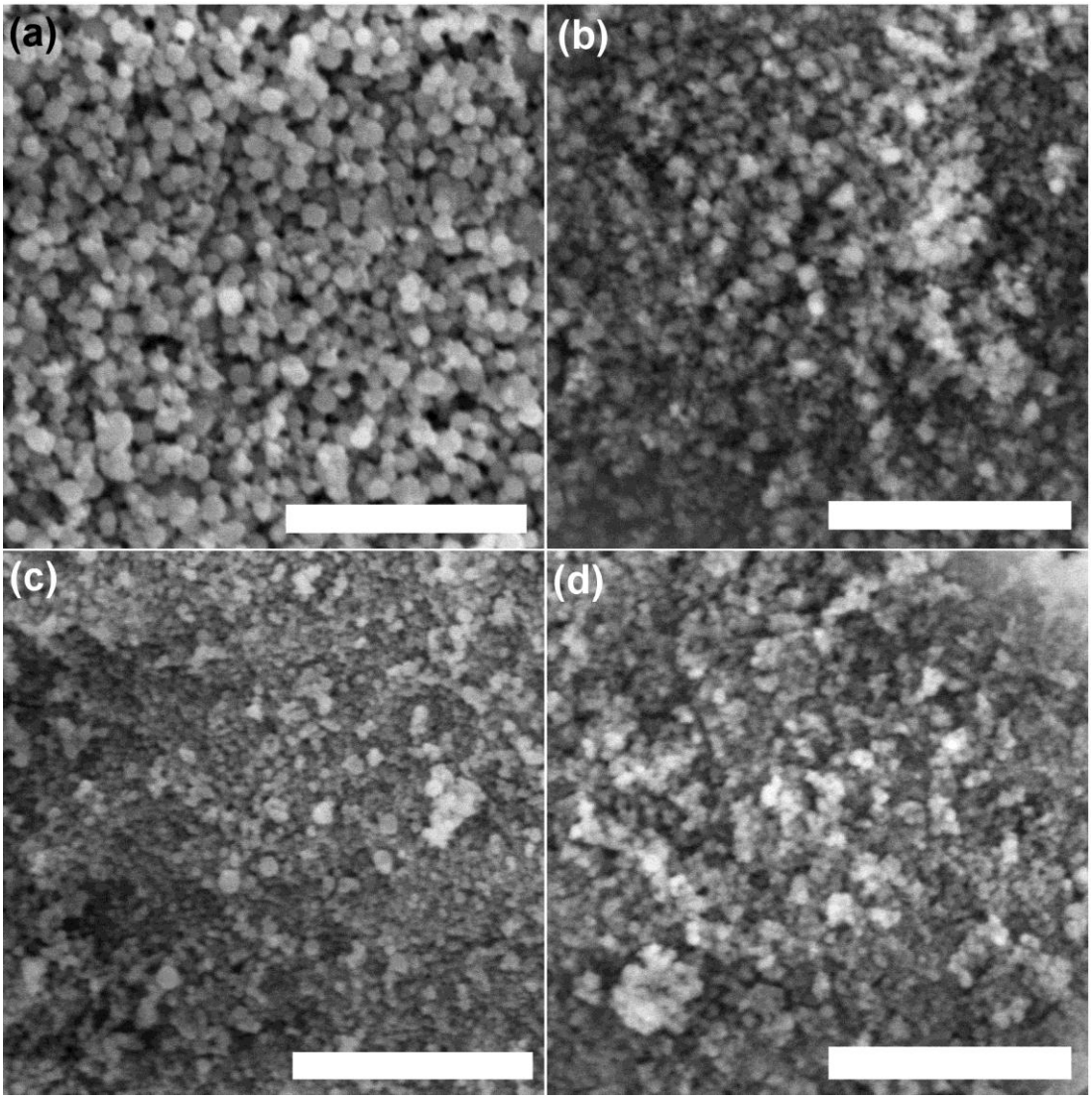

Figure 3.4 SEM images of silica nanoparticles prepared at 50 °C for (a) 0.5 h, (b) 1 h, (c) 2 h and (d) 5 h. The scale bar in each Figure represents 5 μm.

Figure 3.5 shows a histogram of 100 particles of the 0.5 h sample prepared at 50 °C, which is shown in Figure 3.4(a). The average particle size from SEM is 364 nm ± 57 nm. The high deviation, given by the measurements taken on the SEM, is due to the polydispersity present in the sample. In order to fully investigate the influence of time and temperature over resulting particle size, the same reactions were carried out at 75 °C, 85 °C and 100 °C. These results are presented below.

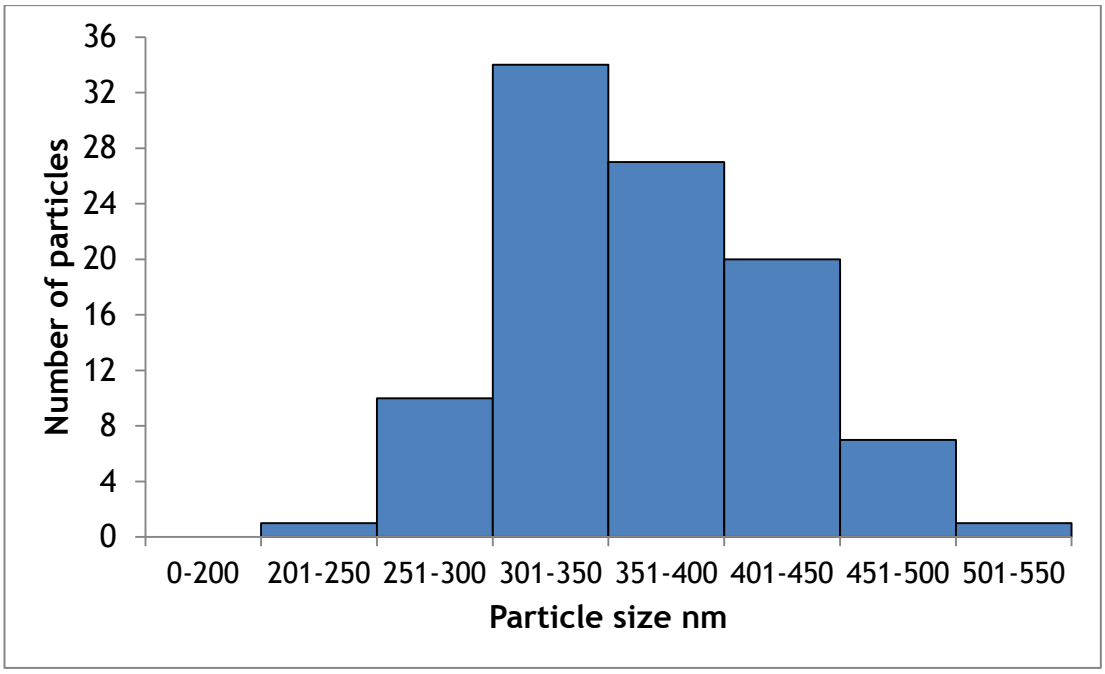

Figure 3.5 A histogram showing the range of particle sizes in Figure 3.4(a) for the sample prepared at 50 °C for 0.5 h. This shows how the majority of particles are between 301 nm and 350 nm. There are no particles found above 550 nm and none lower than 201 nm.

3.2.2 Preparation at 75 °C.

The preparation of silica nanoparticles at 75 °C has been carried out using the same method detailed above. Analysis was performed in a similar manner to monitor particle growth over several weeks and to check precipitated particles immediately after microwave treatment. The initial DLS measurements show the 0.5 h reaction has a Z-average of 89 nm. There is a decrease in these values for 1 h and 2 h to 75.8 nm and 49.5 nm respectively. The 5 h reaction gives the highest initial Z-average of 120.3 nm, but the lowest initial PdI of 0.222. Although the smallest Z-average is shown by the 2 h reaction, this sample also displays the largest polydispersity. All results obtained are shown in Table 3.2 below.

Table 3.2: DLS results obtained for silica nanoparticle growth at 75 °C, recorded over seven weeks. These are taken from averaging the multiple runs performed by the analysis program, and typically show an increase in the Z-average (nm) for the particles with time and a maximum standard deviation of 1.793 nm.

Sample	**Time**	**Initial**		**Week 1**		**Week 2**		**Week 3**		**Final week**	
	(h)	**Z-ave**	**PdI**	**Z-ave**	**PdI**	**Z-ave**	**PdI**	**Z-ave**	**PdI**	**Z-ave**	**PdI**
(e)	**0.5**	89.0	0.290	88.4	0.532	86.0	0.544	94.3	0.499	123.5	0.517
Standard Deviation		0.900	0.017	0.326	0.011	0.696	0.005	0.219	0.010	0.625	0.003
(f)	**1**	75.8	0.287	74.5	0.430	69.8	0.500	72.7	0.467	72.1	0.503
Standard Deviation		0.759	0.017	2.044	0.059	0.860	0.034	0.652	0.003	1.171	0.025
(g)	**2**	49.5	0.539	48.2	0.526	47.9	0.515	46.7	0.512	47.8	0.537
Standard Deviation		0.595	0.004	0.172	0.009	0.085	0.002	0.271	0.006	0.364	0.008
(h)	**5**	120.3	0.222	121.1	0.284	134.5	0.288	122.6	0.285	121.4	0.284
Standard Deviation		0.458	0.007	1.387	0.006	0.361	0.006	1.793	0.001	0.265	0.003

Figure 3.6 shows that for the synthesis performed at 75 °C for 0.5 h, a steady increase in Z-average is noted with a maximum standard deviation of 0.900 nm, along with a sharp increase followed by slight fluctuations in polydispersity showing a maximum standard deviation of 0.017 over a five week period. This increase in polydispersity manifests itself in the initial and final plot intensities of Z-average which reveal the emergence of a second peak.

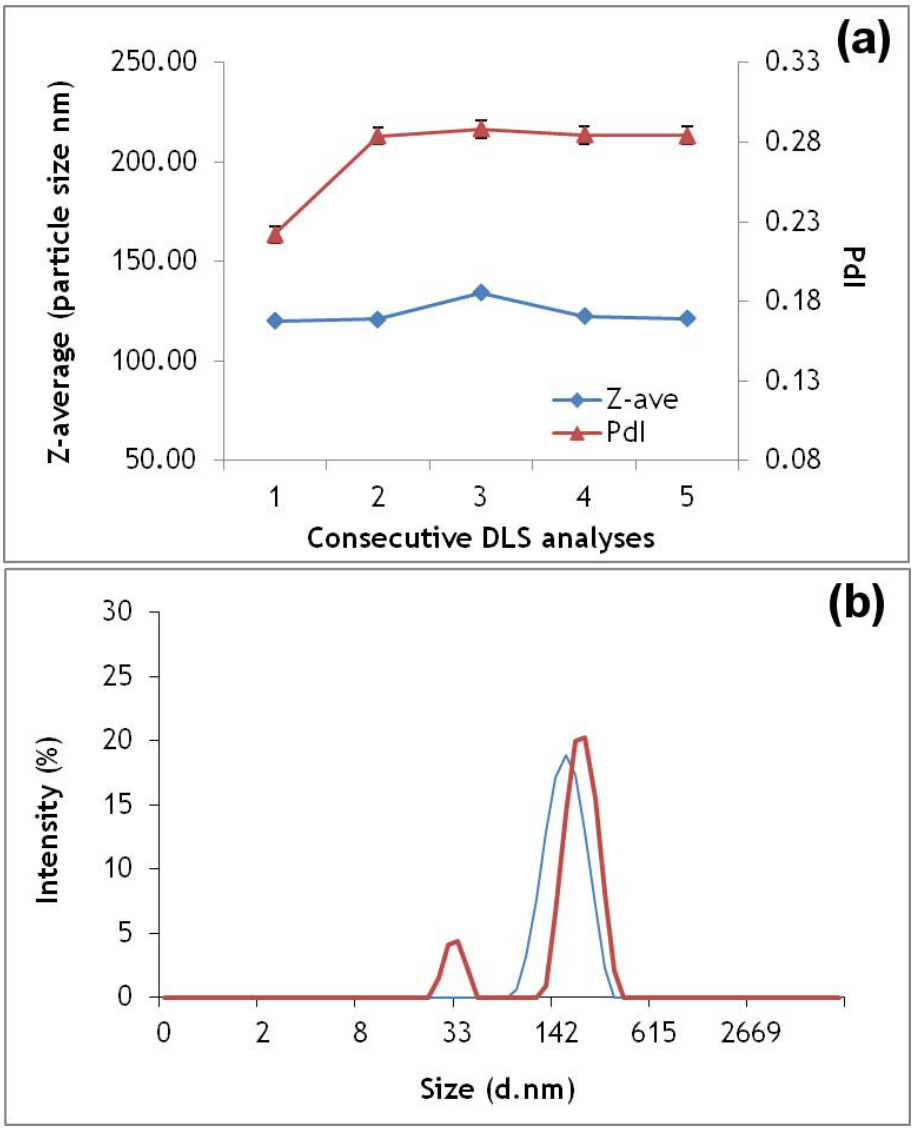

Figure 3.6 (a) Plot of Z-average (blue) and PdI (red) over five analyses. These readings were taken immediately after synthesis and then each week for four weeks. Error bars are also included. (b) Z-average particle size distribution for silica nanoparticles prepared at 75 °C for 0.5 h, obtained from DLS measurements. Blue line is initial analysis and red line is final analysis after five weeks.

As shown in Figure 3.6(a), for the reaction carried out at 75 °C for 0.5 h the Z-averages remain steady until week four where the average particle size begins to increase. This overall increase could be due to the particles aggregating as they age. The short reaction time could again result in the presence of some unreacted TEOS in the reaction mixture after synthesis. However, it is likely there is less unreacted TEOS than in the 50 °C, 0.5 h reaction since subsequent large changes in particle sizes over time which had been observed in that case are not seen here. The polydispersity of this sample has a large initial increase which then steadies off, fluctuating around a value of 0.5. This indicates that as the particles age, several size populations emerge. This could also be an indication of particle agglomeration over time, which is also seen in Figure 3.6(b) where the final DLS Z-average plot of this sample shows two peaks.

Figure 3.7 shows the DLS plots of the initial and final measurements observed for the particle preparations at 75 °C for 1 h, 2 h and 5 h. For the 1 h reaction, the polydispersity increases over time, going from 0.287 initially to 0.503 in the final week of analysis. The 1 h plot (Figure 3.7(a)) is bimodal after initial analysis, with an addition peak seen after the final analysis. As the reaction time increases from 1 h to 2 h, the initial Z-average decreases. The small particle sizes achieved here (49.5 nm) are highly desirable, however there is a doubling in the PdI values (from 0.287 to 0.539), corroborated by the bimodal and multimodal nature of the plots. Although the 5 h reaction gives the largest Z-average, it also displays the lowest PdIs, with a single peak present in the DLS plot after final analysis (Figure 3.7(c)).

It is clear from these results that this reaction temperature results in a high polydispersity for 0.5 h, 1 h and 2 h, which reduces for the 5 h reaction. The best results obtained at 75 °C are the 5 h reactions. Ageing this sample does not cause the average particle size or polydispersity to change greatly, with only a small increase noted. In order to further study these particles before the several week growth period, all reactions were repeated and the particles precipitated out directly after synthesis and studied using IR, DLS and SEM. The IR spectra for these samples are in the Appendices and show similar features at 1375 cm^{-1} for Si-O-Si bonds as noted for the 50 °C preparations.

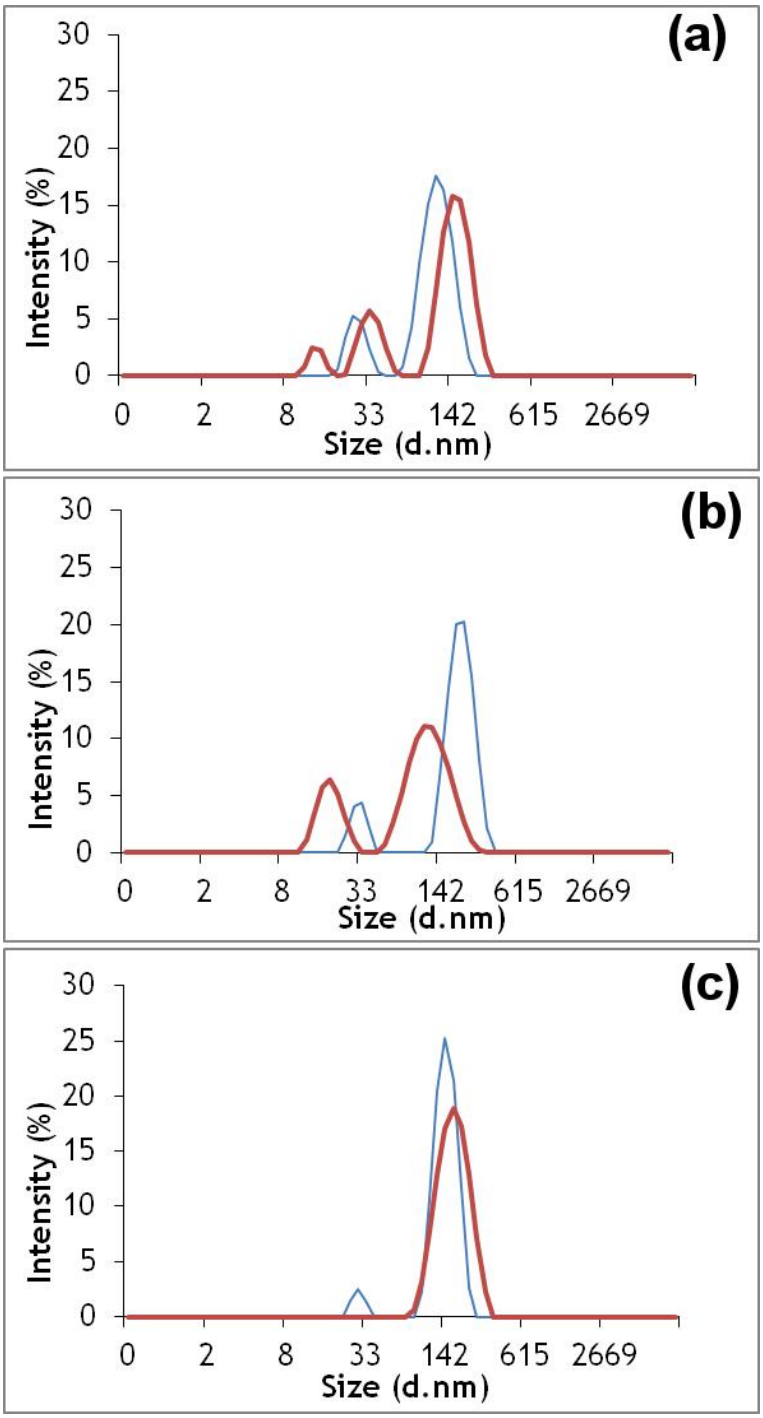

Figure 3.7 DLS Z-average intensity plots for silica nanoparticle samples, prepared at 75 °C for (a) 1 h, (b) 2 h and (c) 5 h. Initial plots are shown in blue, with final plots in red.

SEM images collected for the 5 h reaction show very small but defined, mostly round particles (Figure 3.8(d)). These particles appear to be the most monodisperse of all samples prepared at 75 °C. For example, Figure 3.8(a) shows particles

prepared at 0.5 h have a mixture of larger particles more 0.5 μm and variety of very small particles. These observations are consistent with DLS observations for samples prepared at 1 h (Figure 3.8(b)) and 2 h (Figure 3.8(c)). However, the 2 h synthesis also has a large amount of agglomeration, which can make identifying an accurate particle size difficult.

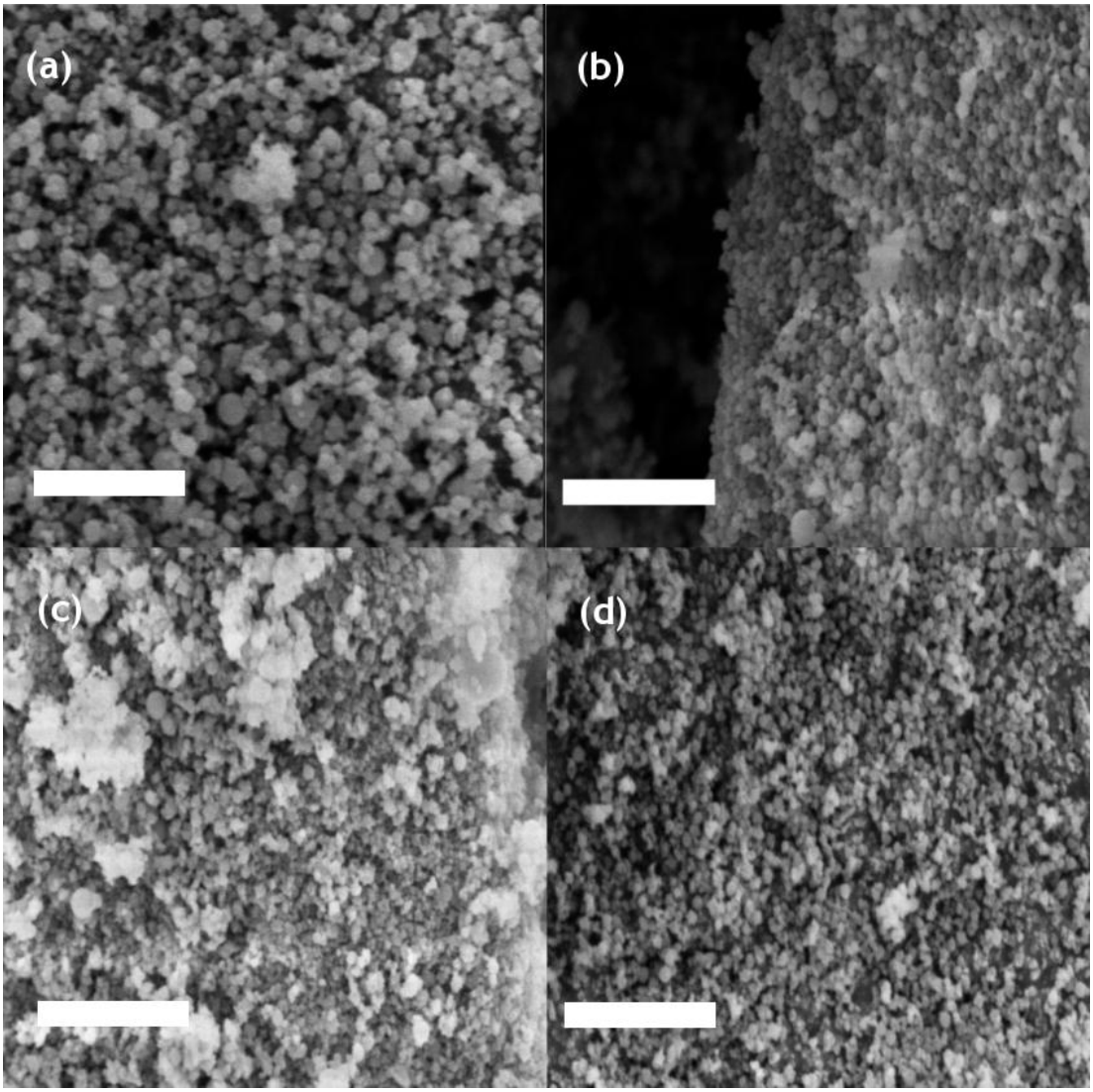

Figure 3.8 SEM images of silica nanoparticles captured at a magnification of 7K. The images show how particle size and shape change as reaction length is increased; (a) 0.5 h, (b) 1 h, (c) 2 h and (d) 5 h. The scale bar in each image is 5 μm.

3.2.3 Preparation at 85 °C.

Silica nanoparticles were prepared in a similar manner at 85 °C, with analysis performed on samples monitored over several weeks and also on dried samples of

immediately precipitated particles. The initial DLS measurements taken show the 0.5 h synthesis has a Z-average of 63.9 nm. There is an increase for 1 h to 66.5 nm and a decrease to 41.4 nm and 60.5 nm for 2 h and 5 h respectively. The largest polydispersity is once again shown by the particles with the smallest Z-average size. Table 3.3 below summarises these observations. For the synthesis performed at 85 °C for 0.5 h, Figure 3.9 shows the steady growth in mean particle size and polydispersity over a five week period, along with initial and final intensity plots.

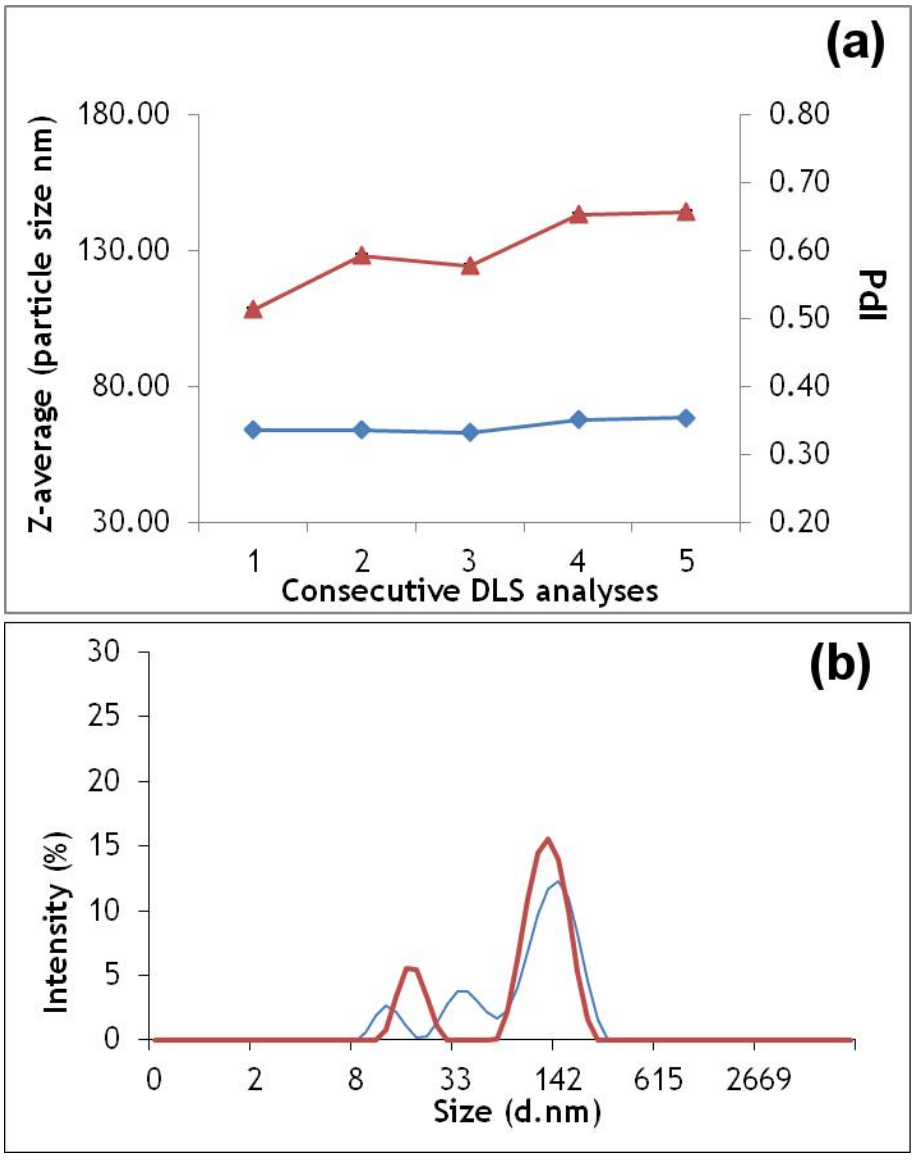

Figure 3.9 (a) Plot of Z-average (blue) and PdI (red) over five analyses. Error bars are included. (b) Z-averages for silica nanoparticles synthesised at 85 °C for 0.5 h, obtained from DLS measurements taken initially (blue) and after 5 weeks (red).

Table 3.3: DLS results obtained for silica nanoparticle growth at 85 °C over four weeks. These Figures are taken from averaging the multiple runs performed by the analysis program. These Figures show a general trend in decreasing the z-average for the particles with time and a standard deviation maximum of 1.565 nm, with a wide distribution in PdI.

Sample	**Time**	**Initial**		**Week 1**		**Week 2**		**Week 3**		**Final week**	
	(hr)	**Z-ave**	**PdI**	**Z-ave**	**PdI**	**Z-ave**	**PdI**	**Z-ave**	**PdI**	**Z-ave**	**PdI**
(i)	**0.5**	63.9	0.514	63.9	0.593	62.9	0.578	67.7	0.654	68.4	0.657
Standard Deviation		0.408	0.004	0.444	0.002	0.249	0.006	0.375	0.004	0.260	0.003
(j)	**1**	66.5	0.478	62.2	0.554	62.7	0.557	73.7	0.612	73.5	0.644
Standard Deviation		1.565	0.025	0.070	0.001	0.406	0.008	0.456	0.007	0.411	0.004
(k)	**2**	41.4	0.632	42.1	0.895	38.2	0.609	38.2	0.587	37.8	0.617
Standard Deviation		0.901	0.040	4.462	0.182	0.306	0.003	0.087	0.005	0.280	0.006
(l)	**5**	60.5	0.580	50.1	0.592	50.4	0.596	47.9	1.000	50.5	1.000
Standard Deviation		1.338	0.030	0.339	0.024	0.125	0.004	0.307	0.000	0.186	0.000

Figure 3.10 shows DLS plots for all other silica nanoparticles prepared at 85 °C for 1 h, 2 h and 5 h. For the 1 h and 2 h reactions, the polydispersity increases over time, with additional peaks in the Z-average intensities noted indicating a number of particle populations exist. Although the Z-average values are low for all samples prepared at this temperature (< 100 nm) with standard deviations not going above 4.462 nm and a minimum of 0.070 nm, the high degree of polydispersity observed is highly undesirable even with such low standard deviations observed for all. The 1 h plot is bimodal after initial analysis and then a third peak appears after final analysis. The polydispersity of the 1 h run, at 0.478, is slightly smaller than that of the 0.5 h reaction (0.514). The observed increase in polydispersity from additional peaks in the Z-average plots is in agreement with the final PdI measurements for the 1 h and 2 h reactions, at 0.644 and 0.617 respectively.

The 5 h plot shows a large change in polydispersity. The PdI of 1.000 for the final DLS measurement of the 5 h reaction indicates that polydispersity is too high to measure accurately. It is clear from these results that this reaction temperature results in a high polydispersity for all reaction times, which is especially high for the 5 h case. The most consistent results obtained at 85 °C are from the 2 h reactions. Although there was a large increase in polydispersity after 1 week, this did not continue and decreased below the original PdI to result in 0.617. This is not as low as previous, lower temperature reactions; however this does indicate that as the sample aged it reduced slightly in both PdI and Z-average.

To prevent any continued growth or increase in polydispersity of the samples, the second batch of silica nanoparticles were precipitated out immediately post synthesis. These precipitated samples are then analysed using IR, DLS and SEM. All IR spectra are included in the appendices and show similar results as observed in the 50 °C and 75 °C cases.

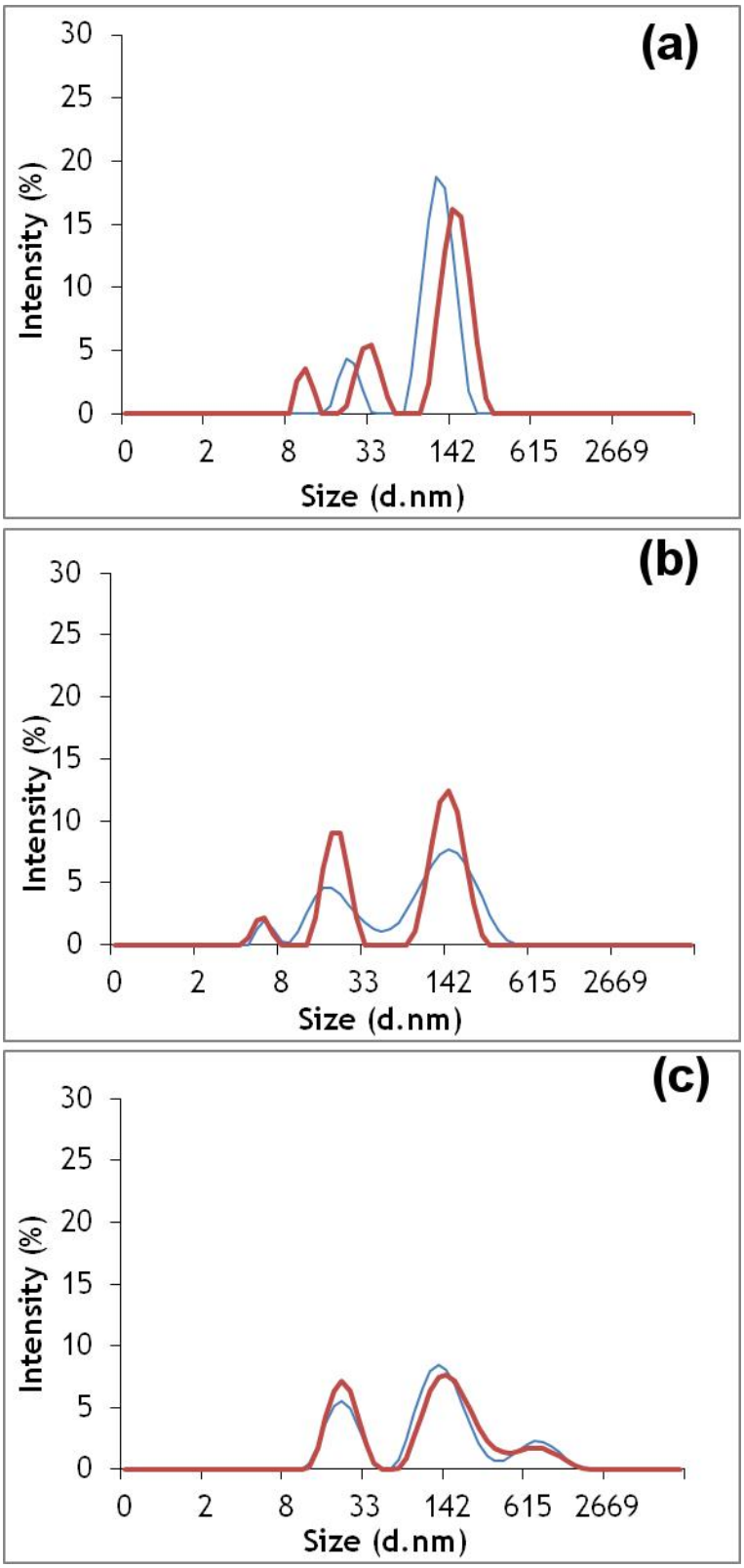

Figure 3.10 DLS intensity plots for silica nanoparticle samples, prepared at 85 °C for (a) 1 h, (b) 2 h and (c) 5 h. The particles display multimodal peak shapes, indicating a high degree of polydispersity. The initial measurement in plotted in blue, with the final measurement shown in red.

SEM images for samples prepared at 85 °C are shown in Figure 3.11. All samples appear polydisperse, with a range of particle sizes observed. The most monodisperse sample appears to be the 1 h sample (Figure 3.11(b)). The 0.5 h reaction shows a number of well-defined, spherical particles. However, there is also a high degree of agglomeration (Figure 3.10(a)). Similar observations can be seen for samples prepared at 2 h (Figure 3.10(c)) and 5 h (Figure 3.10(d)), where smaller particles are observed alongside a few, much larger, particles. The larger particles observed in these samples are from 0.5 μm to 1 μm.

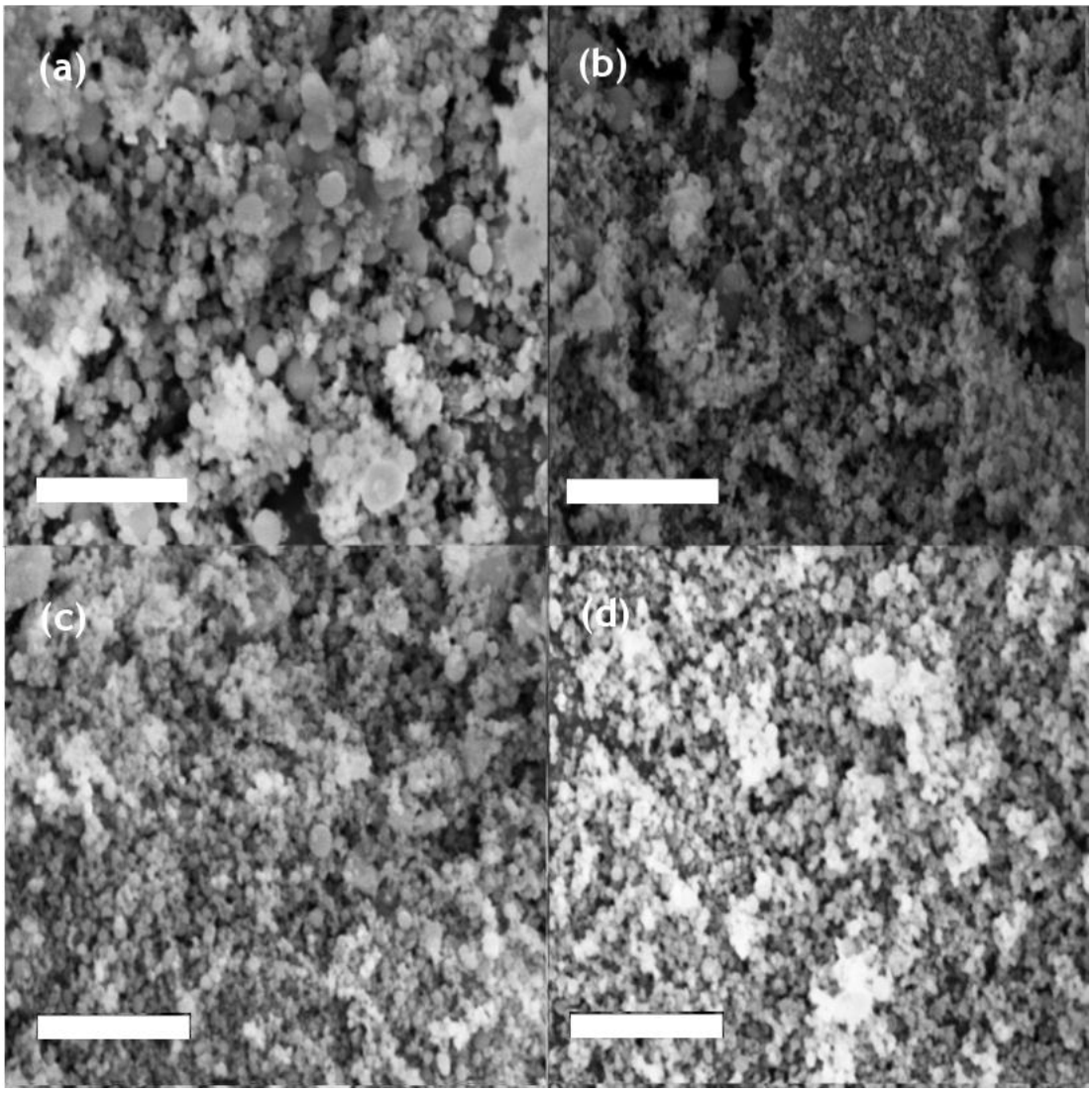

Figure 3.11 SEM images of silica nanoparticles prepared at 85 °C for (a) 0.5 h, (b) 1 h, (c) 2 h and (d) 5 h. The scale bar shown is 5 μm.

3.2.4 Preparation at 100 °C.

Silica particles were prepared in the same manner at 100 °C for 0.5 h, 1 h, 2 h and 5 h. DLS measurements were taken immediately after synthesis and for several weeks after and these results are presented in Table 3.4 below. It shows that the 0.5 h synthesis has an initial Z-average of 77.8 nm. The 1 h and 5 h synthesis have smaller z-averages at 60.9 nm and 64 nm respectively. However the 2 h synthesis has a significantly larger z-average at 180.6 nm. The largest polydispersities are displayed by the particles with the smallest Z-averages. For the 1 h reaction, an initial PdI of 0.627 is seen which does not appreciably decrease over time. Monodispersity is once again shown to be lost with smaller Z-averages.

In the synthesis of silica nanoparticles at 100 °C for 0.5 h, Figure 3.12 shows consistency in Z-average, with a slightly fluctuating polydispersity over a 4 week period, as well as a plot of the intensities showing the initial and final readings for this sample.

As shown in Figure 3.12(a), there is little change in the Z-average over time for the sample prepared at 100 °C for 0.5 h (from 77.8 nm to 77.5 nm). This shows great consistency over time. This indicates that although the reaction time is short, there is likely no unreacted TEOS present in the reaction vessel after removal from the microwave reactor. The PdI of this sample is 0.338 initially, and like the z-average fluctuates a little but returns to a similar value after 4 weeks at 0.333. Such little changes over time also indicate that there is little growth between clusters over time and no appreciable aggregation. Samples prepared at lower temperatures for 0.5 h have shown an increase of PdI over time, highlighting that more growth may have taken place. However the lack of a large change after 4 weeks could again be a result of the increased temperature causing the particles to reach complete growth.

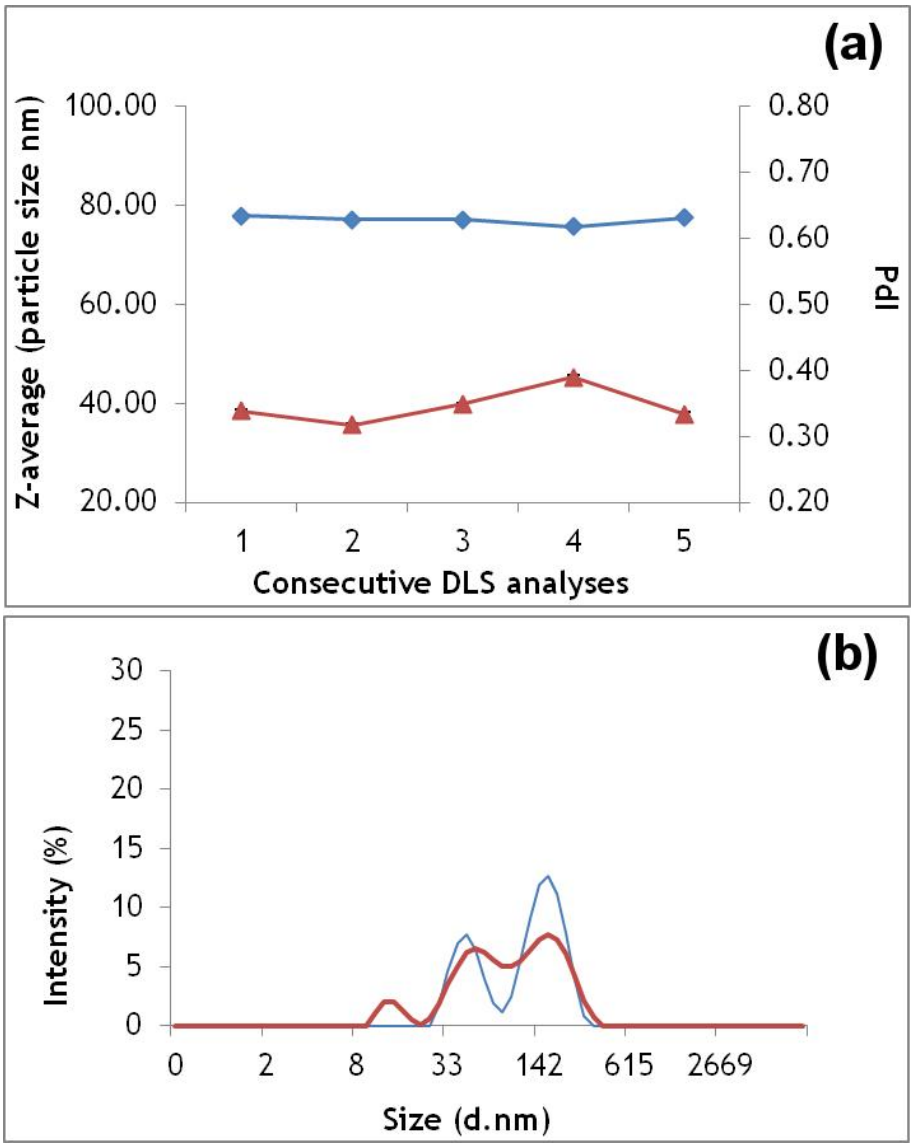

Figure 3.12 (a) Plot of Z-average (red) and PdI (blue) of readings taken immediately after synthesis and then weekly for five weeks. Error bars are included. (b) A graph of intensity against average particle size, showing the distribution of those sizes for silica nanoparticles prepared at 100 °C for 0.5 h, obtained from DLS measurements. The initial value is plotted in blue, with the final observation in red.

Table 3.4: DLS results obtained for silica nanoparticle growth at 100 °C, over four weeks. These are taken from averaging the multiple runs performed by the analysis program. On average, the hydrodynamic radii (nm) and PdI do not change significantly for each sample and show a maximum standard deviation for particle size of 1.099 nm.

Sample	**Time**	**Initial**		**Week 1**		**Week 2**		**Week 3**		**Final week**	
	(hr)	**Z-ave**	**PdI**	**Z-ave**	**PdI**	**Z-ave**	**PdI**	**Z-ave**	**PdI**	**Z-ave**	**PdI**
(i)	**0.5**	77.8	0.338	77.0	0.317	77.0	0.348	75.6	0.389	77.5	0.333
Standard Deviation		0.880	0.003	1.034	0.005	1.099	0.053	0.751	0.003	0.879	0.003
(j)	**1**	60.9	0.627	61.3	0.626	61.12	0.635	73.1	0.684	71.2	0.664
Standard Deviation		0.537	0.008	0.557	0.005	0.348	0.006	0.421	0.003	0.412	0.006
(k)	**2**	180.6	0.130	179.2	0.153	184.4	0.142	186.1	0.130	191.7	0.183
Standard Deviation		0.430	0.004	0.404	0.003	0.597	0.003	0.384	0.009	0.693	0.009
(l)	**5**	64.0	0.480	64.6	0.472	64.8	0.472	67.4	0.278	69.3	0.310
Standard Deviation		0.064	0.005	0.339	0.008	0.060	0.005	0.220	0.006	0.394	0.004

Figure 3.13 below shows the DLS plots of the initial and final readings taken for the 1 h, 2 h and 5 h samples of silica nanoparticles. For the 1 h reaction, the PdI increases from an initial value of 0.627 to 0.664 with minor fluctuations in the measurements in between, with a maximum standard deviation of 0.008. This pattern of a slight increase is also seen with the 2 h reaction time, but with much lower PdI values this time (going from 0.130 to 0.183). For the 5 h preparation, there is an overall decrease in the PdI from initial 0.480 to final 0.310. There is an overall trend of Z-average increase with time, but these are modest and standard deviation has a maximum of 1.034 nm and a minimum of 0.060 nm. Figure 3.13(a) shows that for the 1 h sample, the appearance of another peak in the final analysis supports the high PdI documented in the Table 3.4 above. The 2 h and 5 h plots do not show the presence of any additional peaks and are bimodal in both initial and final analysis. The smaller average particle sizes are more desirable as highlighted previously, however the smaller the z-average the larger the PdI. The 2 h sample has the largest average particle size but conversely has the lowest PdI.

The DLS characterisation for the samples prepared at 100 °C indicates that growth has finished. While lower temperatures showed a change in PdI from initial to final analyses, this temperature shows very little change. There is a degree of polydispersity in all samples. The best results achieved at 100 °C were in the 2 h reaction. While this sample afforded silica nanoparticles at a higher average particle size, initially at 180.6 nm, increasing to 191.7 nm after 4 weeks, the lowest PdI was maintained throughout. Ageing of the samples prepared at this temperature did not appear to affect a great change in polydispersity or average particle size. Additional experiments to obtain precipitated particles were also conducted for the 100 °C reactions. IR spectra are shown in the appendix, with similar Si-O-Si stretches observed as in the case of other reactions.

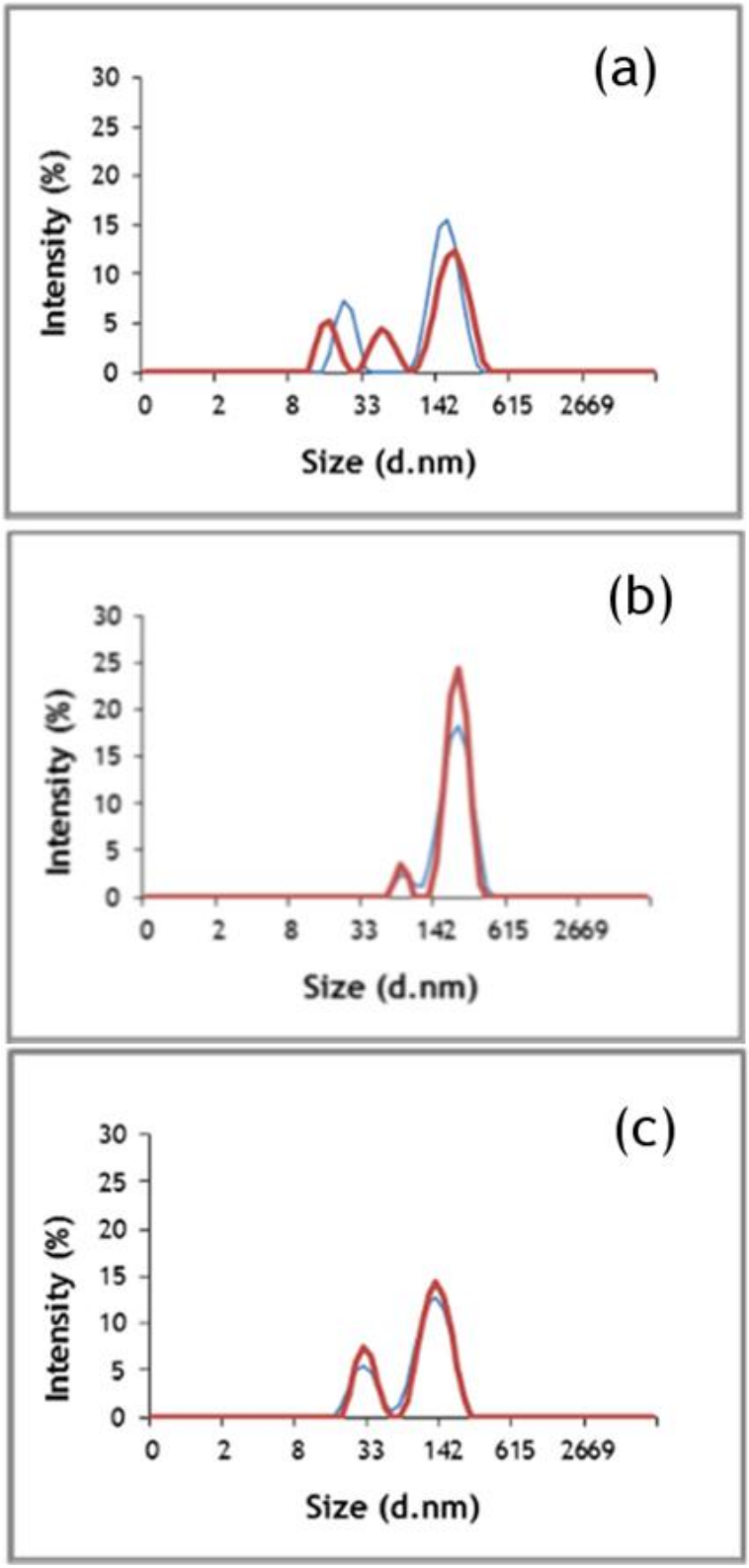

Figure 3.13 DLS Z-average intensity plots for silica nanoparticle samples prepared at 100 °C for (a) 1 h, (b) 2 h and (c) 5 h. The particles are shown to be mostly bimodal with a multimodal plot shown in the final analysis of (a). The initial plots are shown in blue, with the final plots in red.

SEM images are given in Figure 3.14 for the silica nanoparticles prepared at 100 °C. All the images below show very small nanoparticles that are highly agglomerated. The sample that can be seen to have a greater monodispersity is the 2 h reaction (Figure 3.13(c)). The nanoparticles appear to be spherical. Larger particles are also present for the samples prepared at 0.5 h, 1 h and 5 h. For example Figure 3.13(b) shows some larger particles between 0.5 μm and 1 μm, which are no longer spherical.

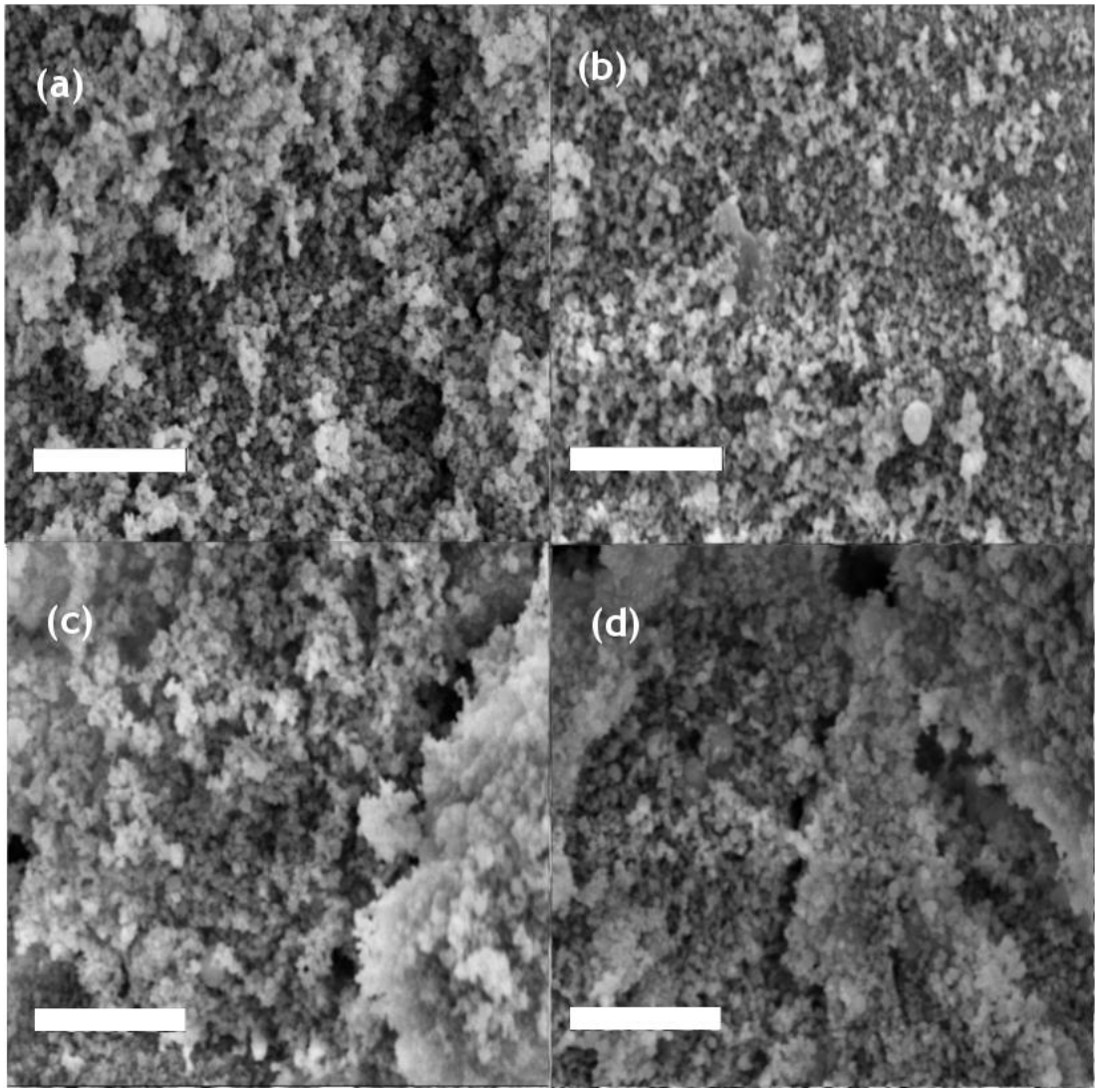

Figure 3.14 SEM images of silica nanoparticles prepared at 100 °C at (a) 0.5 h, (b) 1 h, (c) 2 h and (d) 5 h. There is a high degree of agglomeration noted for these samples. The scale bar in each image is 5 μm.

3.3 Discussion on Silica Nanoparticles

The schematic shown in Figure 3.15 demonstrates how the base catalysed hydrolysis of the silica precursor proceeds to form silica nanoparticles. The microwave method employed above is a modified Stöber synthesis. The original paper reports spherical nanoparticles between 0.05 μm and 2 μm in diameter.[82] The particles prepared in the current work are typically between 30 and 260 nm and are similarly spherical in shape.

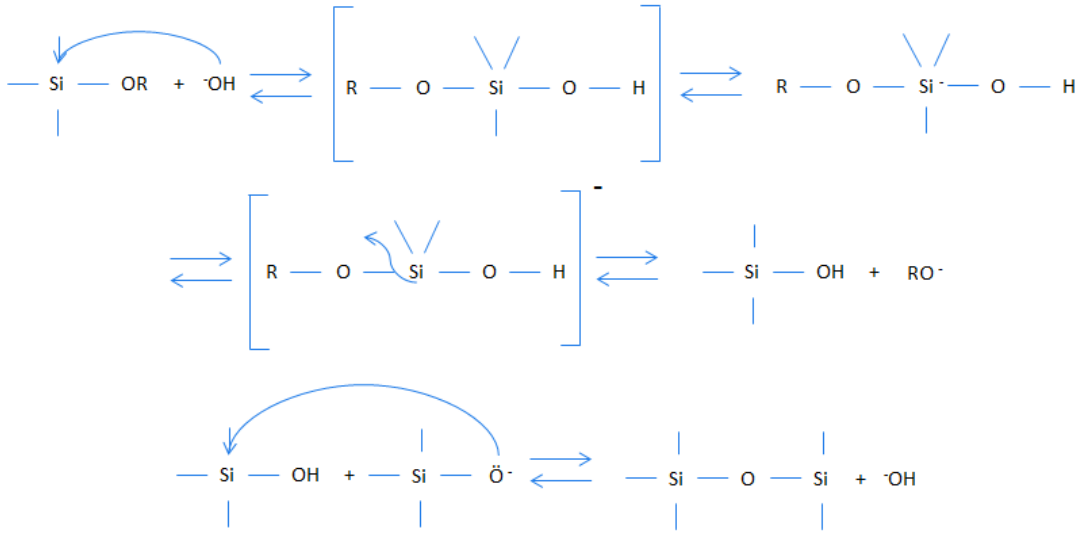

Figure 3.15 Reaction mechanism for the formation of SiO_2 nanoparticles using a base-catalysed condensation of TEOS.[83]

Davies *et al.* documented a synthesis, using TEOS, ammonia, ethanol and water similar to the above synthesis, however with thirteen variations of component volumes. The range of nanoparticle sizes from the synthesis performed by Davies *et al*. is slightly wider, between 32 nm and 262 nm, than the range found by the results detailed here. However the PdI of the reported samples is lower, between 0.072 and 0.206, than the results here.[84]

For microemulsion synthesis, there have been reported variations in particle size and morphology.[85] There have also been smaller particles reported using a two-step hydrolysis and condensation reaction, but non-spherical particles are noted.[86] These particles also display a high polydispersity and reaction times of three days are

required. The reactions here are much shorter for similar particle sizes and low polydispersities (0.5 h, 50 °C).

3.4 Results and discussion of Rhodamine B-labelled silica nanoparticles

The dried particles were re-suspended in ethanol before DLS analysis. The results are shown in Table 3.5 and Figure 3.16. Table 3.5 compares the results obtained for pure SiO_2 nanoparticles and Rhodamine B-doped SiO_2 nanoparticles. Three measurements of each sample were taken. It can be seen that the Z-average remains consistent for the plain silica nanoparticles, with a maximum of 116.1 nm and a minimum of 114 nm. The plain sample also shows a low PdI for all measurements, with an average of 0.105. In contrast, the Rhodamine B-doped sample shows a large amount of variation with a maximum Z-average of 1112.0 nm and a minimum of 772.6 nm, with a much higher average PdI of 0.714.

Table 3.5 DLS results obtained immediately post synthesis for plain silica nanoparticles and Rhodamine B-doped silica nanoparticles at 50 °C for 0.5 h. These figures show each analysis taken during the overall run and then an average of these runs.

Sample	**Measurement 1**		**Measurement 2**		**Measurement 3**		**Average**	
	Z-ave	**PdI**	**Z-ave**	**PdI**	**Z-ave**	**PdI**	**Z-ave**	**PdI**
(a)	116.1	0.118	114.9	0.095	114.0	0.101	115.0	0.105
(b)	1112.0	0.764	898.4	0.757	772.6	0.620	927.7	0.714

DLS plots are shown in Figure 3.16 and show the initial DLS measurements observed for both the plain silica nanoparticles (a) and Rhodamine B-doped silica nanoparticles (b), which were both prepared at 50 °C for 0.5 h.

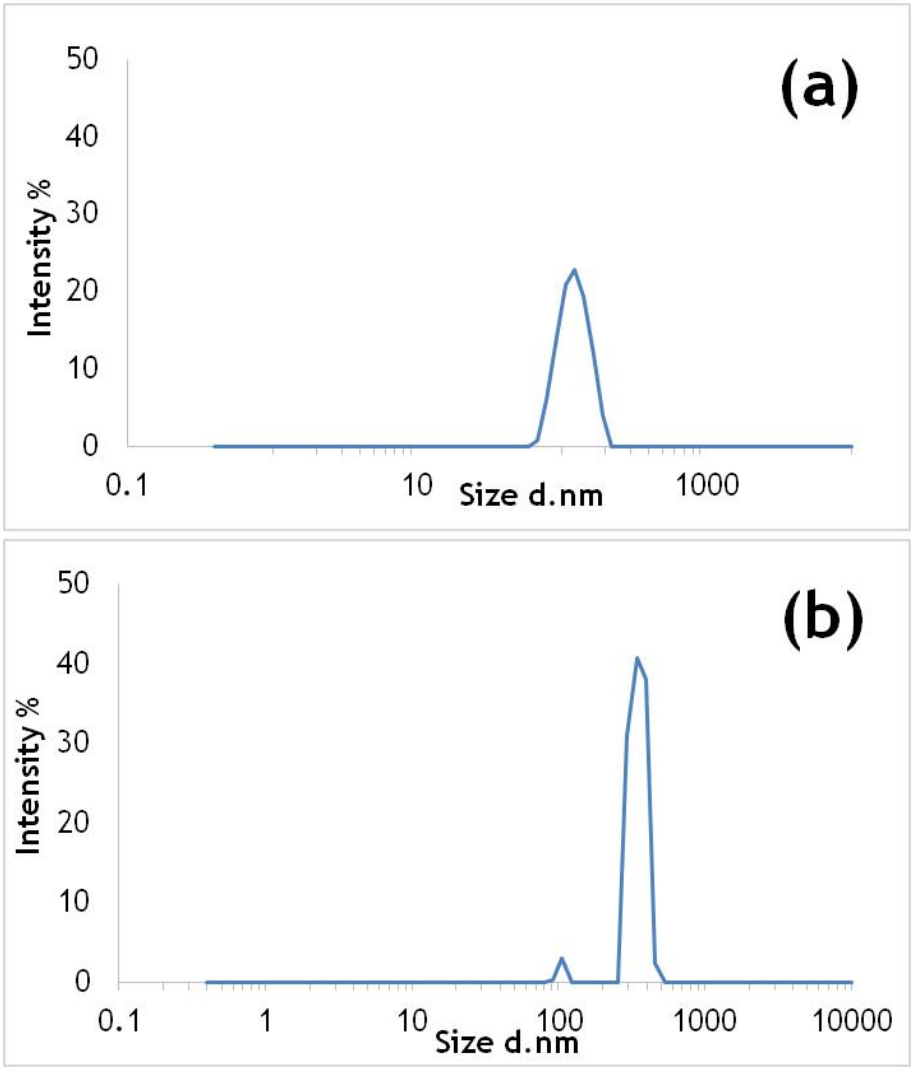

Figure 3.16 DLS intensity plots for the initial analysis of samples immediately post synthesis, prepared at 50 °C for 0.5 h. (a) Plain silica nanoparticles display monomodal behaviour, while (b) Rhodamine B doped silica nanoparticles appear bimodal.

A single peak is noted for the plain silica sample, indicating high monodispersity for this sample. In contrast, the Rhodamine B-doped sample has a much larger size and two peaks, suggesting a polydisperse sample. The Rhodamine B sample also has an unusual shaped peak which reiterates its polydispersivity. The addition of Rhodamine B (Figure 3.17) to the silica nanoparticles may increase electrostatic interactions between neighbouring molecules and particles, which might explain the large increase in Z-average.

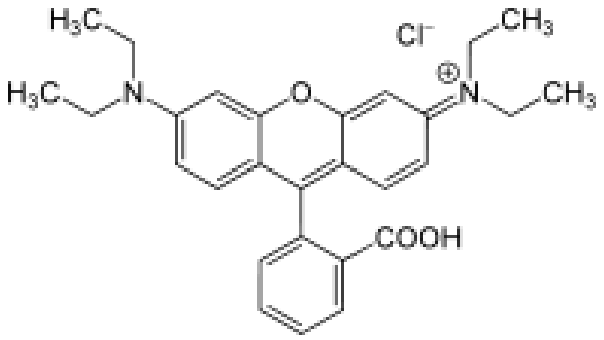

Figure 3.17 Structure of Rhodamine B, which was used to functionalise silica nanoparticles.

The samples were re-suspended in ethanol and subjected to UV irradiation to determine whether the presence of Rhodamine B has bestowed fluorescence properties on these particles. Photographs of the samples are shown in Figure 3.18 and confirm fluorescence in these samples, compared to pure SiO_2 particles. These samples were kept in the dark and the photographs shown in Figure 3.18 were taken two months after initial synthesis. The strong fluorescence still noted for these samples indicates a lack of photodegradation over time.

Silica nanoparticles are able to shield the dye from external oxygen. [87] This shielding is the reason for the extended photostability seen in images in Figure 3.18. The lack of photodegradation after two months means that these samples could be synthesised and stored for use at a later date. The photostability present in the silica doped samples means that bio imaging is a possible application and therefore bioanalysis can be investigated over time.

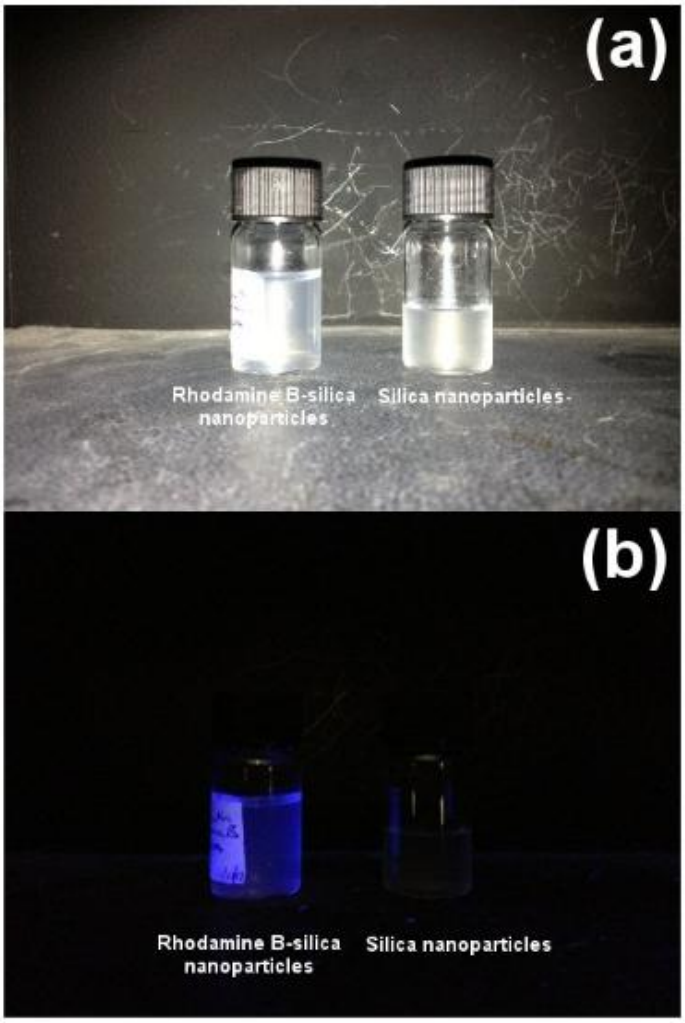

Figure 3.18 Photographs of plain silica nanoparticles and Rhodamine B-silica nanoparticles, suspended in ethanol. (a) Both samples in visible light, (b) samples subjected to UV light at 365 nm, showing the doped sample fluorescing.

4. Gadolinium Oxide and Europium-doped Gadolinium Oxide Nanoparticles

4.1 Results and discussion of Gd_2O_3 and Eu:Gd_2O_3 nanoparticles

Doping gadolinium oxide with europium was carried out to provide fluorescent nanoparticles. Figure 4.1 shows the excitation spectra collected of solid samples of Gd_2O_3 and Eu-doped Gd_2O_3 nanoparticles prepared using the microwave synthesis described in chapter 2.

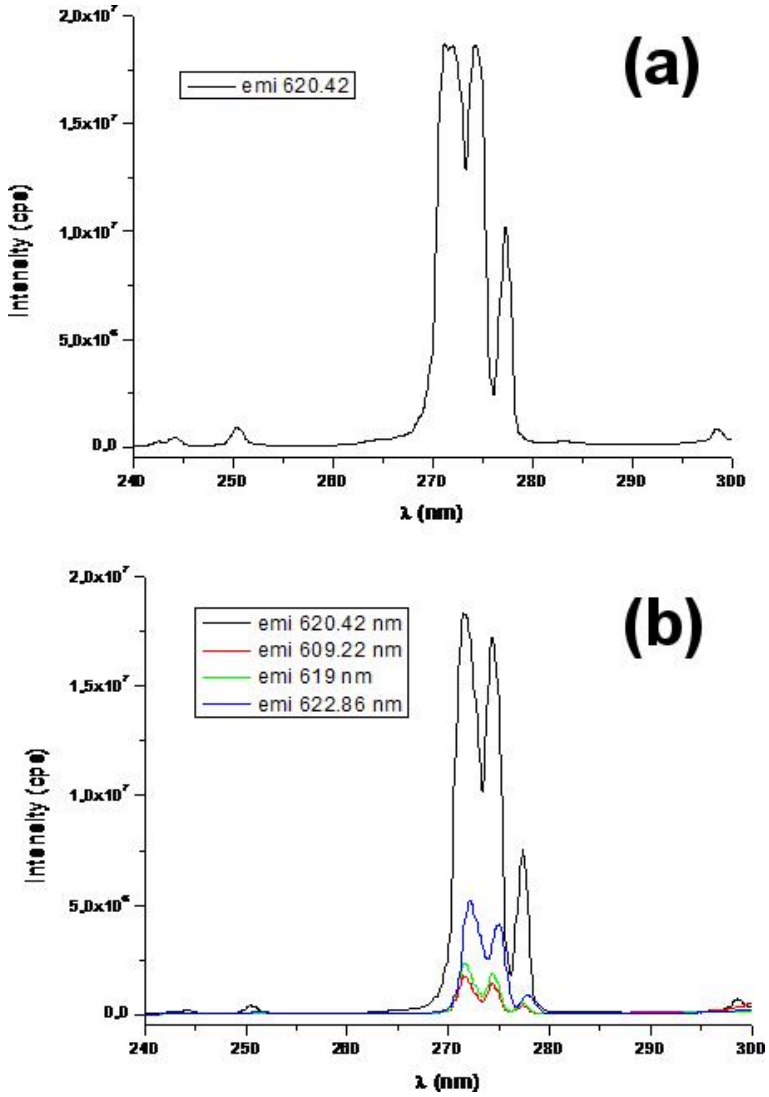

Figure 4.1 Excitation spectra of (a) Gd_2O_3 nanoparticles at an emission wavelength of 620.42 nm (shown on spectra) and (b) Eu:Gd_2O_3 nanoparticles at emission wavelengths of 620.42 nm, 609.22 nm, 619 nm and 622.86 nm (shown on spectra). Spectra were recorded by visiting PhD student Maria Gomes in the Corr Group.

For Gd_2O_3, two large peaks are observed at 272 nm and 274 nm, with a smaller peak at 278 nm. A small peak at 250 nm is also observed. For the Eu-doped Gd_2O_3 sample, similar peaks are observed in the excitation spectra. The corresponding emission wavelength used to obtain these excitation spectra are given in the inset of each figure. These wavelengths are 609.22 nm, 619 nm, 620.42 nm and 622.86 nm. The best excitation spectrum is obtained when an emission wavelength of 620.42 nm is used. The peak in both spectra at 250 nm may be attributed to the charge transfer band of oxygen to europium,[88] while the other peaks correspond to direct excitation of f-electrons. For the Gd_2O_3 sample, the f-f transitions at 272 nm and 274 nm are attributed to $^8S_{7/2} \rightarrow {}^6I_{7/2}$ and $^6P_{7/2}$ transitions.[89] It is difficult to make out any additional peaks in the Eu-doped Gd_2O_3 excitation spectra. Emission spectra of the Gd_2O_3 and Eu-doped Gd_2O_3 nanoparticles are shown in Figure 4.2.

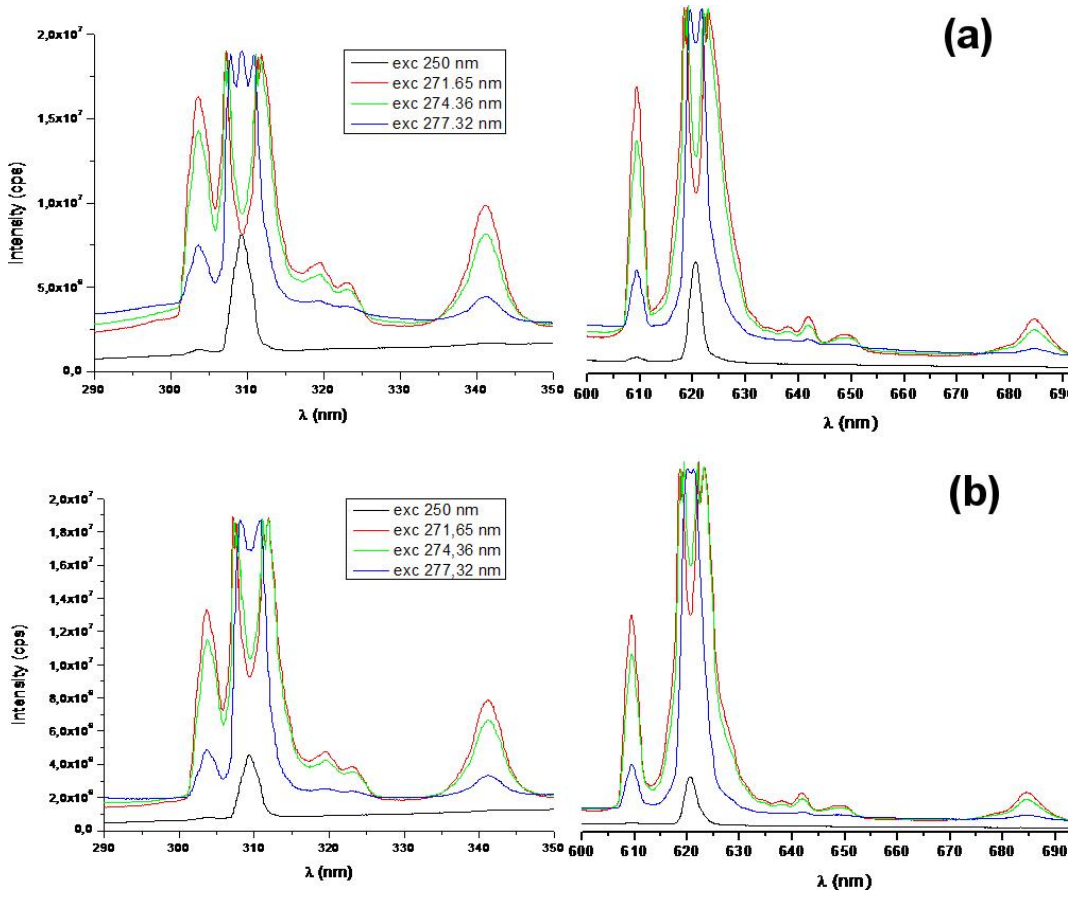

Figure 4.2 Emission spectra for (a) Gd_2O_3 and (b) Eu-doped Gd_2O_3 nanoparticles obtained for different excitation wavelengths of 250 nm, 271.65 nm, 274.36 nm and 277.32 nm. Spectra were recorded by visiting PhD student Maria Gomes in the Corr Group.

Again, similar peaks are observed for both samples. The peaks at 620 nm and 610 nm may be due to the $^5D_0$-$^7F_2$ transition in Eu^{3+}. However, this is also seen in the spectra collected for the pure Gd_2O_3 nanoparticles, so may also come from the $^6G_J \rightarrow {}^6P_J$ transitions of Gd^{3+}. These transitions were also identified by Jayasimhadri *et al.*[89] The peak seen by them at 315 nm is also seen in Figure 4.2 belongs to Gd^{3+}. The powder that was left after drying the europium doped nanoparticles was white in colour, however when exposed to UV light fluoresced bright blue. Unfortunately, due to time constraints and the small product yield, X-ray diffraction analysis was not performed on these samples.

The fluorescence seen, when the powder was exposed to UV light and the spectra in the figures above, demonstrates how these particles would be useful in bioanalysis. The usefulness of Gd_2O_3 nanoparticles increases after dye doping as they are then fluorescent, with exposure to UV light, and magnetic.[89] These nanoparticles therefore have greater potential in bio imaging as they can be directed to the area being investigated through the use of MRI.[90]

5. Conclusions

A successful method for the preparation of monodisperse silica nanoparticles using microwave synthetic approaches has been developed. This has resulted in a faster, low temperature, reproducible method for the preparation of important nanoparticles which could find use as biological labels. In an effort to further establish this, the fluorescent dye, Rhodamine B, has also been incorporated into the silica nanoparticles matrix to provide fluorescent particles. The photostability of these materials has also been established, with no noticeable degradation in fluorescence intensity when placed over a UV lamp noted after two months.

For silica nanoparticles, typical particle sizes of between 37.77 nm and 215.50 nm can be prepared using microwave synthesis methods. However, the polydispersity of these samples is not always low, an important consideration for use in biological systems. For example, the smallest Z-average recorded for particles gave a PdI of 0.617, whereas the largest particles gave a PdI of 0.179. This indicates that while a smaller size is more desirable there seems to be better monodispersity at larger sizes.

It was noted that after several weeks of growth, samples prepared at lower temperatures continued to grow indicating that there are free silica precursor materials still present. This is not the case at higher temperatures, where the Z-averages do not change much over time and increases in PdI may be attributed to aggregation of the particles.

The best conditions for monodisperse particle preparation are found at 50 °C and 0.5 hours, followed by immediate precipitation. These particles are highly spherical and monodisperse according to SEM analysis. This demonstrates the efficiency of using a one-pot microwave synthesis: a variety of particle sizes can be achieved at low temperatures with no additional annealing steps. The synthesis time is much shorter than a number of previous reports. These results are also found to be reproducible.

Varying just two parameters however, does not take into account the effect of increasing or reducing volumes of the starting components and this could provide a starting point for further research in this field in the future.

On incorporation of Rhodamine B into the silica nanoparticles matrix, an increase in Z-average is observed. Due to increased electrostatic interaction, this size increase was expected, however, this is relatively substantial. The fluorescence of this sample was also confirmed under UV irradiation and future experiments could use this one-step procedure for the preparation of fluorescent-silica nanoparticles to include a range of dyes.

Routes to metal oxide nanoparticles have also been investigated, including Gd_2O_3 and Eu-doped Gd_2O_3. These particles were also prepared in just several hours. Emission spectra collected confirm fluorescence of these particles. Although fluorescent nanoparticles comprising Eu:Gd_2O_3 were obtained, the structure of these particles through X-ray diffraction analysis was not confirmed. Also, the fluorescent nature of the particles has not been fully investigated.

6. Further Work

Future work on this system could include varying the concentration of organic dye within the silica nanoparticle in order to establish when self-quenching begins to occur. Other organic dyes could also be incorporated such as tetramethylrhodamine isothiocynate, fluorescein isothiocynate and tris(bipyridine)ruthenium (II) chloride.[91,92,93] This fluorescence combined with the ability of these nanoparticles to be multifunctional means that peptides can be bonded to these samples so that they can then image cells in a targeted manner. The photostability shown by Rhodamine B-silica nanoparticles is further evidence of the effectiveness these samples would have in bioimaging. Fluorescence lifetime measurements could confirm this stability compared to Rhodamine B solutions alone. Silica nanoparticles still maintain their biocompatible nature which would make their use here highly efficient. Future work could also include biological testing of these nanoparticles to determine the toxicity of these particles. Further experiments could use this one-step procedure for the preparation of fluorescent-silica nanoparticles to include a range of dyes.

The use of microwave synthesis as a pathway to these interesting materials has been established, but future work could focus on preparing a series of doped Gd_2O_3 nanoparticles and studying how the fluorescent behaviour changes with rare earth doping content. Future work on these systems could be extended not only in the case of Eu^{3+}, but also to include a range of Ln^{3+} ions.

The future applications of these nanoparticles are restricted only by the choice of molecules they are functionalised with, making these interesting materials in a number of areas including bioimaging.

7. Apendix

7.1 FTIR spectra for silica nanoparticles

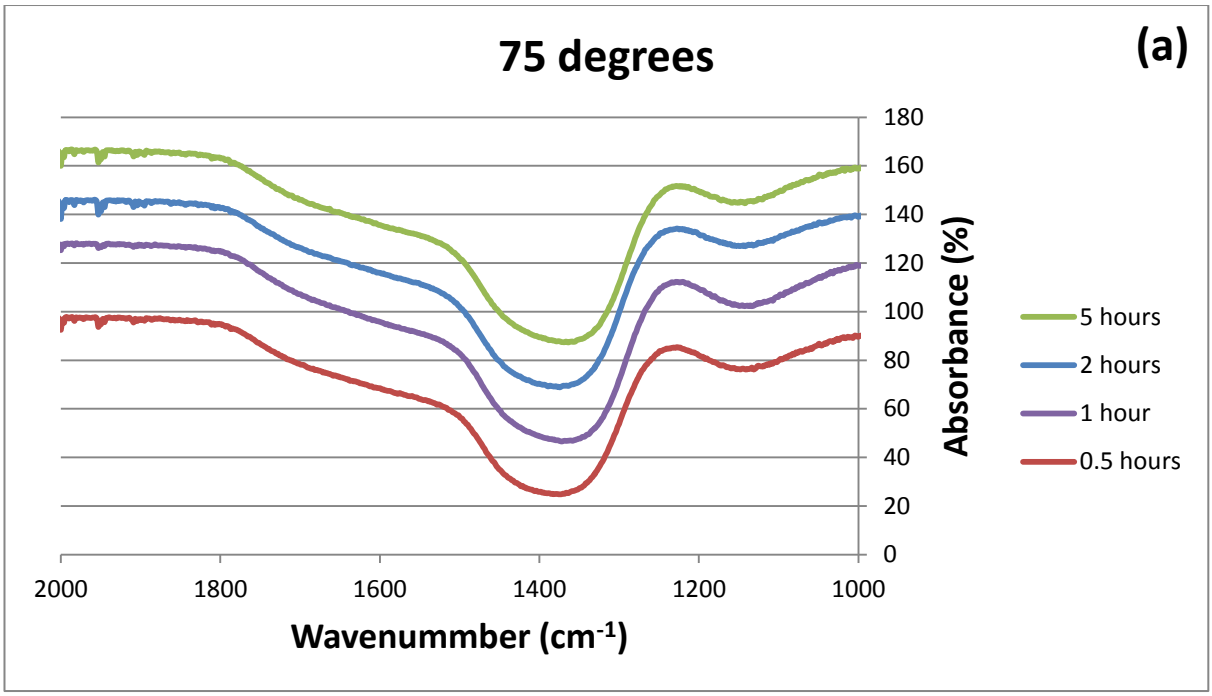

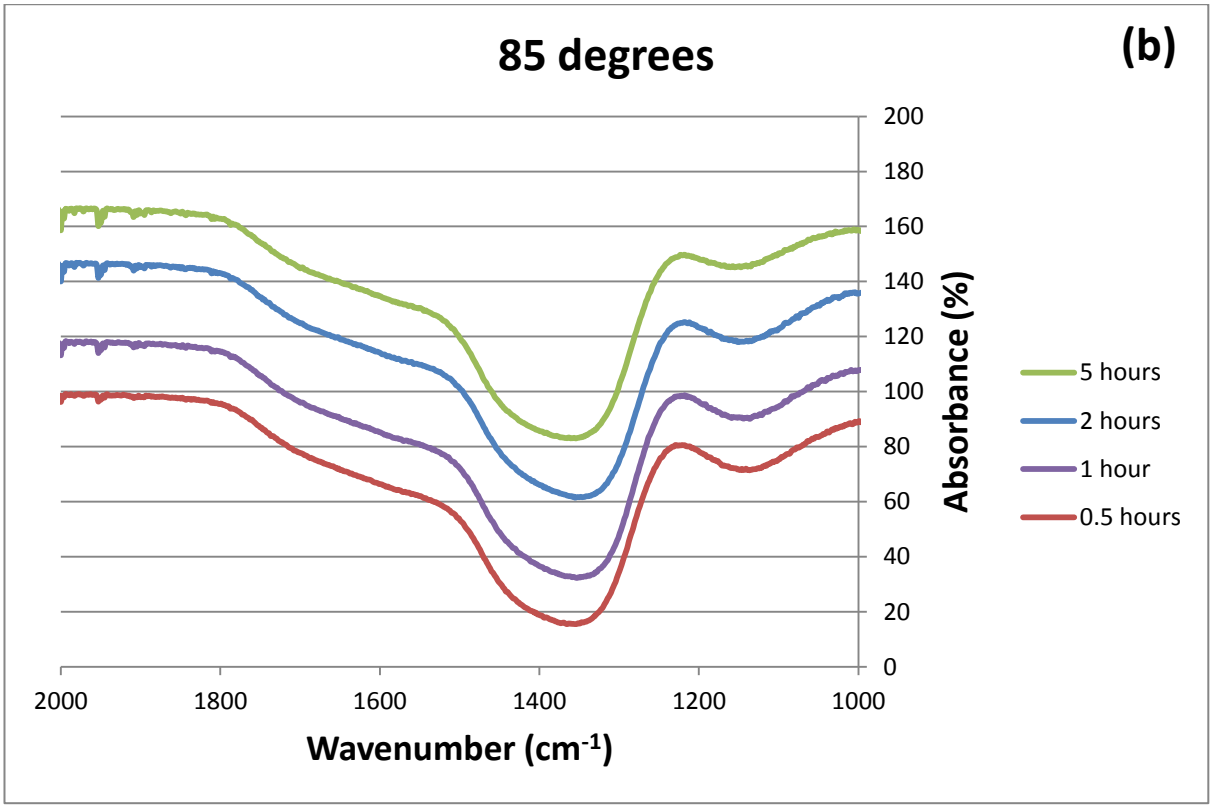

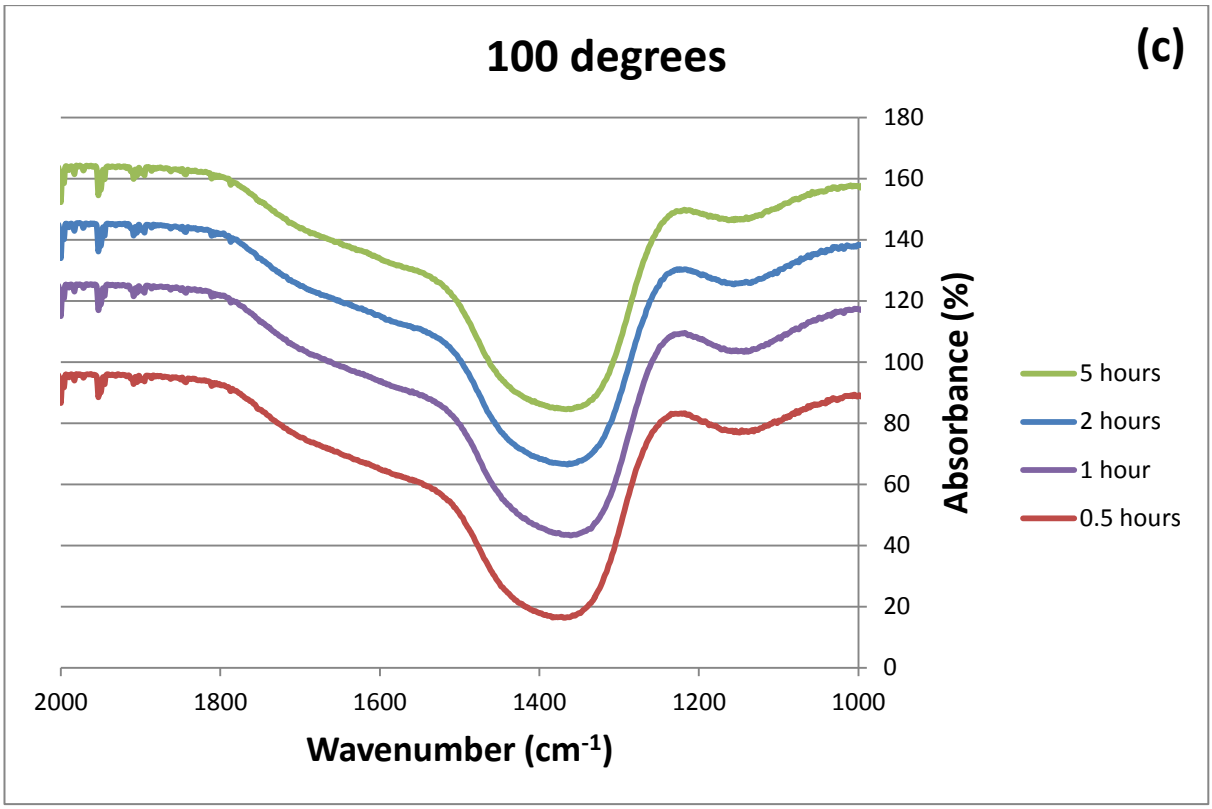

Figure 7.1 IR spectra of dried silica nanoparticles prepared at a) 75 °C, b) 85 °C and c) 100 °C for 0.5 h (red), 1 h (purple), 2 h (blue) and 5 h (green).

7.2 DLS Plots of Z-average and PdI for silica nanoparticles

7.2.1 50 °C

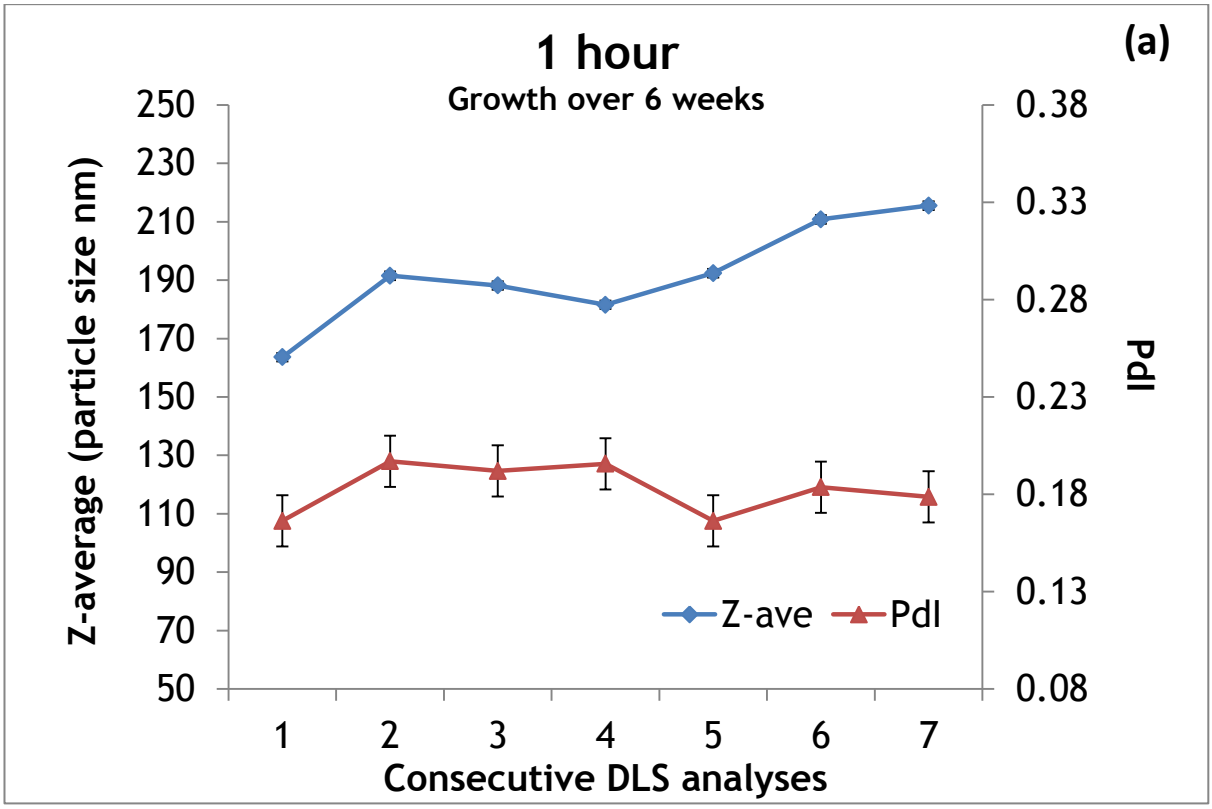

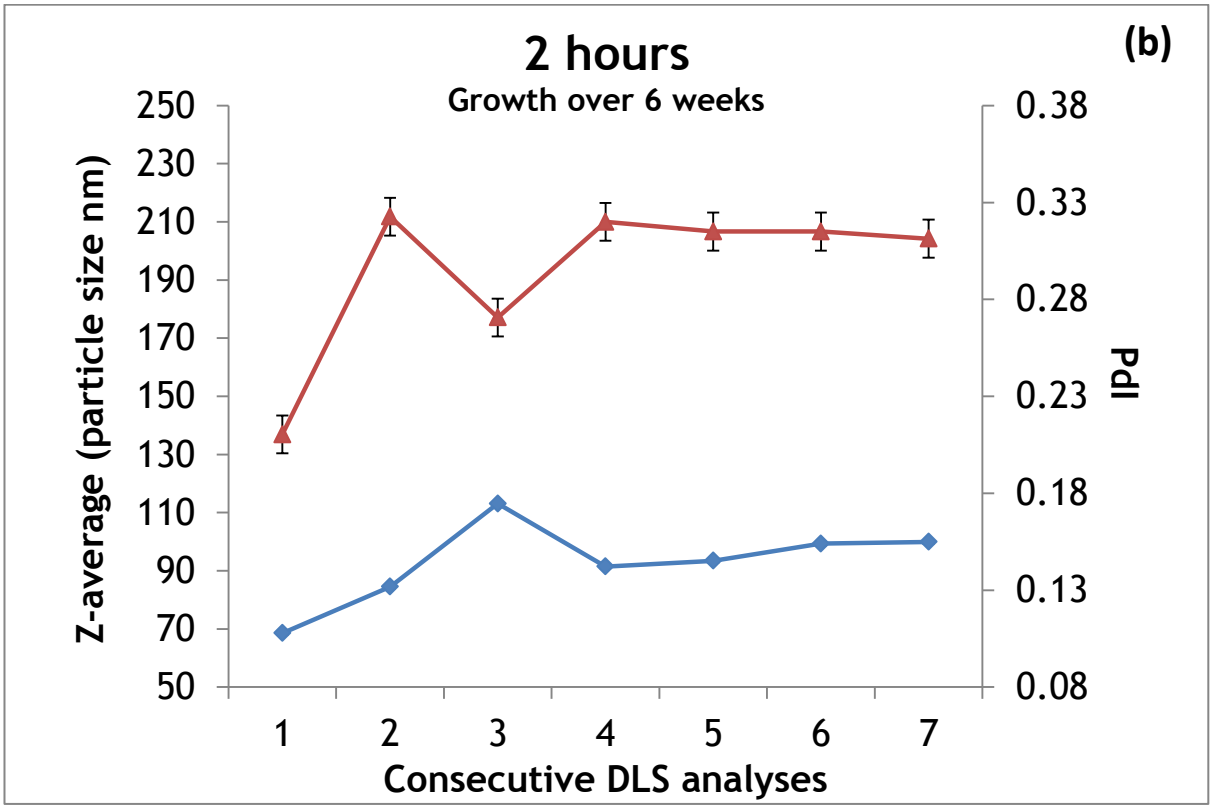

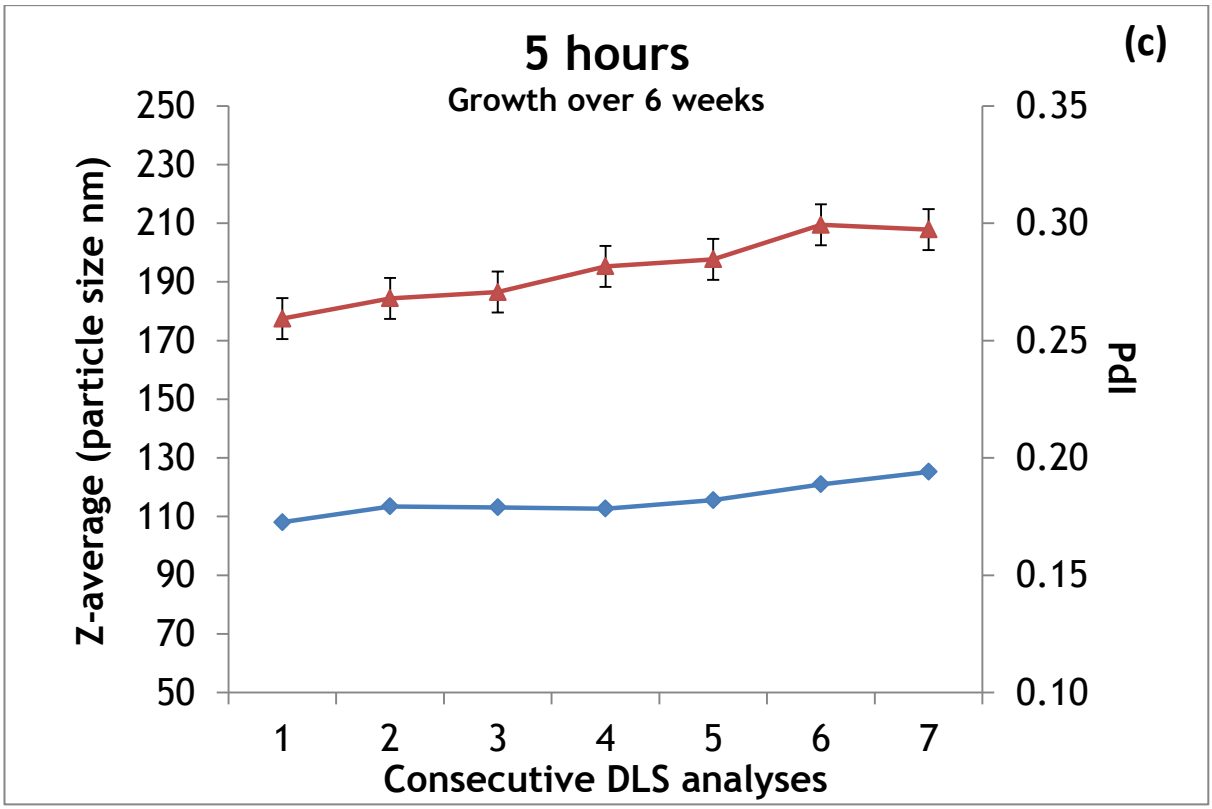

Figure 7.2 Plots of z-average (blue) and PdI (red) over 7 analyses obtained from DLS measurements over (a) 1 h, (b) 2h and (c) 5 h at 50 °C.

7.2.1 75 °C

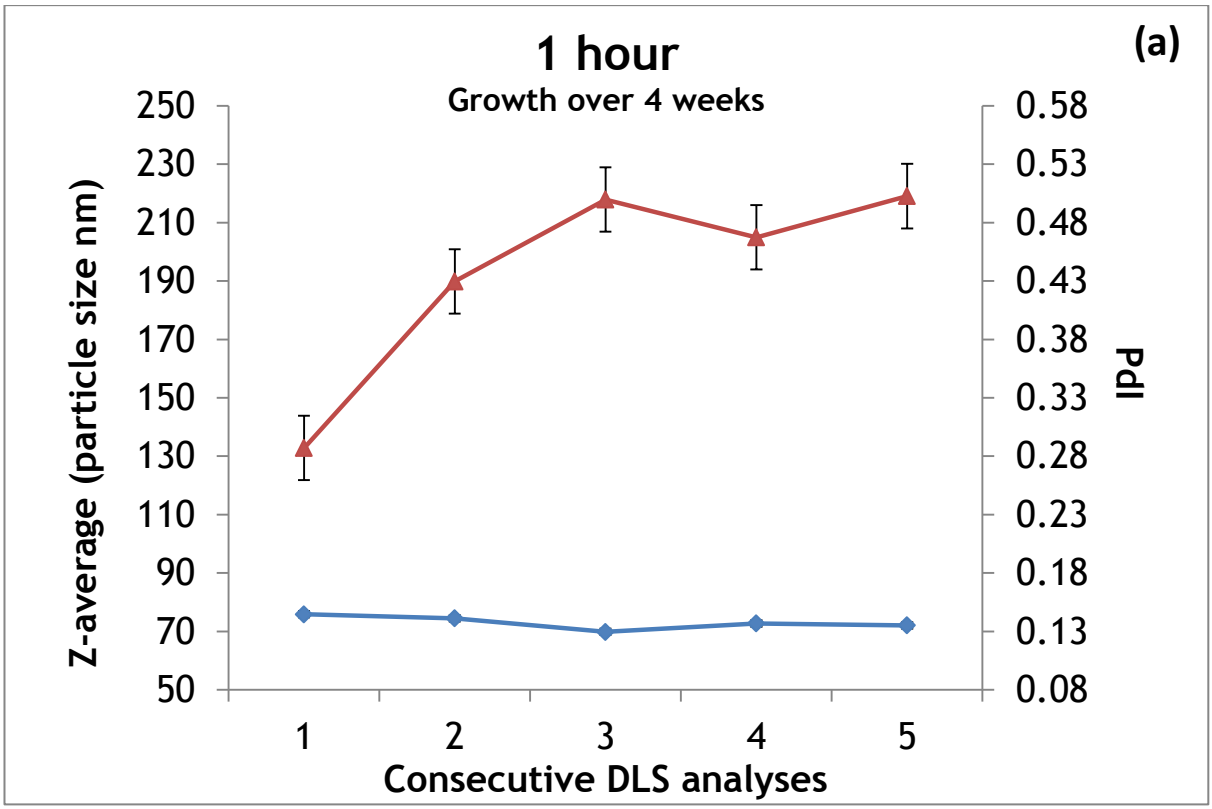
(a)
1 hour
Growth over 4 weeks
Z-average (particle size nm)
250
230
210
190
170
150
130
110
90
70
50
0.58
0.53
0.48
0.43
0.38
0.33
0.28
0.23
0.18
0.13
0.08
PdI
1
2
3
4
5
Consecutive DLS analyses

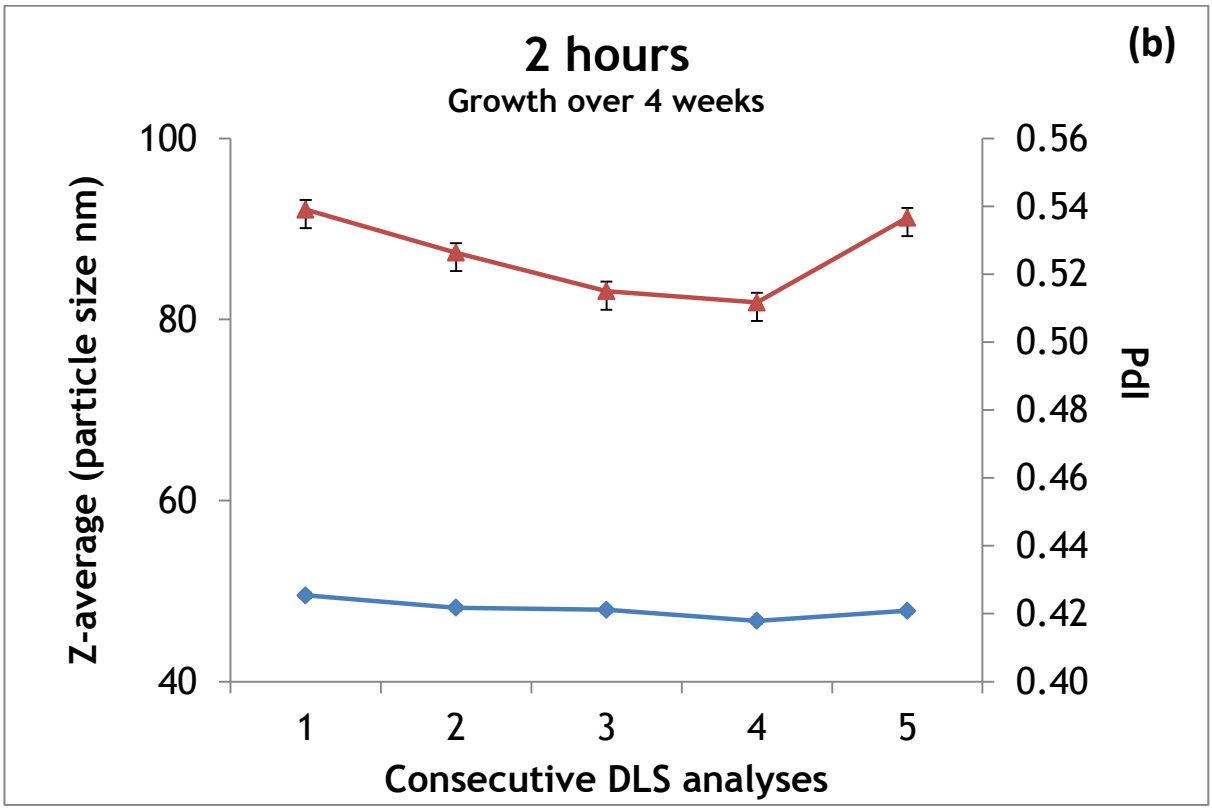
(b)
2 hours
Growth over 4 weeks
Z-average (particle size nm)
100
80
60
40
0.56
0.54
0.52
0.50
0.48
0.46
0.44
0.42
0.40
PdI
1
2
3
4
5
Consecutive DLS analyses

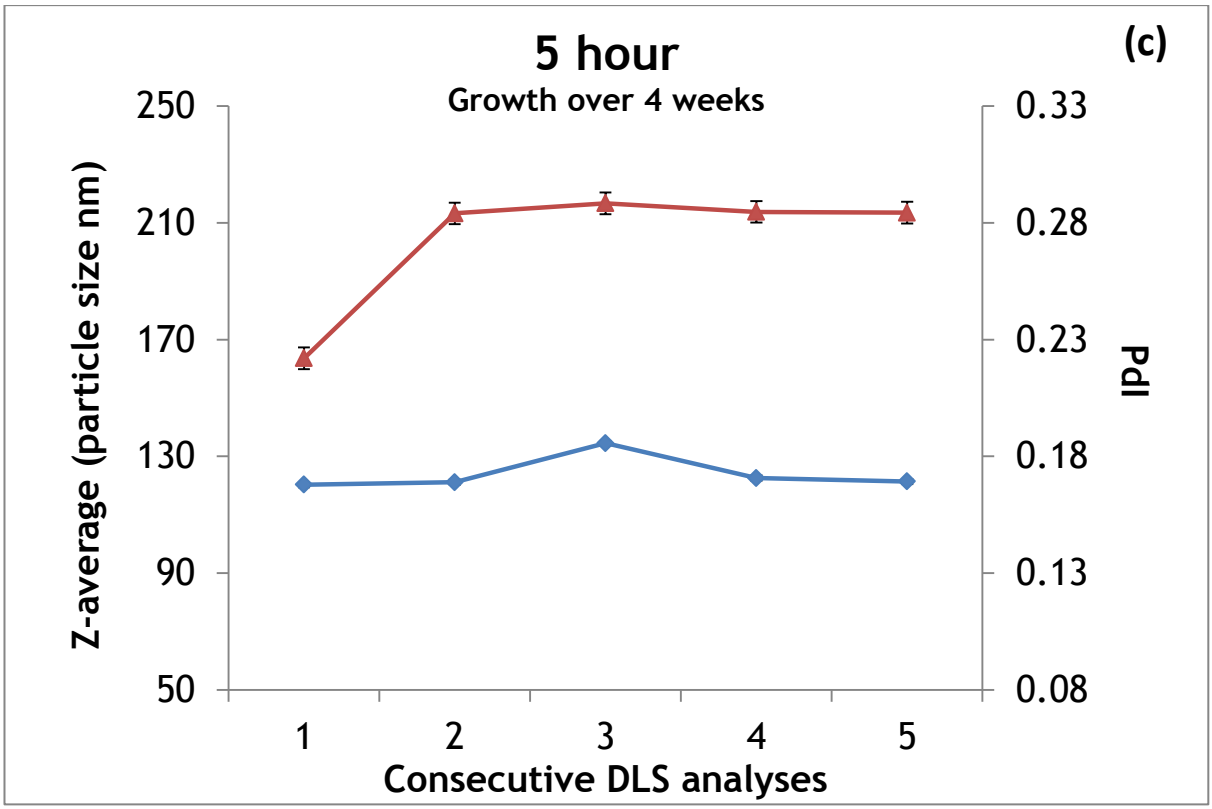

Figure 7.3 Plots of z-average (blue) and PdI (red) over 5 analyses obtained from DLS measurements over (a) 1 h, (b) 2h and (c) 5 h at 75 °C.

7.2.1 85 °C

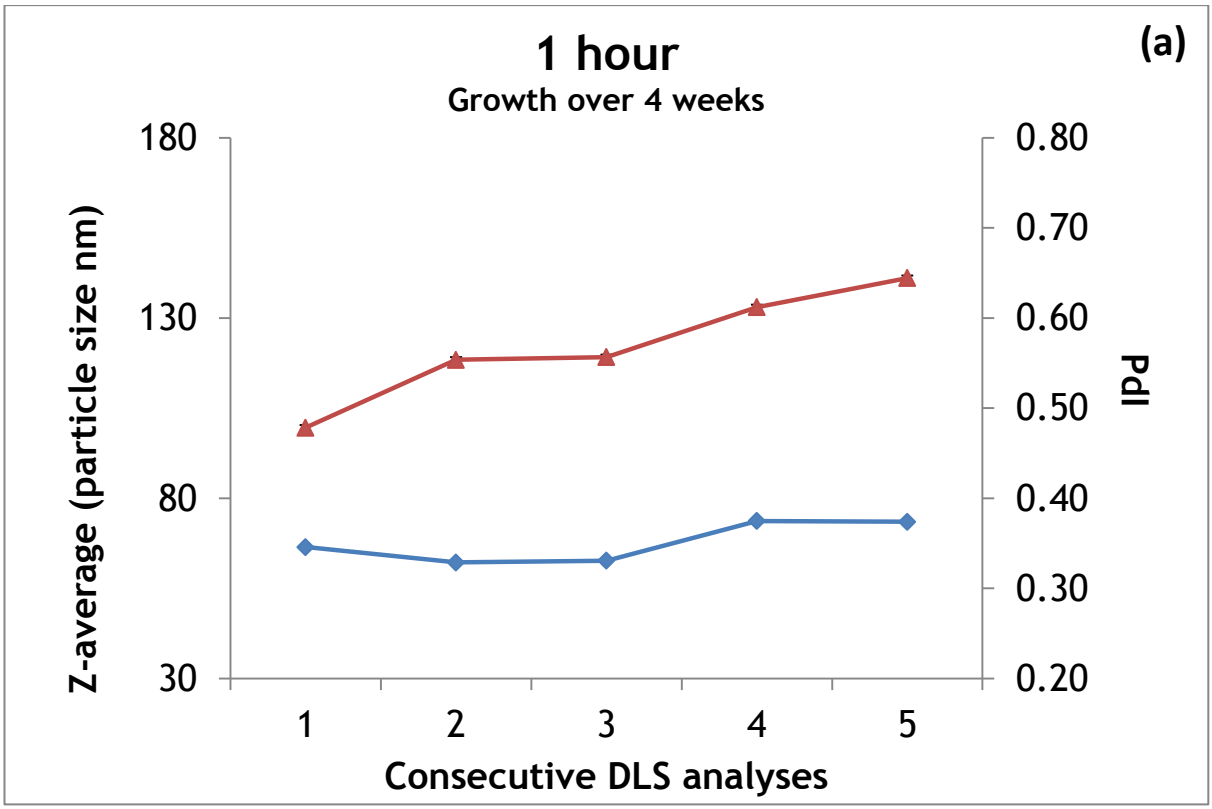
(a)
1 hour
Growth over 4 weeks
Z-average (particle size nm)
180
130
80
30
0.80
0.70
0.60
0.50
0.40
0.30
0.20
PdI
1
2
3
4
5
Consecutive DLS analyses

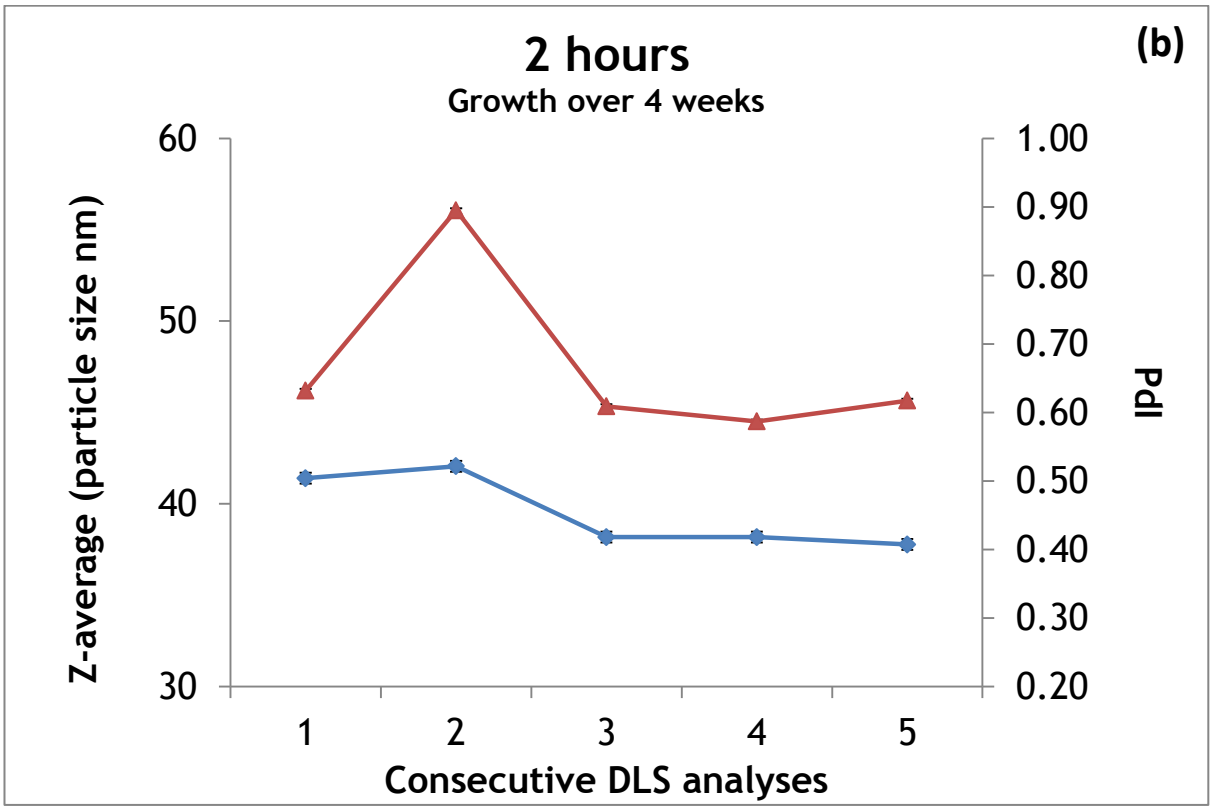
(b)
2 hours
Growth over 4 weeks
Z-average (particle size nm)
60
50
40
30
1.00
0.90
0.80
0.70
0.60
0.50
0.40
0.30
0.20
PdI
1
2
3
4
5
Consecutive DLS analyses

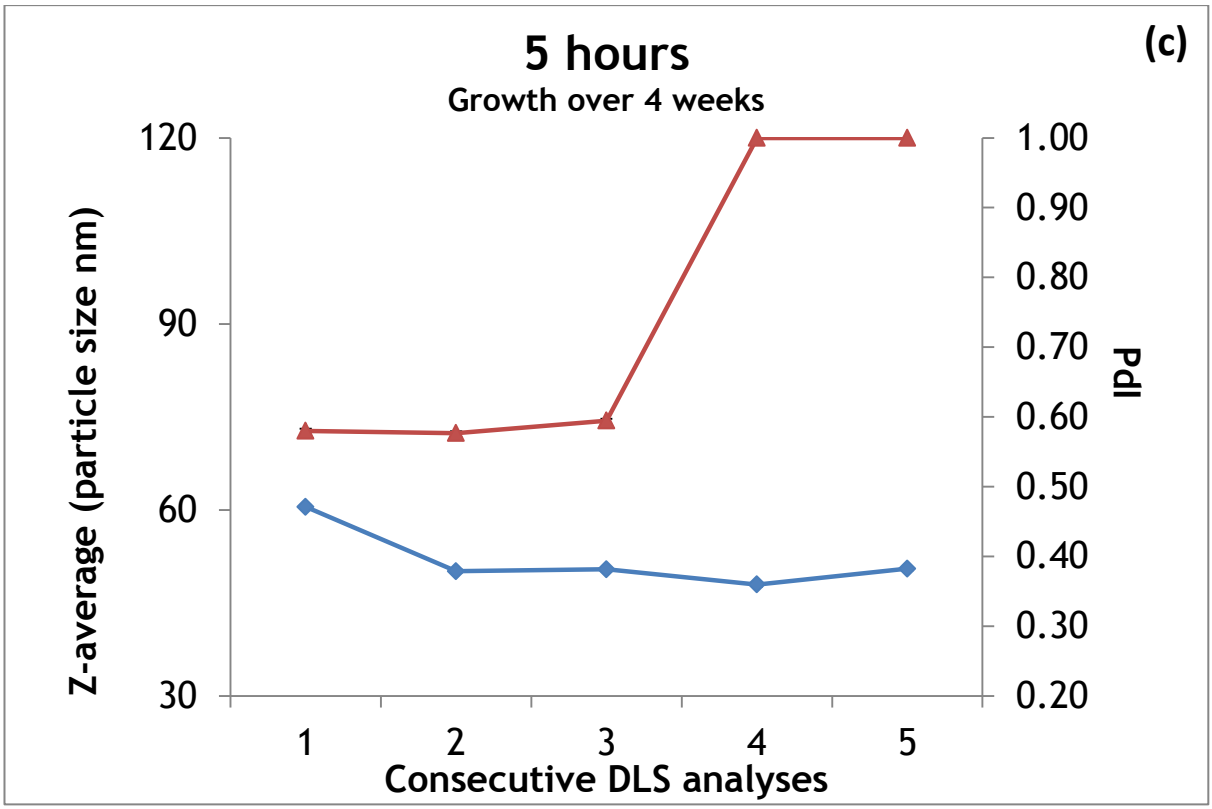

Figure 7.4 Plots of z-average (blue) and PdI (red) over 5 analyses obtained from DLS measurements over (a) 1 h, (b) 2h and (c) 5 h at 85 °C.

7.2.1 100 °C

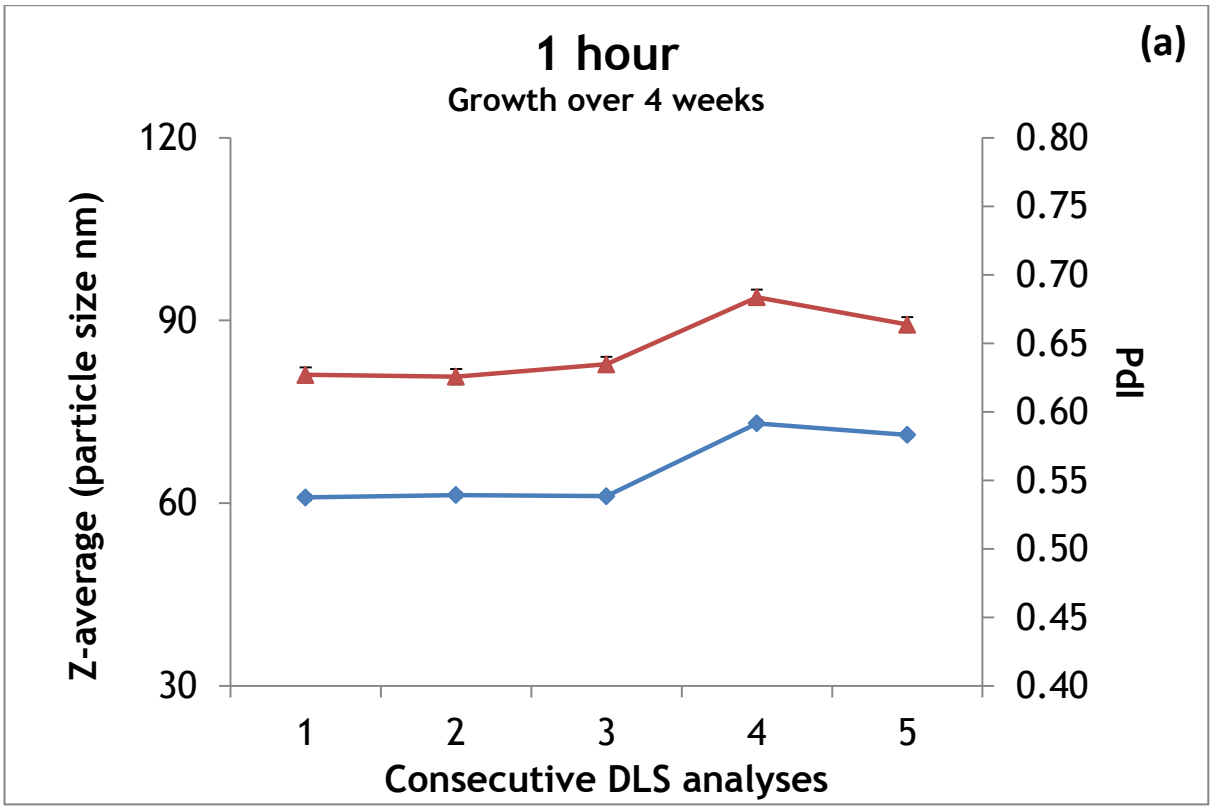
(a)
1 hour
Growth over 4 weeks
Z-average (particle size nm)
PdI
120
90
60
30
0.80
0.75
0.70
0.65
0.60
0.55
0.50
0.45
0.40
1
2
3
4
5
Consecutive DLS analyses

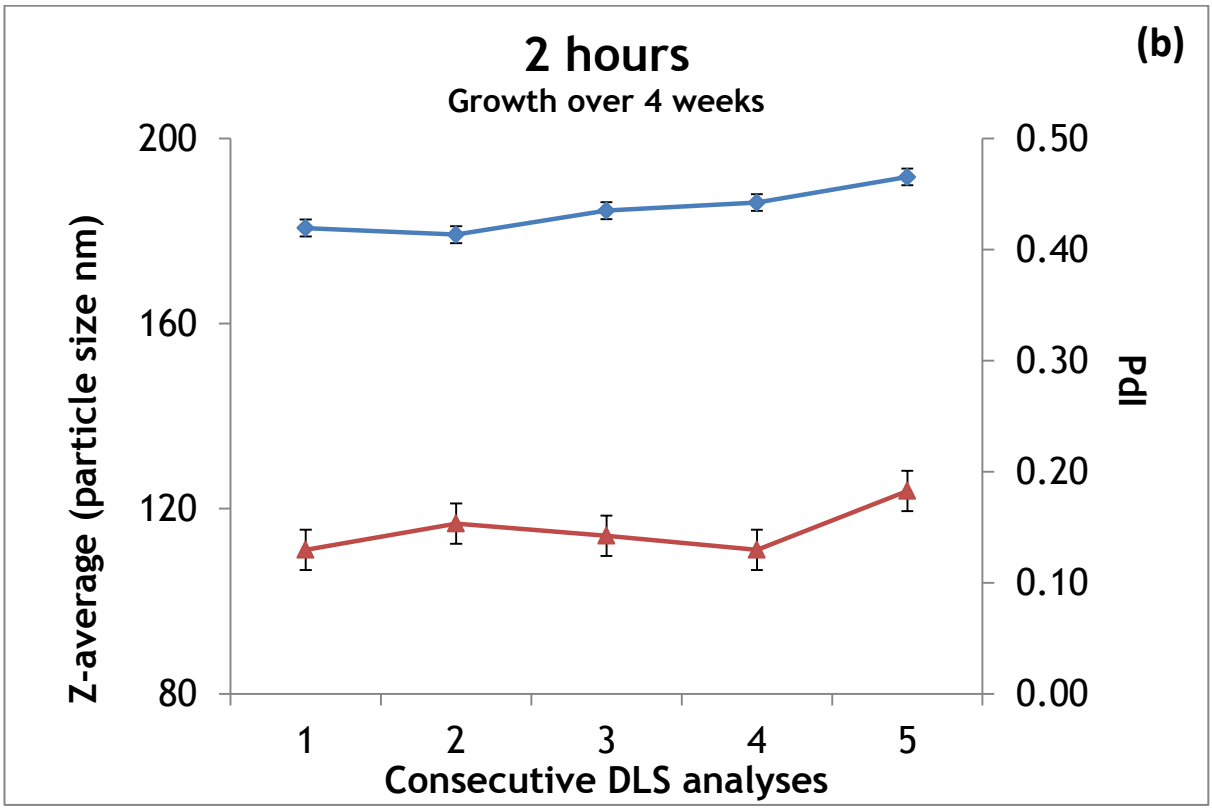
(b)
2 hours
Growth over 4 weeks
Z-average (particle size nm)
PdI
200
160
120
80
0.50
0.40
0.30
0.20
0.10
0.00
1
2
3
4
5
Consecutive DLS analyses

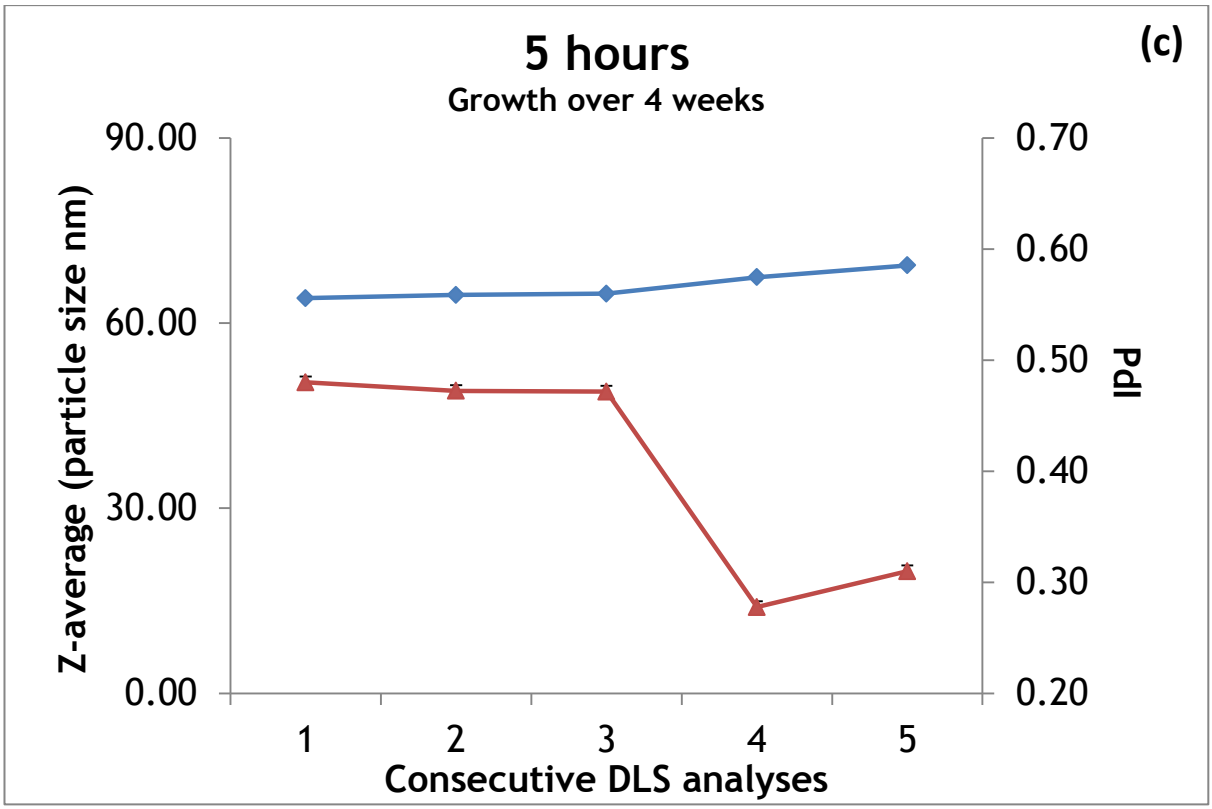

Figure 7.5 Plots of z-average (blue) and PdI (red) over 5 analyses obtained from DLS measurements over (a) 1 h, (b) 2h and (c) 5 h at 100 °C.

7.3 Eu doped Gd_2O_3 emission spectrum

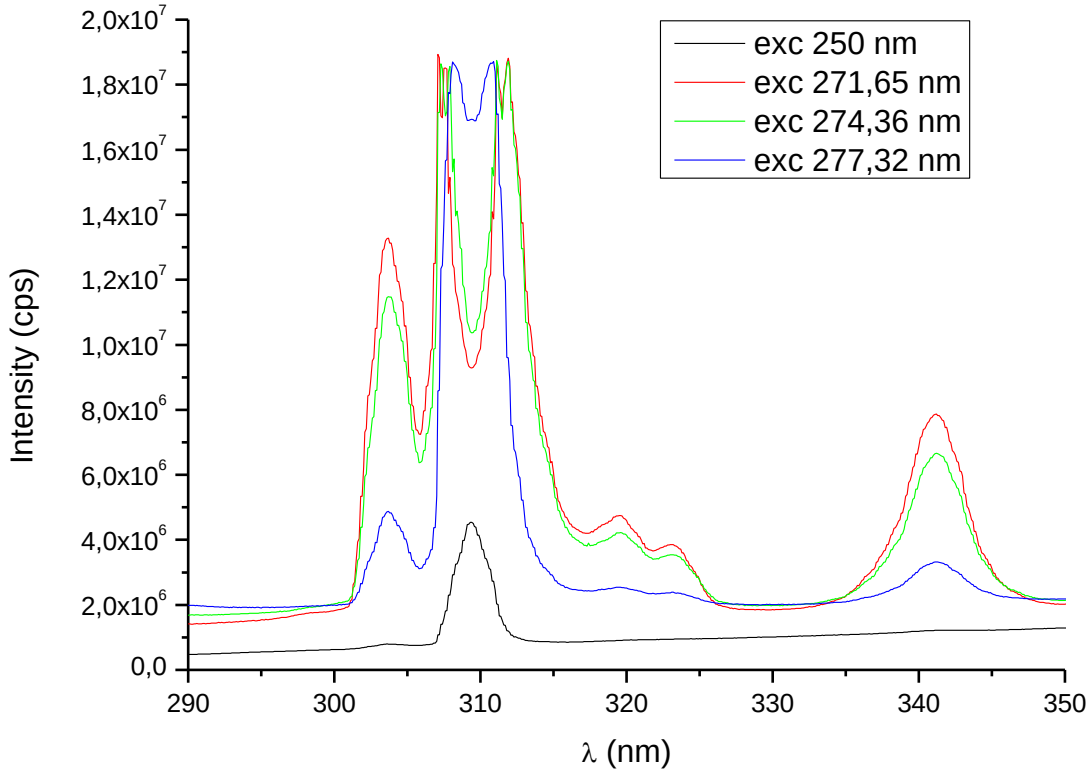

Figure 7.5 Emission spectra of Eu:Gd_2O_3 nanoparticles. Spectra were recorded by visiting PhD student Maria Gomes in the Corr Group. The excitation wavelengths used were 250 nm, 271.65 nm, 274.36 nm and 277.32 nm.

7.4 Gd_2O_3 emission spectrum

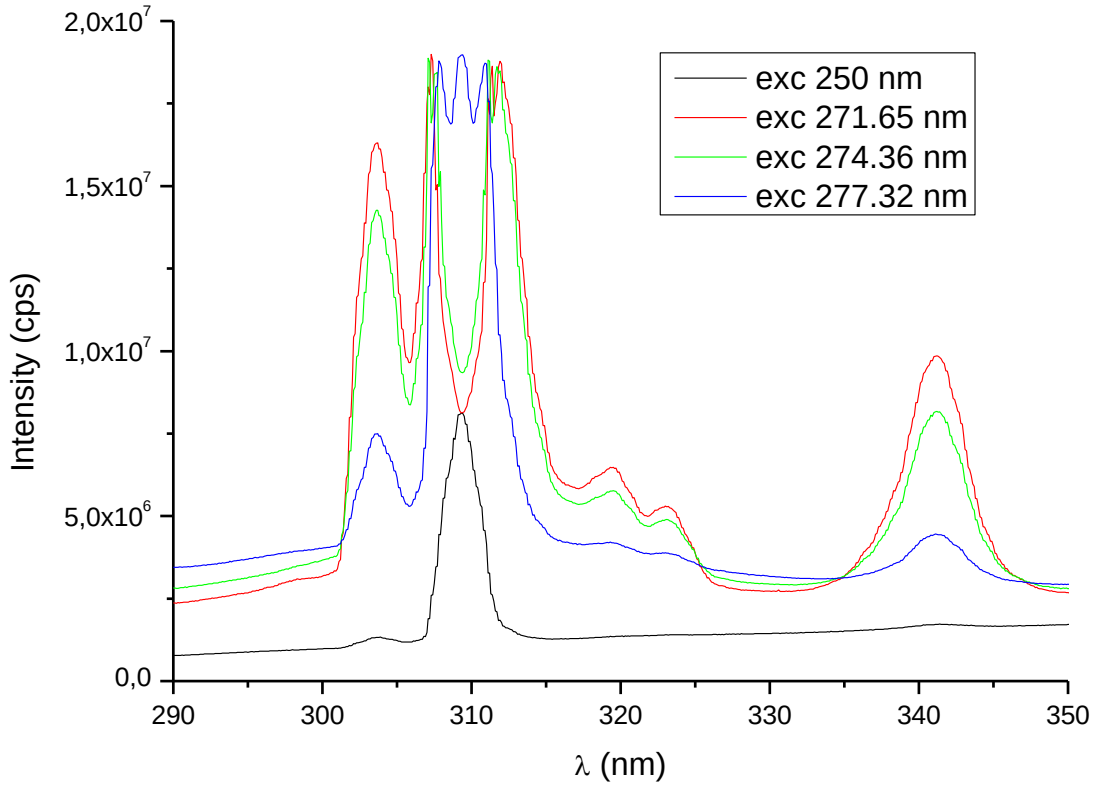

Figure 7.6 Emission spectra of Gd_2O_3 nanoparticles. Spectra were recorded by visiting PhD student Maria Gomes in the Corr Group. The excitation wavelengths used were 250 nm, 271.65 nm, 274.36 nm and 277.32 nm.

References

[1] P. J. A. Borm, D. Robbins, S. Haubold, T. Kuhlbusch, H. Fissan, K. Donaldson, R. Schins, V. Stone, W. Kreyling, J. Lademann, J. Krutmann, D. Warheit and E. Oberdorster, *Particle and Fibre Toxicology*, **2006**, 3, 11.

[2] T. M. Benn and P. Westerhoff, *Environ. Sci. Technol.*, **2008**, 42, 4133.

[3] X. H. Gao, Y. Y. Cui, R. M. Levenson, L. W. K. Chung and S. M. Nie, *Nat. Biotechnol.*, **2004**, 22, 969.

[4] J. P. F. Lagerwall and G. Scalia, *Current Applied Physics*, **2012**, 12, 1387.

[5] A. Nazari, S. Riahi, S. Riahi, S. F. Shamekhi and A. Khademno, *J. Am. Sci.*, **2010**, 6, 102.

[6] C. Rao, H. Matte, R. Voggu and A. Govindaraj, *Dalton Trans.*, **2012**, 41, 5089.

[7] S. Santra, P. Zhang, K. Wang, R. Tapec, W. O'Brien and N. L. Pickett, *Chem. Mater.*, **2001**, 13, 3843.

[8] L. Wang and W. Tan, *Nano Lett.*, **2006**, 6, 84.

[9] M. R. Gwinn and V. Vallyathan, *Environmental Health Perspectives*, **2006**, 114, 1818.

[10] J. H. Warner, A. Hoshino, K. Yamamoto and R. D. Tilley, *Angew. Chem. Int. Ed.*, **2005**, 44, 4550.

[11] X. Michalet, F. F. Pinaud, L. A. Bentolila, J. M. Tsay, S. Doose, J. J. Li, G. Sundaresan, A. M. Wu, S. S. Gambhir and S. Weiss, *Science*, **2005**, 307, 538.

[12] D. L. Green, J. S. Linb, Y-F. Lamc, M. Z-C. Hud, D. W. Schaefere and M. T. Harris, *J. Colloid Interface Sci.*, **2003**, 266, 346.

[13] W. Stöber, A. Fink and E. Bohn, *J. Colloid Interface Sci.*, **1968**, 26, 62.

[14] G-L. Davies, A. Barry and Y. K. Gun'ko, *Chem. Phys. Lett.*, **2009**, 468, 239.

[15] S. Polarz, *Adv. Funct.Mater.*, **2011**, 21, 3214.

[16] S. K. Park, K. D. Kim and H. T. Kim, *Colloids Surf. A.*, **2002**, 197, 7.

[17] K. S. Rao, K. El-Hami, T. Kodaki, K. Matsushige and K. Makino, *J. Colloid Interface Sci.*, **2005**, 289, 125.

[18] G.-M. Gao, H.-F. Zou, D-R. Liu, L-N. Miao, G-J. Ji and S-C. Gan, *Colloids Sur.: A. Physicochem. Eng. Aspects*, **2009**, 350, 33.

[19] R. P. Bagwe, C. Yang, L. R. Hillard and W. Tan, *Langmuir,* **2004**, 20, 8336.

[20] A-H. Lu, E. L. Salabas and F. Schüth. Angew. Chem. Int. Ed. **2007**, 46, 1222 – 1244.

[21] S. Sadasivan, D. H. Rasmussen, F. P. Chen and R.K. Kannabiran, *Colloids Sur.: A. Physicochem. Eng. Aspects*, **1998**, 132, 45.

[22] Z-Z. Li, L-X. Wen, L. Shao and J-F. Chen, *J. Controlled Release*, **2004**, 98, 245.

[23] X. Liu, L. Pan, T. Lv, G. Zhu, Z. Sun and C. Sun, *Chem. Commun.*, **2011**, 47, 11984.

[24] B. Wathey, J. Tierney, P. Lidstrom and J. Westman, *Drug Discovery Today*, **2002**, 7, 373.

[25] D. Wragg, P. Byrne, G. Giriat, B. Le Ouay, R. Gyepes, A. Harrison, A. Whittaker and R. Morris, *J. Phys. Chem. C*, **2009**, 113, 20553.

[26] M. Baghbanzadeh, L. Carbone, P. Cozzoli and C. Kappe, *Angew. Chem. Int. Ed.*, **2011**, 50, 11312.

[27] I. Bilecka and M. Niederberger, *Nanoscale*, **2010**, 2, 1358.

[28] I. Bilecka, I. Djerdj and M. Niederberger, *Chem Commum.*, **2008**, 886.

[29] D. Lovegood, J. R. Owens, M. Seeber, K. G. Kornev and I. Luzinov, Appl. Mater. Interfaces, **2012**, 4, 6875.

[30] N. Chekina, D. Horak, P. Jendelova, M. Trchova, M. J. Benes, M. Hruby, V. Herynek, K. Turnovcova and E. Sykova, *J. Mater. Chem.*, **2011**, 21, 7630.

[31] M. Montalti, L. Prodi, N. Zaccheroni, G. Battistini, F. Mancin and E. Rampazzo, *Proc. SPIE.*, **2006**, 6099, 49.

[32] A. Van Blaaderen and A. Virj, *Langmuir*, **1992**, 8, 2921.

[33] P. Botella, I. Abasolo, Y. Fernãndez, C. Muniesa, S. Miranda, M. Quesada, J. Ruiz, S. Schwartz Jr. and A. Corma, *J. Controlled Release, **2011**, 156, 246.*

[34] Y. Liu, Y. Mi, J. Zhao and S-S. Feng, *Int. J. Pharmaceutics, **2011**, 421, 370.*

[35] I. A. Rahman, P. Vejayakumaran, C.S. Sipaut, J. Ismail and C. K. Chee, *Ceramics Int., **2008**, 34, 2059.*

[36] S. Chandra, K. C. Barick and D. Bahadur, *Advanced Drug Delivery Rev.*, **2011**, 63, 1267.

[37] S. A. Corr, Y. P. Rakovich and Y. K. Gun'ko, *Nanoscale Res Lett.*, **2008**, 3, 87.

[38] O. Veiseh, C. Sun, J. Gunn, N. Kohler, P. Gabikian, D. Lee, N. Bhattarai, R. Ellenbogen, R. Sze, A. Hallahan, J. Olson and M. Zhang, *Nano Lett.*, **2005**, 5, 1003.

[39] D. E. Achatz, F. J. Heiligtag, X. Li, M. Link and O. S. Wolfbeis, *Sensors and Actuators B: Chemical*, **2010**, 150, 211.

[40] H. Mader, X. Li, S. Saleh, M. Link, P. Kele and O. Wolfbeis, *N. Y. Acad. Sci.*, **2008**, 1130, 218.

[41] A. H. Faraji and P. Wipf, *Bioorganic& Medicinal Chem*, **2009**, 17, 2950.

[42] V. Torchilin, *Pharmaceutical Research*, **2007**, 24, 1.

[43] Y. Yamamoto, Y. Nagasaki, Y. Kato, Y. Sugiyama and K. Kataoka, *J. Control. Rel.*, **2001**, 77, *27.*

[44] M. Yokoyama, M. Miyauchi, N. Yamada, T. Okano, Y. Sakurai, K. Kataoka and S. Inoue, *Cancer Res.*, **1990**, 50, *1693.*

[45] G. Yao, L. Wang, Y. Wu, J. Smith, J. Xu, W. Zhao, E. Lee and W. Tan, *Anal. Bioanal. Chem.*, ***2006***, *385, 518.*

[46] P. Sharma, S. Brown, G. Walter, S. Santra and B. Moudgil, *Advances in Colloid Interface Sci.*, **2006**, 123 – 126, 471.

[47] L. Wang, K. Wang, S. Santra, X. Zhao, L. Hilliard, J. Smith, Y. Wu and W. Tan, *Anal. Chem.*, **2006**, 78, 646.

[48] H. Ow, D. R. Larson, M. Srivastava, B. A. Baird, W. W. Webb and U. Wiesner, *Nano Lett.*, **2005**, 5, 113.

[49] A. Burns, H. Ow and U. Weisner, *Chem. Soc. Rev.*, **2006**, 35, 1028.

[50] J. Panyam and V. Labhasetwar, *Advanced Drug Delivery Reviews*, **2003**, 55, 329.

[51] W. Shang, J. Nuffer, J. Dordick and R. Seigel, *Nano Lett.*, **2007**, 7, 1991.

[52] W. Lin, Y-W. Huang, X-D. Zhou and Y. Ma, *Toxicology and Applied Pharm.*, **2006**, 217, 252.

[53] B. Rimal, A. Greenberg and W. Rom, *Curr. Opin. Pulm. Med.*, **2005**, 11, 169.

[54] M. Cho, W-S. Cho, M. Choi, S. J. Kim, B. S. Han, S. H. Kim, H. O. Kim, Y. Y. Sheen and J. Jeong, *Toxicology Lett.*, **2009**, 189, 177.

[55] D. S. Kohane, *Biotechnol. Bioeng.*, **2007**, 96, 203.

[56] K. N. Raymond and V. C. Pierre, *Bioconjugate Chem.*, **2005**, 16, 3.

[57] M. Ahren, L. Selegard, A. Klasson, F. Soderlind, N. Abrikossova, C. Skoglund, T. Bengtsson, M. Engstrom, P-O. Kall and K. Uvdal, *Langmuir*, **2010**, 26, 5733.

[58] F. Fievet, J. P. Lagier, B. Blin, B. Beaudoin and M. Figlarz. *Solid State Ionics*, **1989**, 32–33, 198.

[59] C. Feldmann, *Adv. Funct. Mater*., **2003**, 13, 101.

[60] H-O. Jungk and C. Feldmann, *J. Mater. Sci.*, **2001**, 36, 297.

[61] R. Kennedy and J. Campbell, *J. Phys. C: Solid State Phys.*, **1980**, 13, 5341.

[62] X. Chen, E. Ma and G. Liu, *J. Phys. Chem. C*, **2007**, 111, 10404.

[63] E. M. Goldys, K. Drozdowicz-Tomsia, S. Jinjun, D. Dosev, I. M. Kennedy, S. Yatsunenko and M. Godlewski, *J. Am. Chem. Soc.*, **2006**, 128, 14498.

[64] B. Wathey, J. Tierney, P. Lidstrom and J. Westman, *Drug Discovery Today*, **2002**, 7, 373.

[65] B. L. Hayes, *Microwave Synthesis: Chemistry at the Speed of Light*, **2002**, CEM Publishing, North Carolina.

[66] S. A. Corr, and R. Seshadri, Synthetic Methodologies, Article No.: INO2 04014.01, in *Comprehensive Inorganic Chemistry II* (INO2), **2013**, Elsevier.

[67] A. Einstein, *Ann. Phys*. **1905**, 17, 549.

[68] I. Campbell, *Biophysical Techniques*, **2012**, OUP.

[69] *Zetasizer Nano Series*, **2004**, Malvern Instruments Ltd., Worcestershire

[70] D. E. Koppel, *J. Chem. Phys*., **1972**, 57, 4814.

[71] *Dynamic Light Scattering: An introduction in 30 minutes*, **2014**, DLS Technical note, Malvern Instruments Ltd., Worcestershire.

[72] A. Bandyopadhyay and S. Bose, *Characterisation of Biomaterials*, **2013**, Elsevier.

[73] J. K. G. Dhont, *An Introduction to Dynamics of Colloids*., **1996**, Elsevier.

[74] S. Duckett and B. Gilbert, *Foundations of Spectroscopy*, **1999**, OUP.

[75] *An introduction to electron microscopy*, **2010**, FEI Company.

[76] E. M. Boatman, G. C. Lisensky and K. J. Nordel, *J. Chem. Edu.*, **2005**, 82, 1697.

[77] D. B. Williams and C. B. Carter, *Transmission Electron Microscopy*, **1996**, Plenum, New York.

[78] J. R. Lakowicz, *Principles of Fluorescence Spectroscopy*, **2006**, Springer.

[79] D. S. Kohane, *Biotechnol. Bioeng.* **2007**, 96, 203.

[80] T. Musumeci, L. Vicari, C. A. Ventura, M. Gulisano, R. Pignatello, and G. Puglisi, *J. Nanosci. Nanotechnol.*, **2006**, 6, 3118.

[81] S. Polarz, *Adv. Funct. Mater.*, **2011**, 21, 3214.

[82] W. Stöber, A. Fink and E. Bohn, *J. Colloid Interface Sci.*, **1968**, 26, 62.

[83] T. Sugimoto, *Fine Particles: Synthesis, Characterization, and Mechanisms of Growth*, **2000**, Marcel Dekker Ltd., New York.

[84] G-L. Davies, A. Barry and Y. K. Gun'ko, *Chem. Phys. Lett.*, **2009**, 468, 239.

[85] R. P. Bagwe and K. C. Khilar, *Langmuir*, **2000**, 16, 905.

[86] K. Biswas, J. C. Ray, J-S. Choi and W-S. Ahn, *J. Non-Crystalline Solids*, **2008**, 354, 1.

[87] G. Yao, L. Wang, Y. Wu, J. Smith, J. Xu, W. Zhao, E. Lee and W. Tan, *Anal. Bioanal. Chem.*, ***2006***, *385, 518.*

[88] X. Chen, E. Ma and G. Liu, *J. Phys. Chem. C*, **2007**, 111, 10404.

[89] M. Jayasimhadri, B. V. Ratnam, K. Jang, H. S. Lee, S.-S. Yi and J.-H. Jeong, *Thin Solid Films*, **2010**, 518, 6210.

[90] K. N. Raymond and V. C. Pierre, *Bioconjugate Chem.*, **2005**, 16, 3.

[91] A. Burns, H. Ow and U. Weisner, *Chem. Soc. Rev.*, **2006**, 35, 1028.

[92] H. Ow, D. R. Larson, M. Srivastava, B. A. Baird, W. W. Webb and U. Wiesner, *Nano Lett.*, **2005**, 5, 113.

[93] P. Sharma, S. Brown, G. Walter, S. Santra and B. Moudgil, *Advances in Colloid Interface Sci.*, **2006**, 123 – 126, 471.